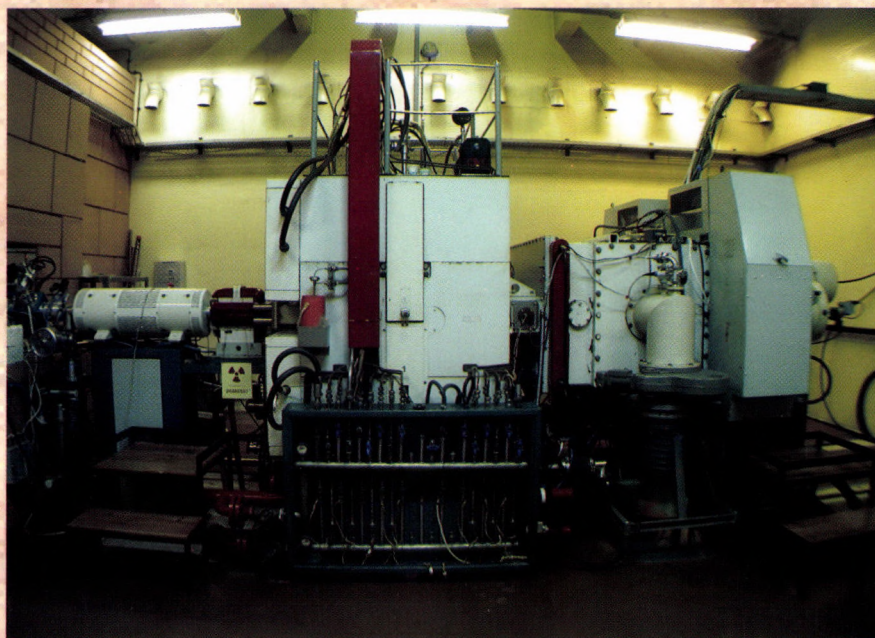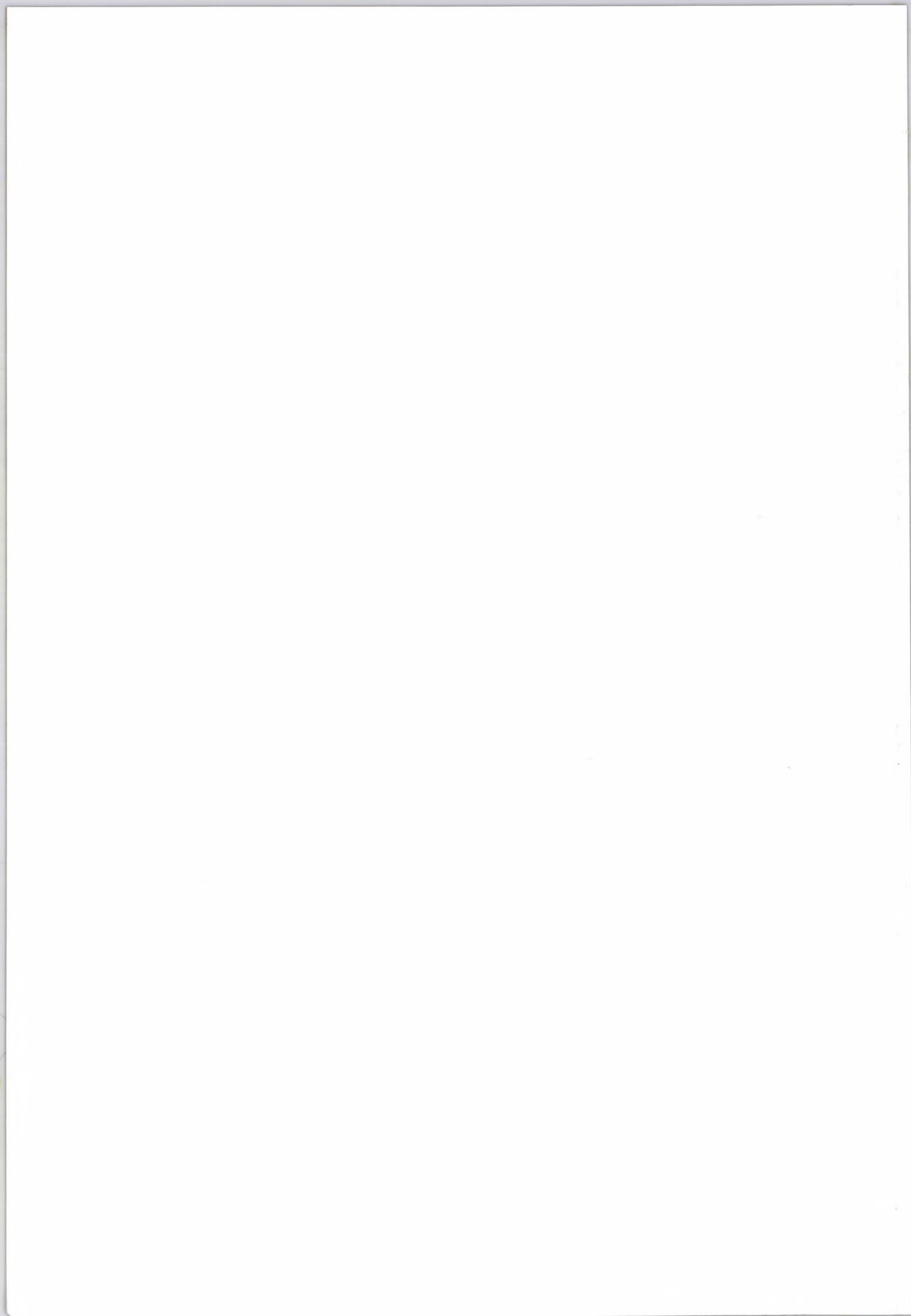# ATOMKI
ANNUAL REPORT
2007

INSTITUTE OF NUCLEAR RESEARCH
OF THE HUNGARIAN ACADEMY OF SCIENCES
DEBRECEN, HUNGARY

INSTITUTE OF NUCLEAR RESEARCH
OF THE HUNGARIAN ACADEMY OF SCIENCES
DEBRECEN, HUNGARY

ANNUAL REPORT
2007

ATOMKI

Preface

This Annual Report has an unusual feature, which is meant to be a constant ingredient of Annual Reports of Atomki in the years to come. From now on, we will have a review on the activity in one of the main research fields of the Institute in each number. The report, included in the present volume covers the activity of the Cyclotron Section. The cyclotron is the largest facility of the Institute, and the Cyclotron Section is responsible for running it and for its use in applied fields.

From among the notable results of the year I mention the following:

We invented a new treatment of the boundary condition for quantum scattering theory. The method is based on a transformation of rotating all physical coordinates into the complex plane. With such a rotation, the outgoing waves can be made square-integrable, which renders this technique useful for the description of resonance states. Now, however, we managed to extend the method to problems that contain both incoming and outgoing waves, i.e., to scattering problems.

In cooperation with a Catania group, the p+p elastic nuclear cross section has been determined under the Coulomb barrier (at 0.1–0.5 MeV) by measuring the cross section of the D(p,pp)n process at a few MeV at the cyclotron. The significance of the indirect method used ('Trojan horse method') is that under the Coulomb barrier the Coulomb effects are overwhelming, while at the energy of this experiment it is negligible. Inside the Trojan horse (i.e., the projectile) the high-energy proton can be carried into the heart of Troy (i.e., the neighbourhood of the other proton) to interact there at very low energy.

We found a two-electron 'cusp' in the collision of two neutral He atoms, which has been a unique observation hitherto. The departure of the two electrons leaves both atoms singly ionized, and the cusp event corresponds to both electrons propagating with the speed of the projectile. Their relative velocity is approximately zero, so the event is in fact a threshold effect. It was observed by detecting the projectile residue as well as the two electrons in triple coincidence.

Filters have been made for medical applications by proton beam micromachining, i.e., by regularly piercing a plastic sheet by a proton beam and chemically etching the tracks.

Following the first volume in 2005, in 2007 Prof. Tibor Fényes published the second volume of his nuclear physics textbook in Hungarian. The subtitle of Volume II is Particles and Interactions. With this, his tremendous endeavour of books (Nuclear Structure in English and Nuclear Physics I–II in Hungarian) has been completed.

The 'honours list' is especially long this year. There were numerous outstanding results by young researchers. The Academy conferred Dr. Zoltán Elekes and Dr. Tamás Vértesi Young Scientists' Awards for their results in the fields of light exotic nuclei and of quantum entanglement, respectively. The Institute itself has issued similar awards to Dr. Gábor Somogyi and Mr. Iván Valastyán. Gábor has had seminal progress in second-order perturbative corrections to quantum chromodynamics, while Iván has produced a very handy software for Cardiotom, a gamma camera for rapid and reliable diagnostics of heart infarction developed for Karolinska Institute, Stockholm. There was also an international youth award conferred to an Atomki member. He is Dr. György Gyürky, his appraised results are in nuclear astrophysics and the award is that of the science academies of the Visegrád countries (Poland, the Czech Republic, Slovakia and Hungary). And I cannot help disclosing an even greater feat of Gyuri Gyürky although that will be the subject of the next Annual Report. He is one of the awardees of the ERC (European Research Council) Starting Grant scheme. The subject of his project is the experimental study of the astrophysical p-process in Debrecen.

And here come the awards received by members of the more mature generation. One of the prizes of the Physics Section of the Academy of Sciences went to Prof. Attila Krasznahorkay for his works on nuclear spectroscopy. The reputable Wigner Prize was awarded to Prof. József Cseh for his works

i

on symmetries in nuclei. To appreciate this, one should know that the money involved in the Wigner Prize is covered by the Paks Nuclear Power Plant. They regard Wigner as a reactor engineer, and the Wigner Prize is usually given to specialists whose work has contributed to the application of nuclear energy. This time one of the candidates was the founder of the Paks Power Plant. The point of the jury was, however, that Wigner was primarily a pioneer of symmetry principles of physics, especially nuclear physics, which is shown by the fact that he was awarded the Nobel Prize for those achievements. Jóska Cseh is the main follower of the Wigner tradition of symmetry considerations in Hungary. This point was honoured by the donators, and the pioneering role of the founder of the Power Station was appreciated by the jury, and thus two full Wigner Prizes were awarded last year.

Prof. Dénes Berényi, who was the Director of this Institute between 1976 and 1990, was conferred an Honorary Degree by the University of Oradea. Oradea (Nagyvárad) is about 35 miles from Debrecen across the Romanian border. Prof. Berényi has been working, with missionary zeal, for bringing together the academic communities of the cross-border region surrounding Debrecen. For about a decade he was responsible for developing close links between the Hungarian Academy of Sciences and the academic circles of the Hungarian minorities over the border, which was an important job after 45 years of cessation during communism. In this position he also layed great emphasis on improving relations with academic institutions in which the majority and minority coexist. That is how he has earned this honour.

Last spring Prof. József Pálinkás MP, former Director of Atomki and present Head of the Physics Department of the University, was elected President of the Centre of Arts, Humanities and Sciences and Vice-Rector of the University. To feature the weight of this Centre within the University, we should mention that it contains 7 of the 15 faculties of the University (the Faculties of Humanities, of Science, of Law, of Economics and Business Administration, of Informatics, of Education and of Music) and 12 of the 20 graduate schools. Thus Prof. Pálinkás is now responsible for running a large portion of the higher education at Debrecen University.

Unlike society by and large, the science community in Hungary is highly meritocratic. That is why membership in the Academy has a tremendous prestige. Last year Prof. Zoltán Trócsányi was elected a corresponding member. He is one of the youngest members of this learned society. He is an expert in perturbative quantum chromodynamics. He teaches at the University of Debrecen, where he usually wins the yearly athletic and swimming competitions of professors, and attracts the most talented students (cf. the award of Somogyi above) to this Institute, where his research work is concentrated.

In boasting of the successes of our colleagues, I should not forget to remember a great loss suffered last year. On 11th October Dr. Éva Csongor, one of the favourites of our professors, a pioneer of environmental physics in Debrecen, and wife of the founding Director, Prof. A. Szalay, died in Budapest after a long disease. She had been teaching the introductory physics course to generations of Debrecen physics students. She had measured the most complete set of radioactivity data of precipitation in the world from the early atomic bomb tests to the Chernobyl disaster. She created the radiocarbon laboratory of the Institute, the only one in Hungary for the time being.

Her most notable pupil was Ede Hertelendi, the impulsive and reckless hero of the history of this Institute, former head of the Section of Environmental Physics, who died in a car accident in 1999.

Well, on 26th October, we inaugurated the new Hertelendi Laboratory for Environmental Studies. The 'new' laboratory is a beautifully re-built re-furbished and re-equipped version of our old laboratory for environmental studies. The reconstruction was financed by the Isotoptech Company, owned largely and managed by one of Ede's pupils, Mr. Mihály Veres. We have been uniting our efforts with Isotoptech in providing measurement services in mass spectrometry and radiocarbon analysis to nuclear industry, to water works, to archaeological museums etc. Now the new laboratory is run jointly. The portrait relief of Ede Hertelendi shown has been put at the entrance to the main premises of the Laboratory.

The central subject of the Physics Days, the annual festivity held in March for the general public,
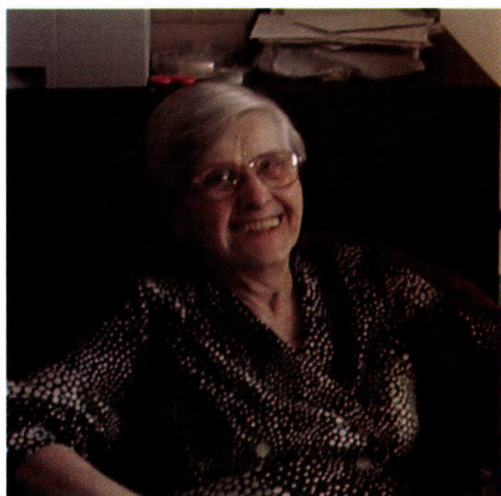
Dr. Éva Csongor (1922–2007)
on her last visit to Atomki,
on 28 August, 2003
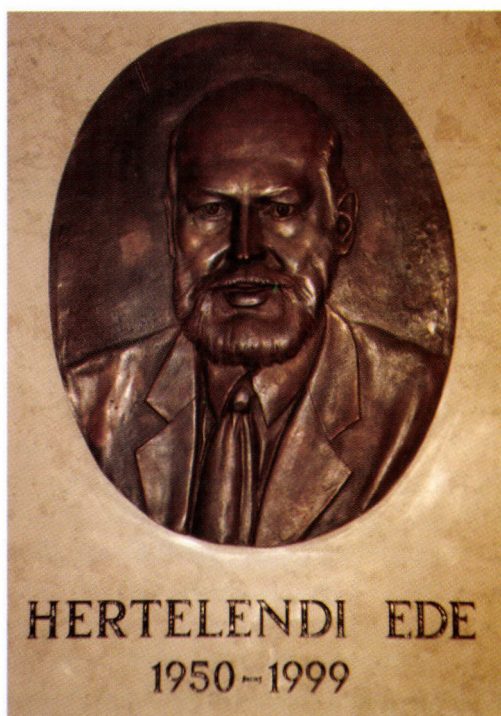
Dr. Ede Hertelendi sculpted by László Aszalós
at the entrance to the Hertelendi Laboratory
for Environmental Studies

was Modelling in Physics. The lectures were the following: 'From measurements to empirical laws' by Dr. K. Tőkési (Atomki), 'A physicist's visit to the zoo' by Dr. Zs. Fülöp

(Atomki), 'The most beautiful models in physics' by Prof. J. Pálinkás (University of Debrecen and Atomki) and 'A simple model for the growth of civilizations' (Prof. T. S. Bíró (Research Institute for Particle and Nuclear Physics, Budapest). On the last afternoon there was a quiz of secondary-school teams to test their knowledge on nuclear energy. This was organized by Dr. I. Uray on the occasion of the debut (http://www.atomki.hu/nupex/) of the Hungarian version of the European nuclear physics website for the general public NUPEX (Nuclear Physics Experience, http://www.nupecc.org/NUPEX/index.htm). While the talks were mostly very enjoyable, the childrens' quiz was very instructive to the organizers. It showed how superficial is the knowledge of the youth educated according to the recipes of the information society.

In May the Hungarian community interested in nuclear energy celebrated the silver jubilee of the International Atomic Energy Agency. IAEA did help us a lot in the early period to develop our research and development infrastucture and our expertise. For example, IAEA contributed to the price of the cyclotron and of the instruments around it by substantial amounts. It also granted scholarships to the science and technical personnel. The staff of Atomki have been acting as IAEA experts in many different countries, and we produced experimental machinery and software ordered by IAEA. IAEA is supporting nuclear data measurements, compilatory work and methodological research here. More details can be found on this in the review by the Cyclotron Section.

We celebrated the Day of Hungarian Science in autumn by a mini-symposium entitled 'Approaching Creation' reviewed the Debrecen contribution to the Compact Muon Solenoid (CMS) detector system we installed at the Large Hadron Collider at CERN (http://www.atomki.hu/CMS-program.pdf).

There were two international symposia held in Atomki. One was to mark the 70th birthday of Dr. Endre Somorjai

(http://www.atomki.hu/somorjai70-program.html), the person, who started research on nuclear astrophysics in Debrecen. Hungarian Civil Service Law has compelled him to retire now, but he is still working with us as a *professor emeritus instituti*, and is still a permanent player of hobby football on the grounds of the Institute.

The other international meeting was the 3rd Japan–Hungary Joint Seminar on Physics in Modern Science and Technology, whose subject was now Progress in Science and Technology with Particle and Photon Beams (http://www.atomki.hu/3.jp-hu/index.html). Parts of this meeting were held at the University of Szeged and at the Research Institute for Particle and Nuclear Physics, Budapest. The Japan–Hungary joint symposia have always been tremendously enjoyable and have been a source of optimism for us. This time we have found out that in detection techniques we are facing problems that are very similar to some problems of the neutrino physicists at RCNP, Osaka, and elsewhere in Japan. To solve these problems with joint efforts, we concluded a cooperation agreement.

Debrecen has become a candidate for hosting the European Spallation Neutron Source (ESS). The ESS project involves an enormous scientific and technological potential for Debrecen as well as for the country. Atomki made its contribution to raising public awareness of all these by holding a mini-symposium (http://www.atomki.hu/ESS/) on the possible use of a neutron source. The speakers included the main promoters of the Hungarian ESS proposal (Prof. F. Mezei, Dr. L. Rosta), the Mayor of Debrecen (Mr. L. Kósa) and some of the leading figures of the University (Prof. J. Pálinkás, Vice-Rector Z. Szilvássy, Prof. Gy. Bazsa) and of Atomki (Dr. A. Fenyvesi).

To conclude this Preface, I have to disclose that this is my last preface to the annual reports. My impression is that writing these prefaces would become a mere routine if I were to write them on and on, and it would be a shame if the reader noticed that I did not put my heart into them. That is why I wanted to stop now. When I made my last application for the directorship, I confided that I would take up this job just up to the end of last year, yet, eventually, I was appointed for the period ending in 2009. After my repeated reminders, the bosses of the Academy realized that I was serious, and provided for a selection procedure to find my successor. I am glad to announce that the procedure started with an international call for application concluded in appointing Dr. Zsolt Fülöp, Deputy Director in 2007, who would also have been my choice. Zsolt is 44 years old, which is a best age to become a boss. Perhaps he can still enjoy it. He is head of the experimental nuclear astrophysics group, a pupil of Prof. Somorjai. He is extremely active, and is not deterred by facing problems, which is shown by the fact that he has 5 (five) children of ages 6 to 16, and he and the family are coping with each other. I am gradually withdrawing from the matters of the Institute, and hope to become a scientist again.

Looking back to the eleven years of my directorship I see a solid tendency of higher and higher performance by the Institute, albeit the fields and forms of the progress have been varied. I feel this tendency prevails even in the more recent years, despite the deteriorating conditions. After the communist times I felt relief from the obligation of finding excuses for doing research. The view that scientific research represents a value by itself was generally accepted at the time when I started my job as director. Now, I think, this opinion would count as politically incorrect. Media imprint on innate naivety and multilateral European misunderstanding have now created a disinformation society in this country (or on the whole continent?), in which all values are shaken, and many people have lost their senses. Our duty in this environment is to show that science still remains one of the cornerstones of society, and scientific research can best benefit society if it is allowed to follow its own instincts.

The financial and personnel conditions in 2007 are given in the pie charts to follow this Preface. This Report, prepared in LaTeX, is available on the web at www.atomki.hu in PDF format.

Debrecen, 15 April 2008

Rezső G. Lovas
former Director

Organizational structure of ATOMKI

Director:	R.G. Lovas, corresponding member of the HAS
Deputy directors:	Zs. Fülöp, D.Sc.
	S. Mészáros, C.Sc.
Finance director:	Dr. M. Pálinkás

- Secretariat (Scientific Secretary: Z. Máté, C.Sc.)
- Library (Librarian: Mrs. M. Nagy)
- Accounting (Head: Mrs. J. Sass)
- Basic Services and Maintenance (Head: Mr. I. Katona)
- Mechanical Workshop (Head: Mr. I. Gál)

Scientific Sections

Division of Nuclear Physics (Head: J. Cseh, D.Sc.)

- Section of Experimental Nuclear Physics (Head: A. Krasznahorkay, D.Sc.)
- Section of Electrostatic Accelerators (Head: I. Rajta, Ph.D.)
    - Nuclear Astrophysics Group
    - Ion Beam Analysis Group
- Section of Theoretical Physics (Head: A. Kruppa, D.Sc.)

Division of Atomic Physics (Head: Á. Kövér, D.Sc.)

- Section of Atomic Collisions (Head: B. Sulik, D.Sc.)
- Section of Electron Spectroscopy (Head: L. Kövér, Ph.D.)

- Section of Environmental and Earth Sciences (Head: Á.Z. Kiss, D.Sc.)
    - Laboratory of Environmental Studies
    - Radon Group
    - K-Ar Laboratory
    - Radiation- and Environmental Protection Group
    - QMS Laboratory
- DE TTK - ATOMKI Department of Environmental Physics (Head: S. Sudár, C.Sc.)
- Cyclotron Section (Head: F. Tárkányi, C.Sc.)
- Section of Electronics (Head: J. Gál, C.Sc.)

Data on ATOMKI

At present the Institute employs 197 persons. The affiliation of personnel to units of organization and the composition of personnel are given below.
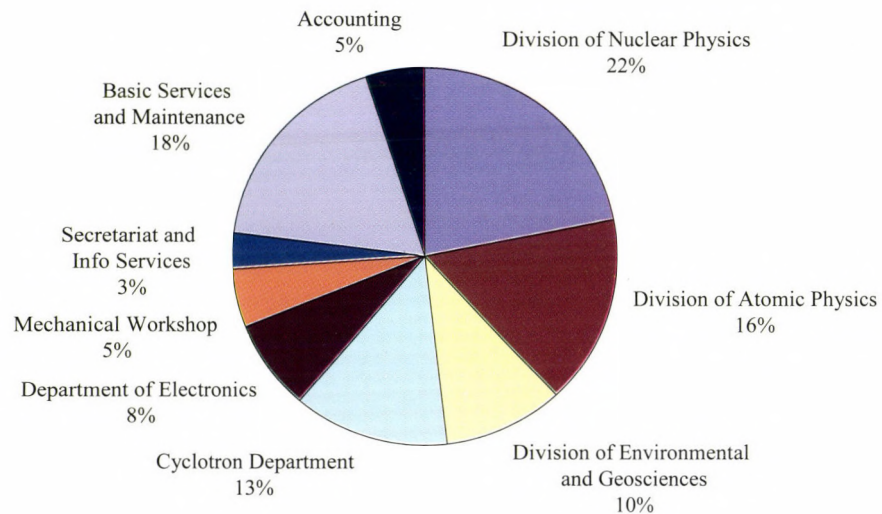

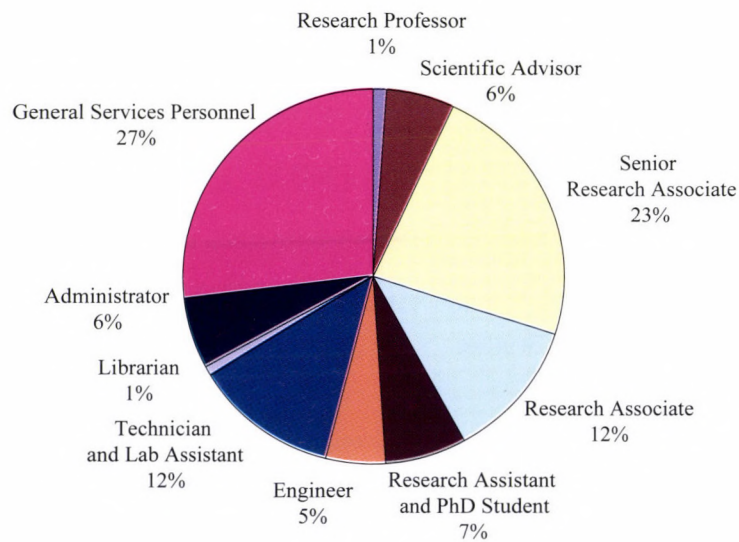**Figure 1.** Affiliation of personnel to units of organization

Figure 2. Composition of personnel

Finance

The total budget of the Institute for the year 2007 was 1299 million Hungarian Forints. The composition of the budget and the share of personnel expenditure within the budget are shown below.
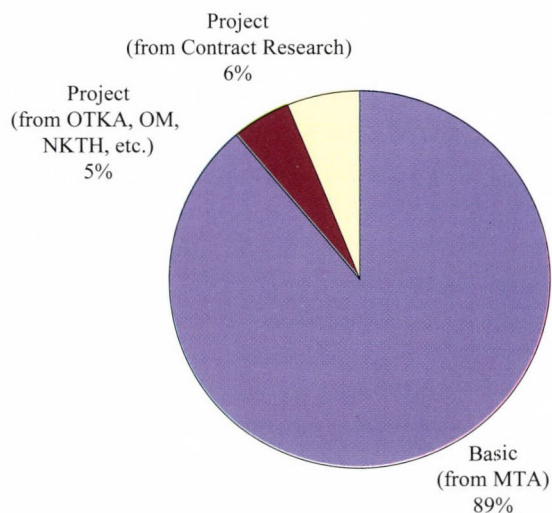

Figure 3. Composition of the budget of the Institute
MTA: Hungarian Academy of Sciences
OTKA: Hungarian Scientific Research Fund
OM: Ministry of Education
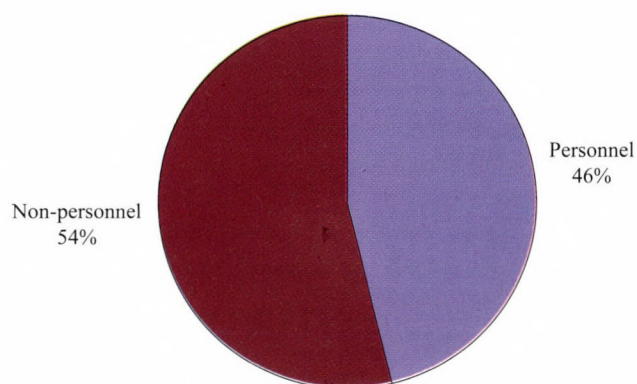*NKTH: National Office for Research and Technology*

Figure 4. Breakdown of expenditure into personnel and non-personnel expenditures

Table of contents

Featured Laboratory: Cyclotron
Status report on the operation of the cyclotron and on the programs of its practical applications   1

1. General Physics

2. Sub Atomic Physics

3. Atomic and Molecular Physics

8. Developments of Methods and Instruments

9. Publications and Seminars

Status report on the operation of the cyclotron and on the programs of its practical applications

F. Tárkányi, I. Ander, L. Andó, F. Ditrói, A. Fenyvesi, B. Király, Z. Kormány, P. Kovács, Z. Kovács, I. Mahunka, É. Pribóczki, F. Szelecsényi, I. Szűcs, Z. Szűcs, S. Takács

1. Main tasks

The main task of the Cyclotron Department is to operate the ATOMKI MGC-20E cyclotron, to support the research in different scientific fields and to use the accelerator in practice related applications. The Cyclotron Laboratory has been installed in a research institute so research is the most important task. Considering that some results of the basic research can be used in different routine applications, the second important task is to help developing systems for this reason. The capacity of the accelerator usually allows making routine applications to ensure the financial background for the service and for the development of the cyclotron.

The cyclotron is applied directly for basic nuclear physics research and it indirectly helps the research in other fields via interdisciplinary studies. It is used in broad scale for different practical applications which have direct results in basic sciences in many cases therefore the classification sometimes is not simple. The irradiations at the cyclotron are dedicated to basic research in the field of nuclear structure and nuclear reaction studies and from other side to the so-called practical applications.

The cyclotron has been in operation in ATOMKI since 1985. Since then the cyclotron has been reliably running with very short undesired breakdowns and it has been used for a wide range of research and application programs. This overview gives a short summary of the status of cyclotron operation and the practical applications and gives some indications on the future plans.

2. Cyclotron operation

The MGC-20E cyclotron of ATOMKI has been the major particle accelerator facility in Hungary since it started operation in 1985. It is a variable energy compact machine which can accelerate particle beams from proton to alpha. For about two decades it was the only cyclotron type accelerator in the country and was used for various research and application programs. In recent years two new dedicated PET-isotope cyclotrons were put into operation (in Budapest and Debrecen) with comparable proton and deuteron final beam energies. Although these new machines are superior in beam intensity and economics of operation, the MGC-20E cyclotron is still the most flexible accelerator facility for research and non-routine application tasks in Hungary. Its sophisticated external beam transport system with advanced beam diagnostics and instrumentation, combined with the broad range of variable beam parameters makes it a unique tool for numerous programs.

The cyclotron operation group has been putting great efforts into new developments and upgrade of various subsystems of the machine in order to increase both reliability and economics of the operation and to extend the lifetime of the facility. Two major reconstruction projects were successfully implemented during the last decade. First the obsolete vacuum and control systems of the cyclotron and beam transport lines were replaced by up-to-date hardware and software components. This project was financially supported by the International Atomic Energy Agency and the design and implementation process was carried out fully in-house by the cyclotron operation group. The radiofrequency system of the cyclotron was later upgraded by the manufacturer of the machine in a project supported by the Hungarian Academy of Sciences. The RF-system was completely redesigned and rebuilt with widely and long-term available components, providing maintainable operation for many years to come.

Table 1. Statistics of cyclotron operation during the last decade

Year	Operation	Maintenance		Breakdown		Availability		Beam tuning		Beam on target	
	(h)	(h)	(%)	(h)	(%)	(h)	(%)	(h)	(%)	(h)	(%)
2007	2951	343	11.6	43	1.5	2565	86.9	172	5.8	1061	36.0
2006	3445	441	12.8	62	1.8	2942	85.4	181	5.3	1690	49.0
2005	3302	418	12.7	42	1.3	2842	86.0	192	5.8	1353	41.0
2004	3554	450	12.6	70	2	3034	85.4	213	6.0	1086	30.6
2003	4051	365	9.0	4	0.1	3682	90.9	250	6.2	1973	48.7
2002	4084	449	11.0	15	0.4	3620	88.6	279	6.8	1791	43.9
2001	4300	483	11.2	66	1.5	3751	87.3	272	6.3	1803	42
2000	4227	412	9.5	22	0.5	3793	90	480	11	1685	40
1999	4265	301	7	76	2	3888	91	546	13	1792	42
1998	4096	752	18	49	1	3295	81	420	10	1520	37
1997	3946	450	11	87	2	3409	87	588	15	1168	30

Table 2. Statistics of cyclotron utilization

Beam on target (h)	1997	1998	1999	2000	2001	2002	2003	2004	2005	2006	2007	Total
Nuclear spectroscopy	314	214	190	590	138	663	568	269	378	359	151	**3834**
Nuclear astrophysics	161	371	813	290	923	496	613	176	489	630	465	**5427**
Radiation tolerance test	114	148	191	72	147	106	50	79	34	142	214	**1297**
Nuclear data	25	53	42	136	29	16	9	157	95	152		**714**
Neutron physics		52	11		13	23						**99**
Medical isotope production	554	655	545	597	553	434	617	280	260	194	96	**4785**
Thin layer activation						56	116	125	97	105	50	**549**
Target technology										108	85	**193**

The cyclotron operation group has been involved in various beam diagnostics and instrumentation projects as well. In collaboration with iThemba LABS in South Africa we have been participating in research and development of different non-destructive beam diagnostics systems for cyclotrons and their beam lines, like beam position monitors (BPM) and beam intensity measuring equipments. The application of the Experimental Physics and Industrial Control System (EPICS) for the existing diagnostics systems is also studied.
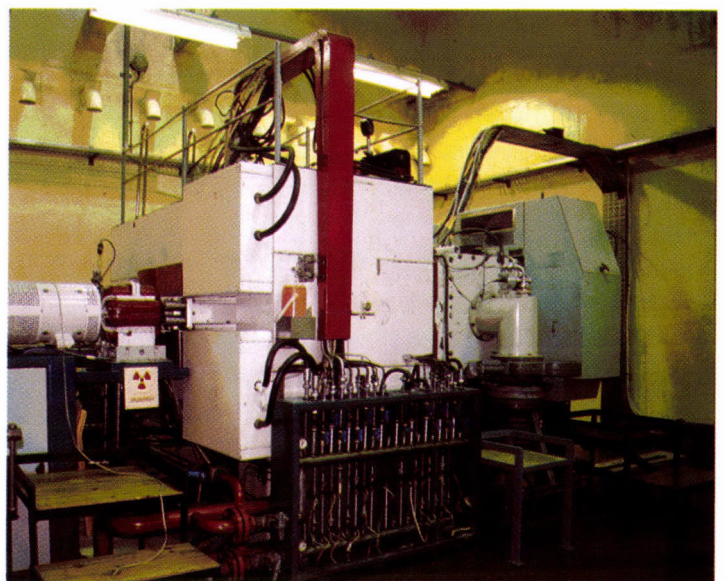
Figure 1. MGC-20E cyclotron of ATOMKI

The expertise of the staff is used in numerous projects managed by various user groups. We provide regular help in the design and construction of mechanics and electronics for new experimental arrangements, like different setups for thin layer activation or development of a pneumatic post system for irradiated target samples.

Main beam parameters

Particle beam	Energy (MeV)	Intensity (µA)		Energy spread of extracted beam	$< 3 \times 10^{-3}$
Proton	2.5 – 18	40		Energy spread of analyzed beam	$< 10^{-3}$
Deuteron	1 – 10	40		Power consumption	200 kW
^{3}He	4 – 26	10		External target locations	9 horizontal,
Alpha	2 – 20	20			1 vertical

Milestones in the cyclotron operation

1980-83	Design and purchase (supported by IAEA)
1984-85	Installation and commissioning
Nov. 1985	Start of operation
1997-99	Reconstruction project (supported by IAEA
	Technical Co-operation Project HUN/4/013)
2003	Renewal of the RF-system of the cyclotron
	(supported by the Hungarian Academy of Sciences)

3. Practical applications

The field of practical applications is very broad and has been flexibly changed in accordance with the continuously varied circumstances. There were some fix factors like cyclotron parameters, in some meaning the traditions, but most of the determining factors were changed continuously like experience, collaborations, technology changes, economic situations and requirements. All practical applications are based on three results of interactions of charged particles with the matter: production of useful radioisotopes, production of fast neutron beam and making radiation damage in irradiated samples.
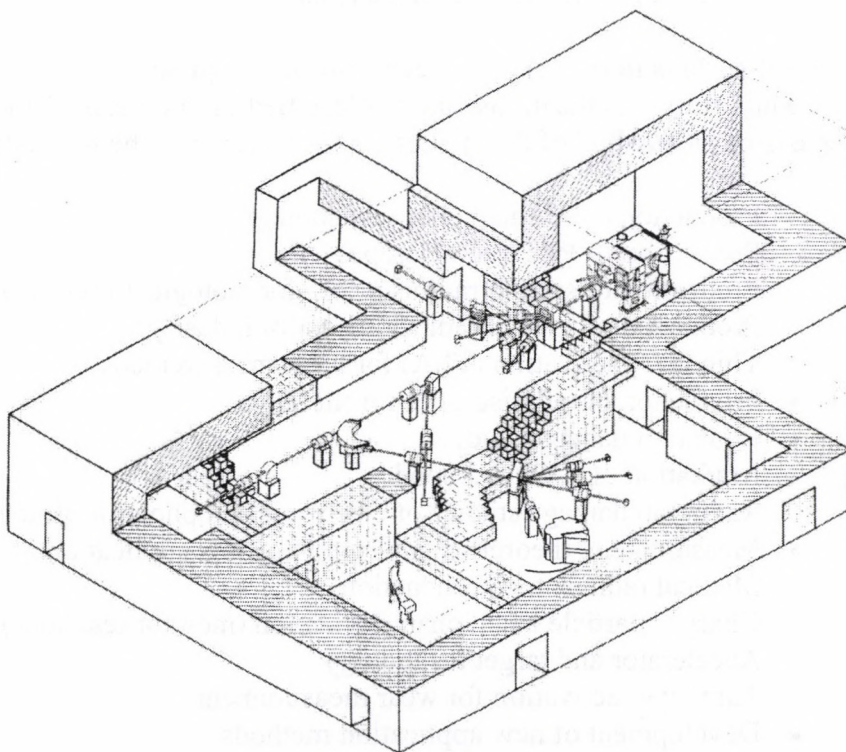
Figure 2. Layout of the protected area

Milestones in the practical applications

1986	Start of SPECT-isotope production
1987	Start of bio-medical and agro-biological applications with fast neutrons
1992	Start of radiation damage studies
1994	Start of PET-isotope production
2002	Start of Thin Layer Activation program for wear studies
2005	Start of CVD diamond irradiations

3.1 Technical background for applications

Five well equipped beam lines/target stations were built for practical applications: two beam lines for radioisotope production, high intensity fast neutron source, TLA beam line and quasi-monoenergetic neutron source. To support proper handling, separation, labeling processes and investigation of patients an analytical and target preparation laboratory, a radiochemical laboratory and a medical unit (including a PET scanner) are available.

3.2 Applications in the past

During the long operation period many applications were stopped due to the less optimal conditions of the cyclotron beam parameters:

- Production of long-lived SPECT radionuclei (^{67}Ga, ^{111}In etc.)
- Production of microfilters via fission products
- Experiments related to neutron therapy
- Irradiations for induction of genetic mutations for breeding purposes
- Charged particle activation analysis

3.3 Applications in the last few years and in the present

The present applications can be classified on the basis of the field of final application or on the basis of the method of the application. According to the methods:

- Production of radioisotopes for labeling
  Production of PET-radioisotopes
  Production of special radioisotopes for biological investigation
  Production of special radioisotopes for industry
  Thin layer activation (TLA) for wear measurement
- Production of radioisotopes for therapy
- Radiation damage studies
  Irradiation of CVD diamond
  Radiation damage studies of electronic and photonic structures, components and devices
- Measurement, theoretical interpretation and application of nuclear reaction data
  Medical radioisotope production
  Charged particle beam characterization (monitor reactions)
  Accelerator and target technology
  Thin layer activation for wear measurement
- Development of new application methods
  New isotope production methods
  New labeling methods
  New data measuring methods
  New data application methods

4
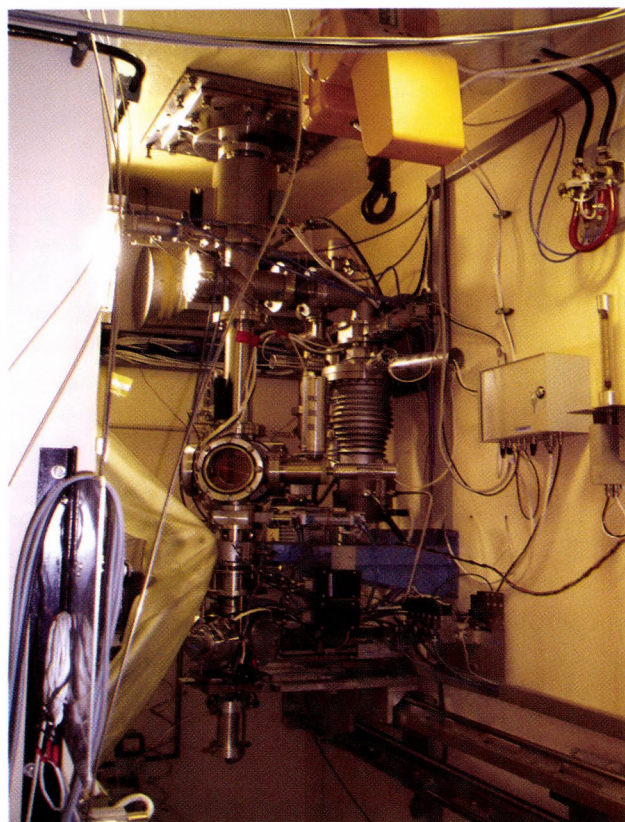
Figure 3. Vertical beam-line for solid, liquid and gas targets
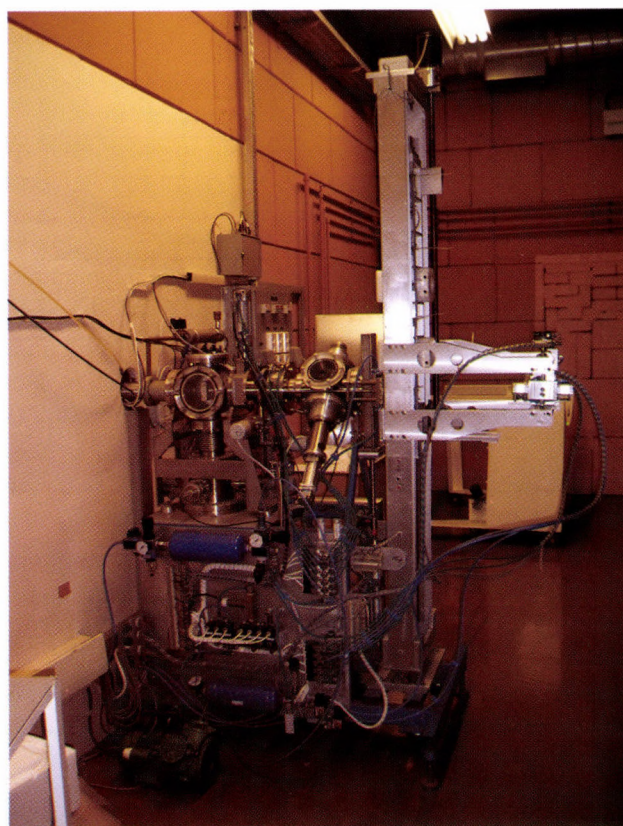
Figure 4. Horizontal beam-line for multipurpose use

4. Production of radioisotopes for labeling

The aim of the application is to follow different biological and industrial processes by detecting radiations of the radioactive decay of inserted radioactive probes or labeled compounds. There are two different methods according to labeling. In the first case the indicator radioactive isotopes are produced separately on a proper target and used for labeling after chemical separation. In the second case the radioactive isotope is directly produced in the sample participating in the investigated process.

4.1 Off-line labeling of biological and industrial processes

There are two high intensity beam lines with special target stations for production of radioisotopes in high yield. The vertical beam line at the ATOMKI cyclotron is a unique station in Europe used routinely in medical isotope production (see Fig 3). The remote controlled vertical beam line is equipped with an automatic target changer for 4 different solid, gas or liquid targets.
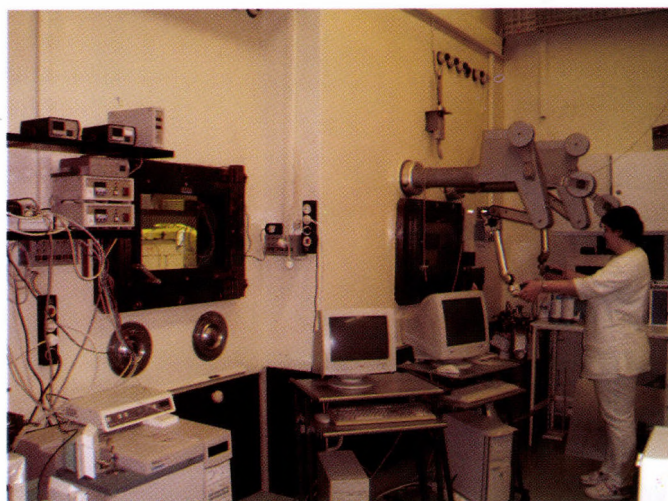
Figure 5. Hot cells with lead-glass windows and manipulators
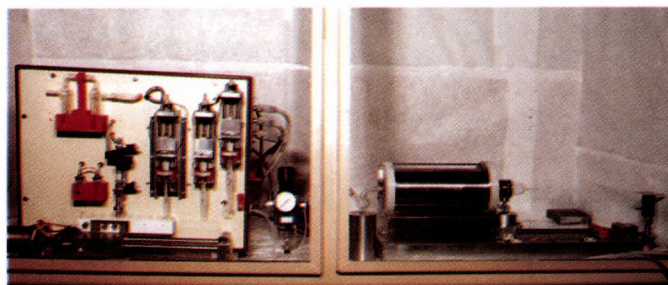
Figure 6. ^{123}I production system
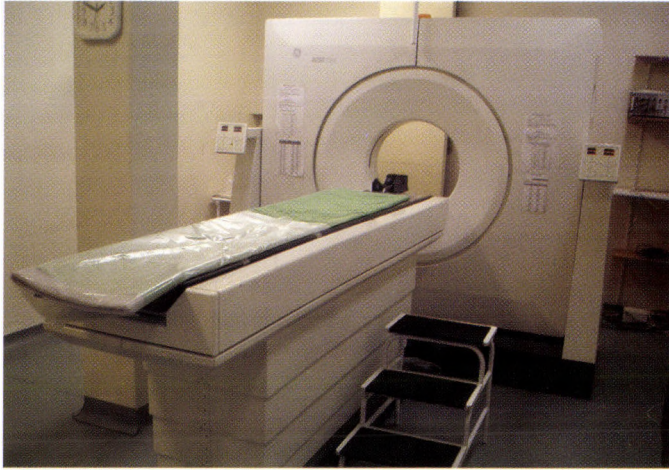
Figure 7. The first PET scanner in Hungary

For medical diagnostic purposes using Positron Emission Tomography the following radioisotopes/labeled compounds have been produced:

- [^{11}C]methionine
- [^{15}O]buthanol, [^{15}O]H$_2$O
- [^{18}F]dezoxy-D-glucose
- [^{124}I] fatty acids, [^{124}I] hyppurate
- ^{76}Br-labelled oligonucleotid

For biological investigations in collaboration with universities the following special radioisotopes were produced:

- ^{24}Na
- ^{43}K
- Rb mixture
- ^{62,65}Zn
- ^{203}Pb

For tracing industrial processes the following special radioisotopes were produced:

- ^{56}Co to test reactor cooling system
- ^{48}V to test oil pipe-lines

For wear studies using implanted radioactivity ^{7}Be was produced in large quantity.

Figure 8. Tracing the sap-flow of plants with radioisotopes in field experiments

4.2 On-line labeling

Main field of the use of the on-line radioisotope labeling method is the Thin Layer Activation (TLA) method where we produce proper radioisotope usually directly in a very thin layer of the investigated sample subject to wear, corrosion or erosion process. At the ATOMKI cyclotron extensive irradiations have been performed for wear studies of

- Engine parts
- Railway wheels
- Machine parts
- Art materials
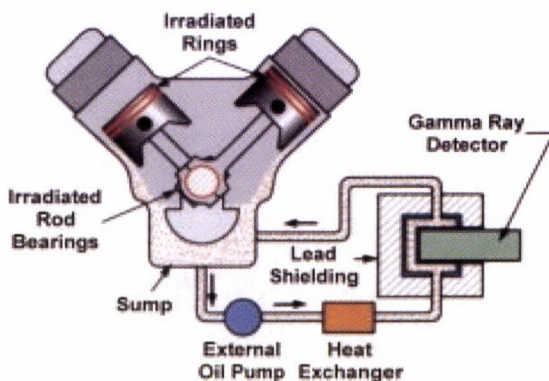
Figure 9. Basic principle of wear measurement
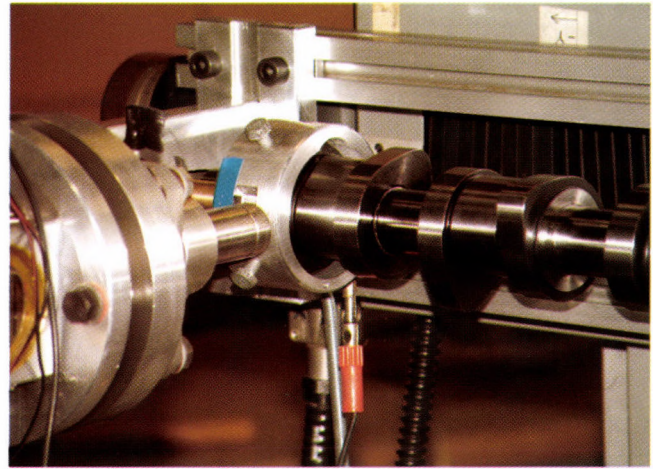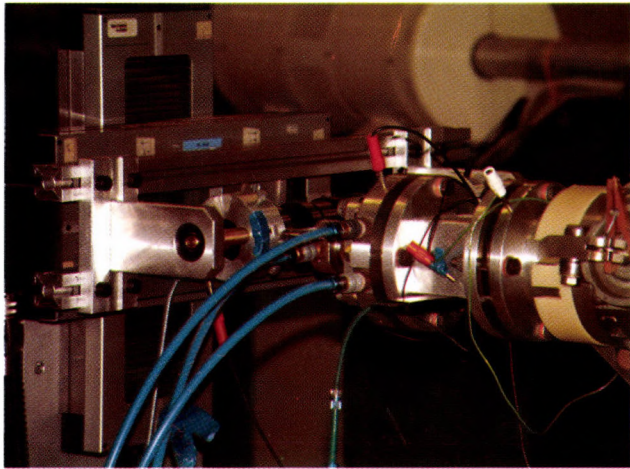
Figure 10 a-b. Thin layer activation irradiation of camshaft

5. Research and applications with fast neutrons

Two beam lines are available for irradiations with fast neutrons. At the high intensity irradiation site a water and He-gas cooled beryllium target is used for producing p+Be and d+Be neutrons with broad spectra mainly for application purposes. The low intensity irradiation site is used for neutron physics research either with broad spectrum d+Be neutrons or with quasi-monoenergetic d+D neutrons produced using a D_2-gas target.

There has been a broad range of research and applications of the neutron sources within the frameworks of numerous collaborations with local groups of ATOMKI, other institutions in Debrecen and collaborators from Hungarian and international institutions.
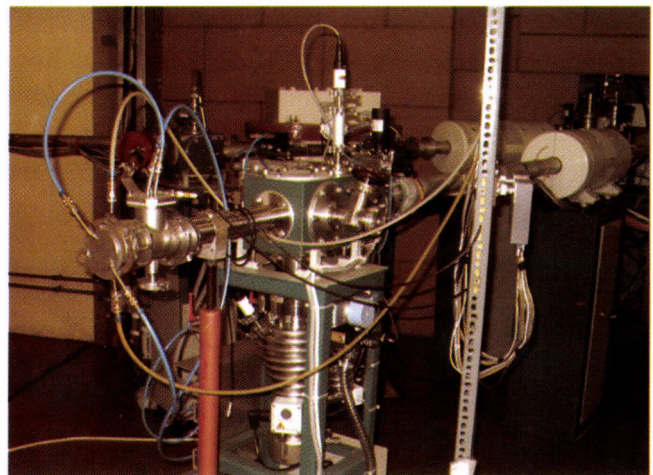
Figure 11. High intensity fast neutron source
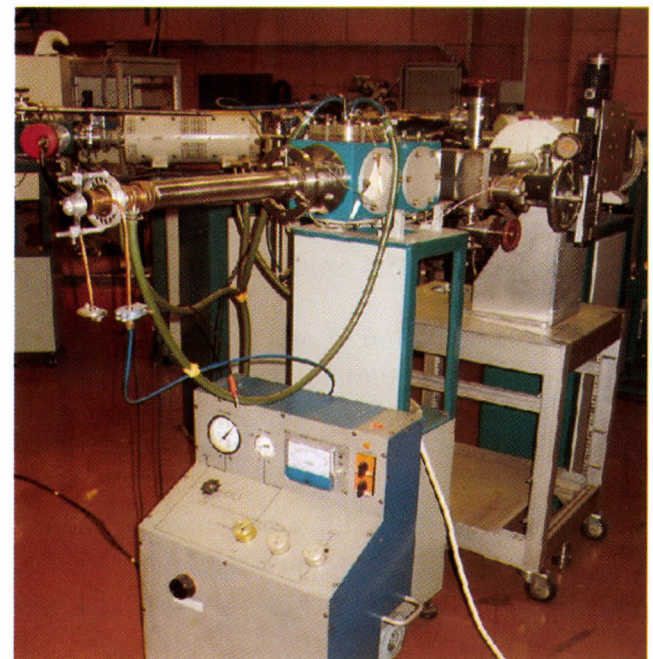
Figure 12. Low energy neutron irradiation site with D_2-gas target and its gas handling system

7

5.1 Neutron physics

- Cross section measurements
- Neutron transport studies
- Integral measurements for validation of evaluated excitation functions and cross section data libraries

New cross section data have been measured for the excitation function of several neutron induced nuclear reactions in the E_n = 6-11 MeV neutron energy range using quasi-monoenergetic neutrons.

A search for discrepancies of cross section data was also performed via integral testing methods. In the first method cross sections integrated for well known broad spectra of d+Be neutrons were measured and compared with data of evaluated libraries and/or results of theoretical calculations for the excitation functions. In the second method, at fast neutron sources (d+Be, d+D, d+T, Pu-Be) with well known spectra, transmission type benchmark neutron transport experiments have been done for bulk media of different shielding materials (graphite, aluminum, iron, lead, bismuth, water, polyethylene and sand). The measured spectra of neutrons (leakage spectra) were compared to results of Monte-Carlo simulations performed using cross section data of different versions of evaluated neutron data libraries (ENDF, JENDL, JEFF). Several discrepancies of cross section data have been found using the two types of integral testing method.

5.2 Bio-medical applications

- Physical dosimetry of mixed neutron-gamma fields
- Radiobiological research with human cells, bacteria and small animals related to fast neutron radiotherapy
- Study of the effects of radio-protector and hypoxic radio-sensitizer compounds in mixed neutron-gamma fields
- Study of the synergic effects of neutron irradiation and infections by bacteria
- Biological dosimetry

These studies provided important radiobiological information that can be used in planning and assessment of effects of fast neutron exposition of human individuals (e.g. fast neutron radiotherapy, radiation protection related issues at nuclear and high energy physics installations and space applications, military applications etc.).

5.3 Agro-biological applications

- Induction of mutations in seeds of hybrids and inbred lines (rice, soybean, wheat, corn, onion, tomato, pea, bean etc.) for breeding purposes
- Study of neutron and gamma photon induced electron traps in different media (milk powder, bones, teeth etc.)

As a major result a new maize gene bank has been available at the Center of Agricultural Sciences of Debrecen University with 1500 maize lines with broad genetic variability, resistance and adaptability. The great genetic variability can be exploited after strict assessment and selection. Up to now three of the lines have been released after investigation of the distinctness, uniformity and stability (often referred to as the "DUS criteria").

5.4 Radiation damage studies with fast neutrons

- Electronic and photonic devices: analogue ICs, memories, ASICs, light sources (LEDs and laser diodes), photo sensors (PM-tubes, a-Si Shottky sensors, p-i-n sensors, CCDs, CMOS active pixel sensors), optical materials (glues, glasses), optical fibers, opto-couplers
- Thin layer structures: $Si-SiO_2$, amorphous Si, SiC, CVD diamonds
- Detectors: silicon diodes, silicon microstrip detectors, parallel plate ionization chambers
- Systems: tiltmeters

5.5 Fast Neutron Activation Analysis (FNAA)

- Materials used for packaging integrated circuits
- ICs produced by flip-chip bond technologies
- Activation of multi-chip modules
- Estimation of the effects of neutron activation on device characteristics of ICs
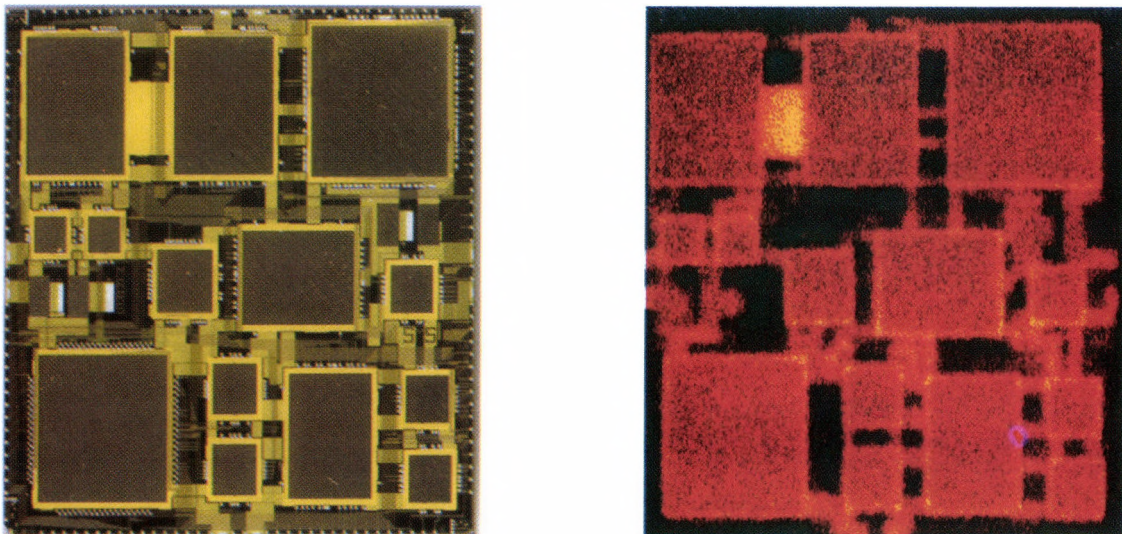
Figure 13. Optical image of a multi-chip module (left) and its autoradiogram after neutron irradiation (right) showing "hot spots" of activation

The aim of the radiation damage and FNAA studies is the development of radiation tolerant components, devices and systems that can operate in radiation environments with neutron component (e.g. nuclear installations, high energy physics experiments, space, avionics and military applications). Most of the results have been used for the development of different sub-systems of the CMS, ATLAS and ALICE high energy physics experiments at the Large Hadron Collider at CERN (Geneva, Switzerland).

Results of the memory tests have been used for selecting the components of the on-board mass storage system of the SMART-1 satellite of the European Space Agency (ESA). SMART-1 spiraled its way to the Moon using solar-electric propulsion and carrying a battery of miniaturized instruments. Because of the small thrust of its ion propulsion engine the satellite was exposed by the harsh radiation environment of the van Allen belts of Earth for weeks during its long journey to the Moon.

6. Investigation of new application methods

Studies of basic processes and search for new or upgraded nuclear methods are required to improve and extend practical applications:

- Dynamic effects in gas targets
- High intensity targets
- TLA with shifted energy primary beam
- Thick target yield measurement by using thin targets
- Nuclear data for TLA
- New radiopharmaceuticals
- New methods of chemical synthesis
- Investigation of new production routes for medical radioisotopes

In connection with development and standardization of new application methods the Cyclotron Department participated in a few IAEA Coordinated Research Projects:

- Thin layer activation for wear measurement
  CRP 1992-1996
  IAEA TECDOC-924
- Standardized high intensity solid targets for cyclotrons
  CRP 2000-2003
  IAEA Technical Report 432
- Improved high intensity gas and liquid targets for cyclotrons
  CRP (in progress)
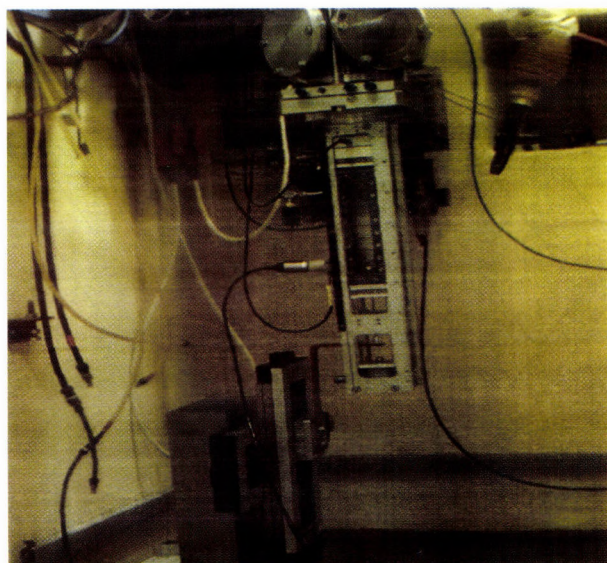
Figure 14. Investigation of static and dynamic effects in interaction of charged particle beam with gas targets
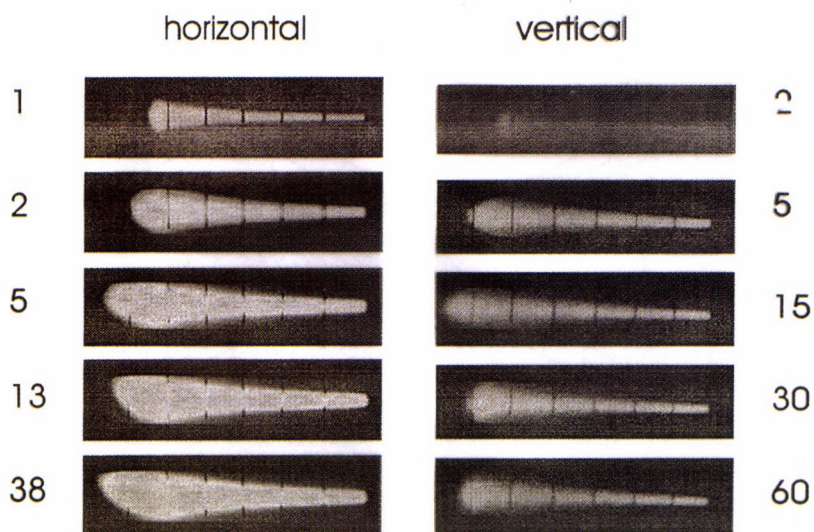
Figure 15. Frames of recorded light emitted by the gas target during bombardment with horizontal and vertical beam for demonstration of the changes of the beam volume in time

7. Investigation of nuclear reaction data for non-energy related applications

Charged particle accelerators are used in broad fields of basic research and in different applications. By using a charged particle accelerator we activate the dedicated target intentionally and simultaneously in a byprocess the accelerator itself, the target system, the beam line devices and the beam shaping devices.

The knowledge of the amount of the produced radioisotopes and/or the primer and secondary radiation is very important for the construction, for the operation and for the dedicated applications. The precise nuclear data help in the optimization of all kind of irradiation. Among the experimental nuclear data the decay data can be measured with fewer uncertainties than the reaction cross sections. The predictivity of the recently used theoretical model codes is not satisfactory in most of the applications.

Measurements of activation cross section data are very important both for the everyday practice and for the improvement of the nuclear reaction theory. We have performed a very extensive study on the application related charged particle induced cross section data practically since the installation of the cyclotron. As a result, our group in collaboration with foreign institutes became one of the most important charged particle data group in the field of low and medium energy reactions.

Our investigations are focused on the following fields:
- Measurement of new experimental data
- Theoretical interpretation of experimental data
- Compilation of the experimental data in standard EXFOR format
- Compilation and critical evaluation of literature data for production of recommended database
- Production of recommended databases for different applications

7.1 Measurement of new experimental data

We performed measurements for

- Production of medical SPECT radioisotopes
- Production of medical PET radioisotopes
- Production of radioisotopes used in internal radiotherapy
- Beam monitor reactions
- Activation data for accelerator based waste transmutation
- International Fusion Materials Irradiation Facility (IFMIF)
- Reactions used in thin layer activation
- Accelerator beam lines and target holding units

Table 3. Measurements of experimental data. In collaboration with foreign laboratories, excitation functions on 50 targets for about 1000 nuclear reactions have been measured

Target	Particle	Investigated reaction products	Medical	Biological, industrial tracer	Monitor	Accelerator technology	TLA
^{9}Be	^{3}He	^{7}Be					^{7}Be
^{nat}B	p, d	^{7}Be					^{7}Be
^{nat}C	^{3}He	^{7}Be					^{7}Be
^{14}N	p, d	^{11}C, ^{13}N, ^{14}O, ^{15}O	^{11}C, ^{13}N, ^{15}O				
^{18}O	p	^{18}F	^{18}F				
^{nat}Ne	p, d, ^{3}He, α	^{18}F, ^{22,24}Na	^{18}F				
^{27}Al	p, d, α	^{22,24}Na		^{22,24}Na	^{22,24}Na	+	^{22}Na
^{35}Cl	α	^{38}K	^{38}K				
^{38,40}Ar	p, ^{3}He, α	^{38}K, ^{43}K	^{38}K	^{43}K			
^{45}Sc	p	^{44,45m}Ti, ^{43,44m,44g}Sc	^{44}Sc			+	^{44m}Sc
^{nat}Ti	p, d, ^{3}He, α	^{48,49,51}Cr, ^{48}V, ^{43,44m,44g,47,48}Sc	^{51}Cr, ^{47}Sc	^{48}V	^{48}V, ^{51}Cr	+	^{48}V, ^{51}Cr, ^{47}Sc
^{nat}V	d	^{48,51}Cr, ^{48}V	^{51}Cr			+	^{51}Cr, ^{48}V
^{55}Mn	p, d	^{52}Fe, ^{52,54,56}Mn	^{52,54}Mn			+	^{54}Mn
^{nat}Fe	p, d, ^{3}He, α	^{56,57}Ni, ^{55,56,57,58,61}Co, ^{52}Fe, ^{52,54,56}Mn, ^{48,51}Cr, ^{48}V, ^{47}Sc	^{52,54}Mn, ^{51}Cr		^{56,57}Co	+	^{56,57}Co
^{59}Co	d, ^{3}He, α	^{60,61,62}Cu, ^{56,57,58,60}Co, ^{54,56}Mn	^{60,61,62}Cu	^{56}Co	^{56,57}Co	+	^{56,57,58}Co, ^{54}Mn
^{64}Ni	p, d, ^{3}He, α	^{62,63,65}Zn, ^{60,61,64,67}Cu, ^{56,57}Ni, ^{55,56,57,58,60,61}Co, ^{52,54,56}Mn, ^{48}V	^{60,61,64,67}Cu, ^{52,54}Mn		^{61}Cu	+	^{65}Zn, ^{56}Ni, ^{56,57,58,60}Co, ^{52,56}Mn, ^{48}V
^{nat}Cu	p, d, ^{3}He, α	^{66,67}Ga, ^{62,63,65}Zn, ^{64}Cu, ^{65}Ni, ^{56,58,60}Co, ^{59}Fe	^{66,67}Ga		^{56,58}Co, ^{62,63,65}Zn, ^{66,67}Ga	+	^{67}Ga, ^{65}Zn, ^{56,58,60}Co, ^{59}Fe
^{nat,66,67,68}Zn	p, d	^{66,67,68}Ga, ^{62,65,69m}Zn, ^{61,64,67}Cu, ^{57}Ni, ^{55,56,57,58,60}Co, ^{52,54}Mn	^{66,67,68}Ga, ^{61,64,67}Cu, ^{62}Zn (^{62}Cu)			+	^{67}Ga, ^{65}Zn, ^{67}Cu, ^{56,57,58,60}Co, ^{54}Mn
^{76,77,80}Se	p	^{75,76,77}Br	^{75,76,77}Br				
^{nat,78,82,83}Kr	p, d, ^{3}He, α	^{79,81,82m,83,84m,84g,86}Rb, ^{82,83,85m,85g,87m}Sr, ^{77,79}Kr, ^{75,76,77}Br	^{75,76,77}Br, ^{81}Rb (^{81}Kr), ^{82}Sr (^{82m}Rb)	^{83}Rb			
^{nat}Rb	p	^{82,83mg,85mg,87m}Sr, ^{81,82m,83,84mg,86mg}Rb	^{82}Sr (^{82m}Rb)				
^{89}Y	p, d	^{86,88,89}Zr, ^{86,87m,87mg,88,90m}Y, ^{82,83,85}Sr, ^{83,84}Rb	^{88,89}Zr, ^{87,88}Y				^{89}Zr, ^{88}Y, ^{85}Sr, ^{83,84}Rb
^{nat}Zr	p, d	^{90,91m,92,95,96}Nb, ^{88,89,95,97}Zr, ^{86,87,88}Y	^{88,89}Zr, ^{87,88}Y			+	^{92m,95}Nb, ^{89,95}Zr, ^{88}Y
^{93}Nb	p, d, α	^{94g,95m,95g,96g,96m}Tc, ^{90,93m}Mo, ^{89,90,91m,92m,95m}Nb, ^{86,87,88,89}Zr, ^{86,87m,87,88}Y	^{94g}Tc, ^{88,89}Zr, ^{87,88}Y			+	^{95m,96mg}Tc, ^{92m,95mg}Nb, ^{89}Zr, ^{88}Y
^{nat,100}Mo	p, d	^{94,95,95m,96,99}Tc, ^{93m,99}Mo, ^{90,92m,95,96}Nb, ^{86,88,89}Zr, ^{86,87,88}Y	^{94,99m}Tc, ^{99}Mo, ^{88}Y			+	^{95m,96mg}Tc, ^{92m,95}Nb, ^{89}Zr, ^{88}Y
^{103}Rh	p, d	^{101,103}Pd, ^{101m,101g,102m,102g}Rh	^{103}Pd			+	^{102g}Rh

Table 3. Measurements of experimental data. In collaboration with foreign laboratories, excitation functions on 50 targets for about 1000 nuclear reactions have been measured (continued)

Target	Particle	Investigated reaction products	Medical	Biological, industrial tracer	Monitor	Accelerator technology	TLA
^{nat}Pd	p, d, α	^{104,105,111m}Cd, ^{103,104mg,105,106m,110m,111,112}Ag, ^{100,101,109,111}Pd, ^{99m,100mg,102}Rh, ^{97}Ru	^{103}Ag (^{103}Pd), ^{104,110m,111}Ag				^{105,110m}Ag, ^{102}Rh
^{nat}Ag	p, d, α	^{108g,108m,109mg,110g,110m,111mg,112m,112mg,107,109}Cd, ^{105,106m,110m}Ag, ^{100,101,103}Pd, ^{99,100,101m,102,105}Rh, ^{97}Ru	^{110,111}In, ^{110}Ag, ^{103}Pd			+	^{110m}In, ^{105,110m}Ag, ^{102}Rh
^{nat,111,112,114,116}Cd	p, d, ^{3}He, α	^{107g,108m,108g,109g,110m,110g,111mg,112m,113m,114m,115m,116m1}In, ^{107,109,111m,115m,115g,117m,117g}Cd, ^{104g,105g,106m,110m,111g,113g}Ag	^{110,111,114m}In, ^{119m}Sn			+	^{110m}In, ^{105g,110m}Ag
^{nat}In	d	^{111,113}Sn, ^{111mg,112m,113m,114m,115m,116m1}In	^{114m}In			+	^{113}Sn
^{nat}Sn	p, d, ^{3}He, α	^{116,117,119m,119g,121m,121g,123m,127m,127g}Te, ^{115,116m,117,118m,120m,122,124,125,126,127}Sb, ^{113,117m,125}Sn, ^{109mg,110m,111mg,114m}In	^{117m}Sn, ^{110m,111mg,114m}In			+	^{121m,125m}Te, ^{120m,124,126,127}Sb, ^{113}Sn
^{nat}Sb	^{3}He, α	^{121,123,124,126}I	^{123,124}I				^{126}I
^{122,123,124,nat}Te	p, d	^{121,123,124,126,128,130g}I, ^{121g}Te	^{123,124}I				^{126}I
^{124,nat}Xe	p, d, α	^{122m,123,127,129,130m,132,134,135m,136,138}Cs, ^{121,122,123,133m,135m,135g}Xe, ^{121,123,124,126,130,131,133}I, ^{129m,129g,131m,131g,133m,135m,137m,139}Ba	^{131}Ba (^{131}Cs), ^{123,124}I				
^{124,nat}Xe	p, d, α	^{122m,123,127,129,130m,132,134,135m,136,138}Cs, ^{121,122,123,133m,135m,135g}Xe, ^{121,123,124,126,130,131,133}I, ^{129m,129g,131m,131g,133m,135m,137m,139}Ba	^{131}Ba (^{131}Cs), ^{123,124}I				
^{133}Cs	p	^{128,129,131,133m}Ba, ^{129,132}Cs, ^{127,129m,131m}Xe	^{131}Ba (^{131}Cs)				
^{nat}Ba	p	^{132mg,133,135}La, ^{129m,129g,131m,133m,133g,135m}Ba, ^{129,132,134}Cs	^{131}Ba (^{131}Cs)				
^{nat}Nd	d	^{139}Ce, ^{139,140}Nd, ^{143,144,146,148}Pm	^{140}Nd (^{140}Pr)				
^{141}Pr	p, d	^{139,140,141}Nd, ^{142}Pr	^{140}Nd (^{140}Pr), ^{139}Pr				
^{nat}Er	p, d, α	^{166,167,169}Yb, ^{163,165,166,167,168,170}Tm, ^{161,169,169,171}Er, ^{166,167}Ho	^{167,170}Tm, ^{165,169}Er, ^{166}Ho				
^{169}Tm	p, d	^{169}Yb, ^{167,168,170}Tm	^{169}Yb, ^{170}Tm				
^{nat}Yb	p, d, α	^{170,171,172,173,175,177m,178m,179m,180m}Hf, ^{169,170,171mg,172mg,173,174g,177g}Lu, ^{169,175,177mg}Yb	^{169,175}Yb, ^{177}Lu				
^{nat}Ta	d, α	^{178,182}Ta, ^{181}W, ^{181,182m,183,184m,184g}Re	^{181}W			+	^{182}Ta, ^{183,184m,184g}Re
^{nat}W	p, d	^{181,182m,182g,183,184m,184g,186g}Re, ^{187}W, ^{177,183}Ta	^{186}Re			+	
^{nat}Re	p, d	^{181,182m,182g,183,184m,184g,186g,188g}Re	^{186,188}Re				
^{192}Os	p, d	^{192}Ir, ^{193}Os, ^{186}Re	^{192}Ir, ^{186}Re				
^{nat}Ir	p, d	^{188,189,191,193m}Pt, ^{185,186g,187,188,189,190g,192g,194g,194m2}Ir, ^{185}Os	^{191,193m}Pt, ^{192g,194}Ir		^{195m,197}Hg	+	^{190,192}Ir
^{nat}Pt	p, d, ^{3}He, α	^{191m,191g,192,193m,193g,195m,195g,197g,199}Hg, ^{191,192,193,194,195,196mg,196m2,198m,198g,199,200m,200g}Au, ^{188,189,191,195m,197m,197g}Pt, ^{188,189,190,192,194m}Ir	^{198g,199}Au, ^{191,195m}Pt, ^{192}Ir			+	^{195,196mg}Au, ^{188}Pt, ^{190,192}Ir
^{197}Au	p, d	^{195m,195g,197m}Hg, ^{195,196,198m,198g}Au	^{198g}Au			+	^{195,196}Au
^{nat}Tl	d	^{202,203,204m}Pb, ^{202}Tl, ^{203}Hg	^{203}Pb				
^{nat}Pb	p, d	^{201,202,203,204,205,206,207}Bi, ^{201,202m,203}Pb, ^{201,202}Tl	^{206}Bi, ^{201}Tl			+	^{205,206}Bi
^{209}Bi	^{3}He, α	^{208,209,210,211}At, ^{210}Po	^{211}At				

Table 4. Accelerators used in measurements

| Accelerator	k-value	Laboratory, City	Beam
SSC	220	iThemba Labs, Somerset West (ZA)	p
Cyclone	110	UCL, Louven La Neuve (BE)	p, d
AVF	110	CYRIC, Sendai (JP)	p, d
AVF 930	90	NIRS, Chiba (JP)	p, ^{3}He, α
CGR 560	40	VUB, Brussels (BE)	p, d, α
U 120M	37	INR, Rez (CZ)	p
CS 30	26	Mount Sinai Medical Center, Miami (USA)	p
CV 28 JULIC	28 45	FZ Julich, Julich (DE)	p, d, ^{3}He, α
MGC 20	20	Abo Akademi, Turku (FI)	p, d, ^{3}He, α
MGC 20	20	ATOMKI, Debrecen (HU)	p, d, ^{3}He, α

7.2 Theoretical interpretation of experimental data

At the beginning we made a few theoretical calculations by using the ALICE-IPPE and STAPRE codes. Later a collaboration was developed with the well-known, well-experienced theoretical group at the Institute of Physics and Power Engineering, Obninsk, Russia. They have made systematic calculations for our measurements and evaluations by using the ALICE-IPPE, GNASH and EMPIRE-II statistical and pre-compound model codes. For the interpretation of the deuteron induced reactions DWBA (Distorted Wave Born Approximation) calculations have been developed and a semi-empirical modification on the statistical codes have been done taking into account direct stripping processes. For some nuclear reactions the TALYS general code has also been used by the group at Cyclotron and Radioisotope Center, Tohoku University, Sendai, Japan.

The aims of the model calculations are:

- to check the prediction capacity of different model codes using a-priori calculations
- to have a preliminary knowledge on the behavior of the excitation functions before the experiment and during the data evaluation
- to evaluate contradicting experimental data measured earlier (effective threshold energies, energy shifts, significant differences in absolute values)
- to estimate contributions from nuclear reactions on different stable isotopes of the given element and from parent decays in the case of cumulative processes
- to estimate radionuclide impurities from residual nuclei having unfavorable decay characteristics (large $T_{1/2}$, no gamma etc.)
- to prepare recommended database

14

7.3 Compilation of experimental data in standard EXFOR format

The practical applications are supported with the collection of experimental data and of the main measuring circumstances in an easy usable computer format. Experimental results published in any publications and reports are collected in a standard EXFOR (CSSR) format. The ATOMKI Nuclear Reaction Data Group has participated in the compilation work since 1992. Fig. 16 shows the retrievals of this database from the IAEA homepage and its mirror sites. In 2007 about 22000 retrievals was detected which proves the usefulness of the EXFOR database. Nowadays, in the newest papers authors refer directly to this database because it contains checked and in some cases updated data. The ATOMKI is a member of the International Nuclear Reaction Centre Network.
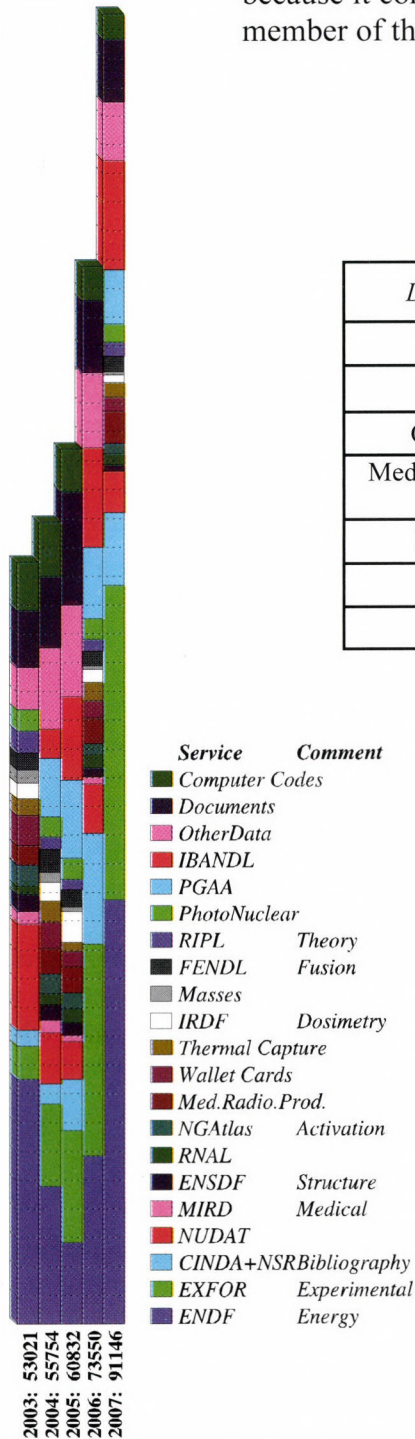
Database/Year	2004	2005	2006	2007
ENDF	9574	5663	11703	29648
EXFOR	5733	7846	14840	22061
CINDA+NSR	1414	3492	7746	5069
Medical Radioisotope Production	1800	1837	1779	2296
Photonuclear	1414	1461	1458	1286
PGAA	4084	5431	5040	3829
IBANDL	2044	5806	6967	7593

Service — Comment
- Computer Codes
- Documents
- OtherData
- IBANDL
- PGAA
- PhotoNuclear
- RIPL — Theory
- FENDL — Fusion
- Masses
- IRDF — Dosimetry
- Thermal Capture
- Wallet Cards
- Med.Radio.Prod.
- NGAtlas — Activation
- RNAL
- ENSDF — Structure
- MIRD — Medical
- NUDAT
- CINDA+NSR — Bibliography
- EXFOR — Experimental
- ENDF — Energy

2003: 53021
2004: 55754
2005: 60832
2006: 73550
2007: 91146

Figure 16. Nuclear Data Services: web statistics

15

7.4 Compilation and critical evaluation of literature data for recommended database

Different applications need different nuclear data and different specific nuclear reactions. It is very important to select the most reliable experimental data from the huge datasets, to correct them to the recent reference data and to prepare a recommended dataset in a handbook for special applications. Taking into account that experimental data are not available in the whole energy range of interest the gaps should be filled by systematics or by theoretical calculations. Preparation of recommended databases therefore is a task for a scientist (or a group of scientists) expert in measurements, data handling and theory.

The ATOMKI Nuclear Reaction Data Group participated in the following recommended databases:

Production of diagnostic SPECT radioisotopes
- CRP 1996-2001
- 16 reactions
- IAEA TECDOC-1211
- http://www-nds.iaea.or.at/medical/

Production of diagnostic PET radioisotopes
- CRP 1996-2001
- 10 reactions
- IAEA TECDOC-1211
- http://www-nds.iaea.or.at/medical/

Monitoring beam parameters
- CRP 1996-2001
- 22 reactions
- IAEA TECDOC-1211
- http://www-nds.iaea.or.at/medical/

Production of therapeutic radioisotopes
- CRP 2002-2007
- 34 reactions
- IAEA TECDOC (in progress)
- http://www-nds.iaea.org/radionuclides/index.htmlx

The data evaluation work is very time consuming and the efforts are appreciated by users in different applications. The recommended database for production of diagnostic radioisotopes and the beam monitor reactions has been used by about 2000 users (see Fig. 16) every year, which shows its importance and usefulness.

8. International collaborations

1. CERN LHC CMS collaboration
   Radiation tolerance tests of components of particle detector systems and their electronics that operate in radiation environment of the CMS experiment

2. EU-FP6 SME DIAMOND
   Development of an innovative, accurate, monolithic CVD diamond array based radiation dosimeter system

3. HAS – FZK (Forschungszentrum Karlsruhe) collaboration
   Thermonuclear fusion related research and developments:
   a. Study of displacement cascades and helium behavior in beryllium by molecular dynamics simulations
   b. Development of methods and techniques for chemical analyses of tritium and its compounds

4. HAS – FWO (Cyclotron Laboratory, Vrije Universiteit Brussel, Belgium) collaboration
   Nuclear reaction data for practical applications

5. ATOMKI – CYRIC (Cyclotron and Radioisotope Center, Tohoku University, Sendai, Japan) collaboration
   Nuclear reaction data for medical applications and accelerator technology

6. ATOMKI – IPPE (Institute of Physics and Power Engineering, Theoretical Department, Obninsk, Russia) collaboration
   Theoretical calculations of nuclear reaction data

7. ATOMKI – IAEA collaboration
   Coordinated Research Projects (CRPs) on
   a. Recommended database for production of therapeutic radioisotopes
   b. High intensity liquid and solid targets
   c. Nuclear Reaction Data Centre network

8. ATOMKI – TUW/AC^{2}T (Technische Universitat Wiena and Austrian Competence Center for Tribology)
   Thin layer activation for wear studies

9. HAS – JSPS and bilateral cooperation with National Institute for Radiological Research, Chiba, Japan
   Production of PET radioisotopes and radiopharmaceuticals for biology and human diagnostics, continuous from 2000

10. TéT cooperation with iThemba Laboratory for Accelerator Based Sciences, Somerset West, South-Africa
    Investigation of methods for preparation of new PET and therapeutic radioisotopes and labeled compounds, continuous from 2001

11. Cooperation between Academies (Abo Akademi, Department of Chemical Processes, Turku, Finland)
    Study of conversion of ^{11}C-labeled compounds on zeolite-type catalysers, continuous from 2003

9. Applications obtained

- National Scientific Research Fund
  Radiochemistry: 5 applications, continuous from 1987
  Nuclear data measurement: 3 applications,
  1998–2001, 2002–2005 and 2006–2009

- FP-6
  SME DIAMOND 2005-2007

10. Publication activity
The results of the research work related to the cyclotron studies during the last 20 years were published in international journals and the usefulness of our work is reflected in numerous citations:

- Scientific paper, book, thesis: ~470 (SCI ~250)
- Independent foreign references: ~1320 (SCI ~660)

1.1 Joint discussion of the real and $\mathcal{PT}$-symmetric Rosen–Morse I potentials

G. Lévai

With the introduction of $\mathcal{PT}$-symmetric quantum mechanics the $\mathcal{PT}$-symmetric version of a number of exactly solvable potentials has been generated. These potentials are invariant under the joint action of the $\mathcal{P}$ space and $\mathcal{T}$ time reflection operations, *i.e.* they obey the $V^*(-x) = V(x)$ relation. $\mathcal{PT}$-symmetric systems may possess *real* energy eigenvalues, but the pseudo-norm of the wave functions defined by the $\mathcal{PT}$-inner product $\langle\psi|\phi\rangle_{\mathcal{PT}} \equiv \langle\psi|\mathcal{P}\phi\rangle$ is indefinite, so their probabilistic interpretation can be restored only by introducing a further $\mathcal{C}$ charge operator in the metric.

The type I Rosen–Morse potential can be defined on the $x \in [0, \pi]$ domain as

$$V(x) = \frac{s(s+1)}{\sin^2(x)} - 2i\Lambda \cot(x) , \qquad (1)$$

and its energy eigenvalues are

$$E_n = (s-n)^2 + \frac{\Lambda^2}{(s-n)^2} . \qquad (2)$$

The corresponding eigenfunctions can be witten in terms of Jacobi polynomials

$$
\begin{aligned}
\psi_n(x) &= C_n(1 + i\cot(x))^{\frac{\alpha_n}{2}}(1 - i\cot(x))^{\frac{\beta_n}{2}} \\
&\times P_n^{(\alpha_n, \beta_n)}(-i\cot(x)) , \qquad (3)
\end{aligned}
$$

where $\alpha_n = s - n + \frac{\Lambda}{s-n}$ and $\beta_n = s - n - \frac{\Lambda}{s-n}$.

The Rosen–Morse I potential (1) can be considered as the generalization of the symmetric Pöschl–Teller hole (with $\Lambda = 0$), which, in turn can be viewed as the extension of the infinite square well (with $s = 0$). This is also seen in the structure of the energy spectrum (2), which follows a quadratic dependence on the principal quantum number n and is perturbed slightly when the odd potential term is switched on ($\Lambda \neq 0$) in (1).

The real Rosen–Morse I potential is obtained if Λ is chosen to be purely imaginary: $\Lambda = i\lambda$. This potential has been interpreted as the Kepler problem on the hypersphere, and it has also been applied as a quark-di-quark potential to account for the energy spectrum of (N and Δ) baryon resonances. The $\mathcal{PT}$-symmetric version of (1) is obtained if Λ is real:

$\Lambda = \lambda$. In the latter case the $\mathcal{P}$ space reflection operation has to be defined as reflection around $x = \pi/2$.

The study of the $\mathcal{PT}$-symmetric Rosen–Morse I potential [1] has been inspired by a similar analysis of the $\mathcal{PT}$-symmetric Scarf I potential [2], in which the odd imaginary component is of the type $i\cot x / \sin x$. The $\mathcal{PT}$-normalization constants of its eigenfunctions have been determined and these results have been used by others to derive the $\mathcal{C}$ charge operator of this problem in a closed analytic form. The importance of this result lies in the fact that previously the $\mathcal{C}$ operator has been determined for other systems by perturbative and approximative techniques.

The main results derived for the $\mathcal{PT}$-symmetric Rosen–Morse I potential are the following [1]. *i)* Closed analytic form has been given for the $\mathcal{PT}$-normalization constants of its eigenfunctions and it has been shown that the pseudo-norm follows the same $(-1)^n$ type behaviour as in the case of the $\mathcal{PT}$-symmetric Scarf I potential. The normalization constants have also been given in closed analytic form for the eigenstates of the *real* potential for the first time. *ii)* It has been shown that in contrast with the Scarf I potential, there is no parameter domain in which both eigenfunctions can be regular at the boundaries. *iii)* It has been demonstrated that similarly to the Scarf I potential, the spontaneous breakdown of $\mathcal{PT}$ symmetry cannot be defined for the Rosen–Morse I potential either, because the transition (corresponding to $s = -\frac{1}{2} + i\sigma$) would imply strongly attractive inverse-square-type singularities at the boundaries.

Another important aspect of the $\mathcal{PT}$-symmetric Rosen–Morse I and Scarf I potentials is that they can be used to generate the angular component of non-central $\mathcal{PT}$-symmetric potentials in 2 or 3 dimensions.

[1] G. Lévai, submitted to J. Phys. A.

[2] G. Lévai, J. Phys. A **39** (2006) 10161.

19

1.2 $\mathcal{PT}$ symmetry breaking in non-central potentials

G. Lévai

$\mathcal{PT}$-symmetric systems represent a special example for non-hermitian problems in quantum mechanics. The Hamiltonian of these systems is invariant under the simultaneous action of the $\mathcal{P}$ space and $\mathcal{T}$ time inversion operations. They resemble hermitian problems in that they typically possess *real* energy spectrum. However, increasing non-hermiticity, *e.g.* the imaginary potential component the real energy eigenvalues merge pairwise and turn into complex conjugate pairs and at the same time, the energy eigenstates cease to be eigenstates of the $\mathcal{PT}$ operator. The mechanism of this spontaneous breakdown of $\mathcal{PT}$ symmetry has been investgated in one spatial dimension, and our aim was to extend these studies to higher dimensions [1,2].

Assuming that the solutions of the Schrödinger equation

$$-\Delta\psi(\mathbf{r}) + V(\mathbf{r})\psi(\mathbf{r}) = E\psi(\mathbf{r}) \qquad (4)$$

can be obtained by the separation of the radial and angular variables, we substitute $\psi(r,\theta,\varphi) = r^{-1}\phi(r)\sin^{-1/2}\omega(\theta)\tau(\varphi)$ in (4), where $r \in [0,\infty)$, $\theta \in [0,\pi]$ and $\varphi \in [0,2\pi]$. Further, we assume that the angular components of the wave function satisfy

$$\omega'' = (P(\theta) - p)\omega , \qquad (5)$$

$$\tau'' = (K(\varphi) - k)\tau , \qquad (6)$$

where $\tau(\varphi)$ has to be defined with periodic boundary conditions. Then the complete three-dimensional problem becomes solvable if the non-central potential takes the form

$$V(r,\theta,\varphi) = V_0(r) + \frac{K(\varphi)}{r^2\sin^2\theta} + \frac{P(\theta)}{r^2} - \frac{k-1/4}{r^2\sin^2\theta} . \qquad (7)$$

Here $V_0(r)$ is a central potential appearing in

$$-\phi'' + \left[V_0(r) + \frac{1}{r^2}\left(p - \frac{1}{4}\right)\right]\phi - E\phi = 0 . \qquad (8)$$

Note that (8) is formally identical with a conventional radial Schrödinger equation complete with a centrifugal term.

In order to solve (4) properly, the state-dependence of (7) has to be eliminated, *i.e.* its dependence on k has to be cancelled by combining the last two terms. This effectively means that (5) has to be solved with a potential $P(\theta)$ that contains a $\sin^{-2}\theta$ type term.

Next we investigate under which conditions the non-central potential (7) exhibits $\mathcal{PT}$ symmetry. It is seen that space reflection $\mathcal{P} : \mathbf{r} \to -\mathbf{r}$ implies that $\mathcal{P}$ can be factorized into two angular terms as $\mathcal{P} = \mathcal{P}_\theta\mathcal{P}_\varphi$, where $\mathcal{P}_\theta\theta = \pi - \theta$ and $\mathcal{P}_\varphi\varphi = \varphi + \pi$. Note that these angular $\mathcal{P}$ operators differ from the usual space reflection operator defined in one dimension as $\mathcal{P}x = -x$. Applying the above $\mathcal{P}$ operator, the $\mathcal{PT}$ invariance of (7) implies $V_0(r) = V_0^*(r)$, $P^*(\pi - \theta) = P(\theta)$, $K^*(\varphi + \pi) = K(\varphi)$ and $k^* = k$, *i.e.* the centrally symmetric component of the potential has to be real, while the two angular potentials have to exhibit a kind of $\mathcal{PT}$ symmetry themselves, furthermore, the eigenvalue of the azimuthal equation (6) has to be real. Note that the last condition can be dropped if the last two terms of (7) can be combined. This can happen when the state-dependence of the potential is eliminated by applying the $\mathcal{PT}$-symmetric Scarf I or Rosen–Morse I potentials in the polar equation (5) [2]. This finding confirms the results of an earlier study, *i.e* that the angular variables are essential in introducing $\mathcal{PT}$ symmetry [1].

The spontaneous breakdown of $\mathcal{PT}$ symmetry occurs when the energy eigenvalues turn into complex conjugate pairs. This can happen if the eigenvalue p of the polar equation becomes complex, *i.e.* if the $\mathcal{PT}$ symmetry of (5) is spontaneously broken [2]. The spontaneous breakdown of $\mathcal{PT}$ symmetry in non-central potentials has been discussed previously only in two dimensions [1]. The results of that study can also be used to introduce the spontaneous breakdown of $\mathcal{PT}$ symmetry in the three-dimensional case via the azimuth angle component of the potential (7).

[1] G. Lévai, J. Phys. A **40** (2007) F273.

[2] G. Lévai, J. Phys. A, in press.

2.1 The LUNA ^{3}He$(\alpha, \gamma)^7$Be experiment with on-line method

Gy. Gyürky, Z. Elekes, Zs. Fülöp, E. Somorjai, for the LUNA collaboration

The ^{3}He$(\alpha, \gamma)^7$Be reaction plays a crucial role in two distinct fields of nuclear astrophysics: in the hydrogen-burning of the Sun (and similar main sequence stars) and in the big-bang nucleosynthesis. In the pp-chain of solar hydrogen burning the ^{3}He$(\alpha, \gamma)^7$Be reaction is the starting point of the 2nd and 3rd branches of the chain from where the high energy ^{7}Be and ^{8}B neutrinos are originated. On the other hand, the rate of the ^{3}He$(\alpha, \gamma)^7$Be reaction determines the primordial ^{7}Li abundance which provides a stringent test of the big-bang nucleosynthesis models. Therefore, the precise knowledge of the astrophysically relevant low energy cross section of ^{3}He$(\alpha, \gamma)^7$Be is of high importance.

The LUNA collaboration has carried out a research program aiming to measure the ^{3}He$(\alpha, \gamma)^7$Be cross section with high precision at low energies. In the first phase of the experiments, the cross section has been determined with the activation technique measuring the decay of the produced ^{7}Be nuclei. The measurements have been carried out at energies between $E_{c.m.} = 93$ and 170 keV [1,2], lower than ever reached before.

The research program has been completed by the on-line measurement where the prompt γ-radiation from the reaction has been measured. Similarly to the activation, the on-line experiments have been carried out at the LUNA-2 400 kV accelerator at the Gran Sasso National Laboratory in Italy. An intense (300 μA) ^{4}He beam bombarded a differentially pumped windowless ^{3}He gas target. The prompt γ-radiation has been measured with an ultra low background HPGe detector. The cross section has been determined at three energies: $E_{c.m.} = 93$, 106 and 170 keV. In order to investigate the possible difference between the cross sections measured with the on-line and activation methods, simultaneously with the on-line experiment the activation measurement has been repeated. Perfect agreement has been observed between the two methods [3].

With our new high precision results the uncertainty of the ^{8}B and ^{7}Be solar neutrino fluxes from the ^{3}He$(\alpha, \gamma)^7$Be reaction rate is reduced form about 8% to 3% and the solution of the ^{7}Li problem of primordial nucleosynthesis based on the limited knowledge of this reaction rate is excluded.

[1] D. Bemmerer *et al.* (LUNA Collaboration), Phys. Rev. Lett. 97 (2006) 12502.

[2] Gy. Gyürky *et al.* (LUNA Collaboration), Phys. Rev. C 75 (2007) 035805.

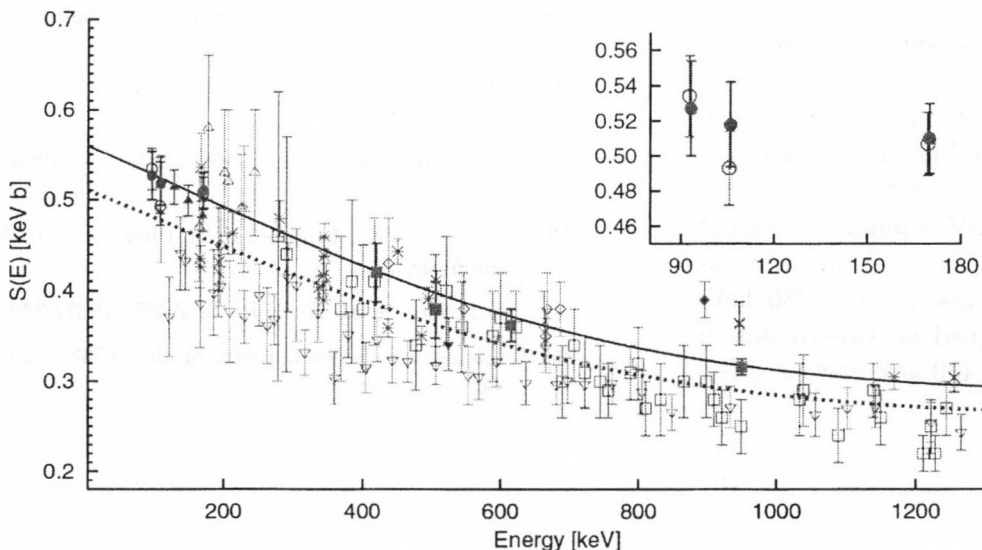[3] F. Confortola *et al.* (LUNA Collaboration), Phys. Rev. C 75 (2007) 065803.

Figure 1. Astrophysical S factor of the ^{3}He$(\alpha, \gamma)^7$Be reaction from the present and previous works. The inset shows the LUNA data obtained with the activation and on-line method. For further details see ref. [3].

2.2 Ground state capture in $^{14}N(p,\gamma)^{15}O$ at LUNA

Zs. Fülöp, Gy. Gyürky, Z. Elekes, E. Somorjai for the LUNA Collaboration

The $^{14}N(p,\gamma)^{15}O$ reaction is the slowest process in the hydrogen burning CNO cycle and thus of high astrophysical interest. This reaction plays a role for the neutrino spectrum of the Sun as well as in the age determination of globular clusters. The reaction was recently studied in three experiments at energies ranging from $E_{cm} = 70$ to 480 keV [1-3]. A significant reduction of the ground state contribution has been found [1,2]. However, the analysis was hampered by the fact that the usage of large detectors in close geometry has as a consequence that the "ground state contribution" is masked by summing–in due to coincidence events from the cascade transitions in ^{15}O. Necessary corrections were of the order of a factor two to four, thereby increasing the uncertainty. Moreover, an R–matrix analysis revealed that below the 259 keV resonance the data followed primarily the low energy wing of the resonance. These data could not probe the behavior of the interference structure, which is needed for reliable extrapolation, due to a minimum of the S–factor curve near $E_{cm} = 160$ keV.

The value of $S_{gs}(0)$ depends on the Γ_γ of the subthreshold state at 6.79 MeV excitation energy in ^{15}O. The influence of a change in Γ_γ of the subthreshold state is illustrated in figure 1 where Γ_γ ranges from 0.6 (dashed line), 0.8 (solid line) to 1 eV (solid thin line). When lowering the width of the subthreshold state $S_{gs}(0)$ decreases, the destructive interference minimum moves to lower energies and hence recovers much earlier at higher energies, i.e. the cross section is expected to be larger at energies above the 259 keV resonance. For the above range in Γ_γ one expects a change in cross section of a factor of three around 330 keV. We have therefore designed an experiment in the energy range 300 to 400 keV using a BGO

shielded Clover detector [5] to reduce significantly the summing–in contributions from the true coincidence events from the ^{15}O cascade transitions. The ground state transition has been investigated at center of mass energies of 318, 334 and 353 keV, respectively, using the LUNA-II accelerator at the LNGS underground laboratory in Italy.

The preliminary analysis proved that the summing-in corrections have been reduced to less than 30%. Further analysis to determine the relevant S-factor values and their impact on the $S_{gs}(0)$ is in progress.
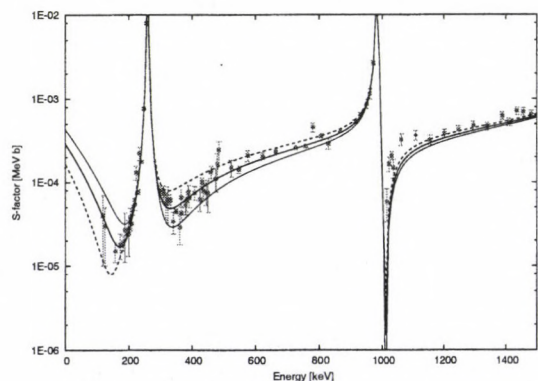

Figure 1. Astrophysical S–factor literature data [1,2,4] for radiative proton capture to the ground state of ^{15}O as a function of center of mass energy illustrating the influence of change in Γ_γ of the subthreshold state where Γ_γ ranges from 0.6 (dashed line), 0.8 (solid line) to 1 eV (solid thin line).

[1] A. Formicola, LUNA Collaboration, Phys. Lett. B591 (2004) 61.

[2] R.C. Runkle et al, Phys. Rev. Lett. 94 (2005) 082503.

[3] A. Lemut, LUNA Collaboration, Phys. Lett. B634 (2006) 483.

[4] U. Schröder, et al, Nucl. Phys. A467 (1987) 240.

[5] Z. Elekes, et al, Nucl. Instr. Meth. A503 (2003) 580.

2.3 The disappearance of $N{=}20$ magicity studied in neutron-rich ^{23}O nucleus

Z. Elekes, Zs. Dombrádi, S. Bishop[a], Zs. Fülöp, J. Gibelin[b], T. Gomi[a], Y. Hashimoto[c], N. Imai[a], N. Iwasa[d], H. Iwasaki[e], G. Kalinka, Y. Kondo[c], A.A. Korsheninnikov[a,f], K. Kurita[g], M. Kurokawa[a], N. Matsui[c], T. Motobayashi[a], T. Nakamura[c], T. Nakao[e], E.Yu. Nikolskii[a,f], T.K. Ohnishi[a], T. Okumura[c], S. Ota[h], A. Perera[a], A. Saito[e], H. Sakurai[e], Y. Satou[c], D. Sohler, T. Sumikama[a], D. Suzuki[g], M. Suzuki[g], H. Takeda[e], S. Takeuchi[a], Y. Togano[g], Y. Yanagisawa[a]

The stability of the shell closures are marked by the size of the shell gaps measured as the energy difference between the single particle states belonging to different major shells. Going from ^{30}Si to ^{24}O, the $N{=}20$ shell gap is expected to gradually decrease, and $N{=}14,16$ shell gaps develop instead. Therefore, our aim was to determine the location of the excited states in ^{23}O, which directly gives the single particle energies suitable to deduce the size of the $N{=}16$ and $N{=}20$ shell closures, via invariant mass spectroscopy combined with the (d,p) neutron transfer reaction.

The experiment was carried out at RIKEN where a 94 $A{\cdot}$MeV energy primary beam of ^{40}Ar with 60 pnA intensity hit a ^{9}Be production target of 3 mm thickness. The total intensity was approximately 1500 cps having an average ^{22}O intensity of 600 cps. The separation of ^{22}O particles was complete. The secondary beam was transmitted to a CD$_2$ target of 30 mg/cm^2. The reaction occurred at an energy of 34 $A{\cdot}$MeV. The scattered particles were detected and identified by a 2×2 matrix silicon telescope placed 96 cm downstream of the target. The first two layers were made of strip detectors (with 5 mm width of each strip) to measure the x and y positions of the fragments. The protons emitted backward in the reaction were detected by 156 CsI(Tl) scintillator crystals read out by photodiodes. The neutrons coming from the decay of the produced ^{23}O nuclei excited above the neutron separation energy were detected by a neutron wall. The energy of the neutrons was deduced from the TOF while the hit position was determined by identifying the rod that fired (in vertical direction) and by the time difference between the two photomultipliers attached to the ends of the rods (in horizontal direction).

The excitation energy spectrum of ^{23}O shown in Figure 1 was reconstructed from the momentum of the neutron and the heavy ion

^{22}O by calculating the invariant mass and using the known neutron separation energy (2.74 MeV). Two peaks are clearly visible at 4.00(2) MeV and 5.30(4) MeV in the spectrum.
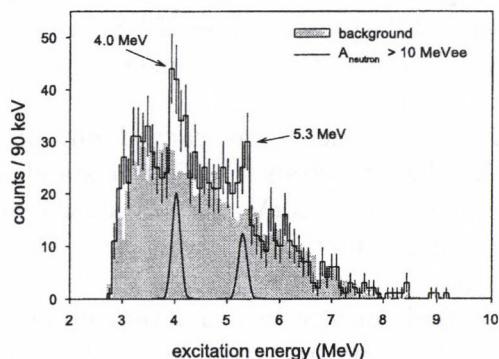

Figure 1. Reconstructed excitation energy spectrum of ^{23}O. A$_{neutron}{>}10$ MeVee. Shaded spectrum represents the background.

The (d,p) reaction populates the single particle states of ^{23}O. From a comparison with shell model calculations, the first one is the neutron $d_{3/2}$ state, the energy of which gives the $N{=}16$ shell closure to be 4 MeV. This is large enough to explain why ^{24}O is the last bound oxygen isotope. The second excited state observed in the present experiment does not have any counterpart in the sd model space, and corresponds to a state from the fp shell. Its energy relative to the $d_{3/2}$ state determines the strength of the $N{=}20$ shell closure to be 1.3 MeV and provides a direct evidence for the disappearance of the $N{=}20$ shell closure at $Z{=}8$.

a) RIKEN
b) Institut de Physique Nucléaire
c) Tokyo Institute of Technology
d) Tohoku University
e) University of Tokyo
f) Kurchatov Institute
g) Rikkyo University
h) Kyoto University

2.4 Observation of excited state in ^{41}Si

D. Sohler, Zs. Dombrádi, B. Bastin[b], S. Grévy[a], O. Sorlin[a], N.L. Achouri[b], J.C. Angélique[b], F. Azaiez[c], D. Baiborodin[d], R. Borcea[e], C. Bourgeois[c], A. Buta[e], A. Burger[f,g], R. Chapman[h], J.C. Dalouzy[a], Z. Dlouhy[d], A. Drouard[f], Z. Elekes, S. Franchoo[c], S. Iacob[e], B. Laurent[b], M. Lazar[e], X. Liang[h], E. Lienard[b], J. Mrazek[d], L. Nalpas[f], F. Negoita[e], N.A. Orr[b], Y. Penionskhevitch[i], Zs. Podolyak[j], F. Pougheon[c], P. Roussel-Chomaz[a], M.G. Saint-Laurent[a], M. Stanoiu[c,k], I. Stefan[a], F. Nowacki[l], A. Poves[m]

Recently, the collapse of the Z=14 and N=28 shell closures has been revealed in very neutron-rich Si and P nuclei [1]. In order to further explore the behaviour of these shell gaps, we studied the excited states of ^{41}Si by in-beam γ-ray spectroscopy from fragmentation of radioactive beams.

The experiment was carried out at the GANIL facility, France. First a stabil 4μA ^{48}Ca beam at 60 MeV/u was fragmented on a ^{12}C target in the SISSI device. The primary reaction products were selected by measuring their energy loss and time-of-flight at the ALPHA spectrometer. The cocktail beam impinged onto a secondary ^{9}Be target placed in the dispersive focal plane of the SPEG spectrometer which was tuned to maximise the transmission of ^{42}Si. The secondary reaction products were unambiguously identified by their ΔE and positions determined by ionisation and drift chambers, furthermore by their TOF and residual energies measured by a plastic scintillator at the focal plane of SPEG. To detect γ rays, the secondary target was surrounded by an 4π array of 74 BaF$_2$ scintillators. The γ-ray spectra were obtained by selecting event-by-event the incoming nuclei and the ejectiles after the secondary target. The γ rays were corrected for Doppler shifts due to the in-flight emission by the fragments.

As it can be seen in figure 1, a clear peak on a low background at 659±14 keV energy appears in the γ-ray spectrum of ^{41}Si. This finding is in accordance with the 770 keV energy of the first 2$^+$ excited state in ^{42}Si with N=28 and Z=14 [1]. Along the N=28 isobaric line the next double magic nucleus is ^{48}Ca. In the neighbouring odd-N nucleus ^{47}Ca the energy of the first excited state was measured to

be 2014 keV. Comparing with that of ^{47}Ca the low energy value of the first excited state obtained in ^{41}Si can be interpreted as a further indication of the disappearance of the N=28 spherical shell closure at Z=14.
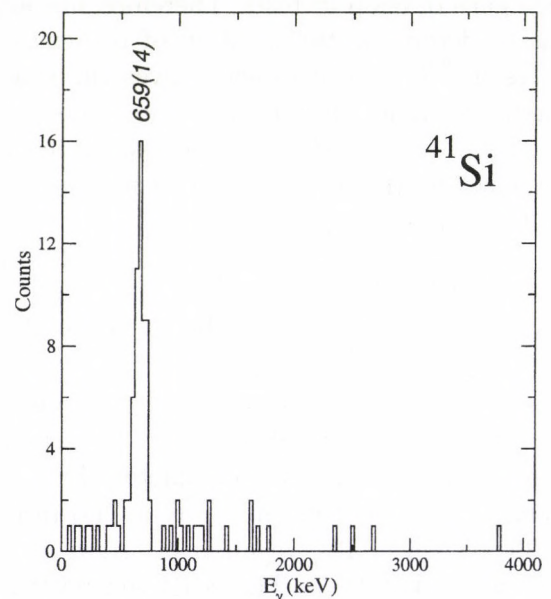

Figure 1. Gamma-ray energy spectrum detected in coincidence with ^{41}Si nuclei.

a) GANIL, Caen, France
b) LPC, Caen, France
c) IN2P3-CNRS, Orsay, France
d) NPI, Rez, Czech Republic
e) IFIN-HH, Bucharest-Magulere, Romania
f) DAPNIA/SPhN, CEA Saclay France
g) Universität Bonn, Germany
h) University of Paisley, Scotland, UK
i) FLNR, JINR, Dubna, Russia
j) University of Surrey, Guildford, UK
k) GSI, Darmstadt, Germany
l) IreS, Strasbourg, France
m) Universidad Autónoma de Madrid, Spain

[1] B. Bastin et al., Phys. Rev. Lett. 99, 022503 (2007)

2.5 Study of proton-induced reactions for the astrophysical p process

G.G. Kiss, Gy. Gyürky, A. Simon, Zs. Fülöp, E. Somorjai, T. Rauscher[a]

The stable proton-rich nuclei with charge number Z≥34 are called p-nuclei [1]. It is generally accepted that the main stellar mechanism synthesizing these nuclei - the so-called p-process - is initiated by consequtive (γ,n) photodisintegration reactions on preexisting more neutron-rich seed nuclei. In the production of the light p nuclei (γ,p) reactions are playing dominant role. Moreover, it has been stated that (p,n) reactions on s or r seed nuclei can give an important contribution to the abundances of the light p nuclei [2]. Cross section data of (p,n) reactions in the energy and mass region relevant for the p process is scarce.

Recently the cross section of the ^{70}Ge(p,γ)^{71}As and ^{76}Ge(p,n)^{76}As reactions had been derived at ATOMKI [3]. The proton capture data had been excellently reproduced and the (p,n) data had been reasonably described by the statistical model calculations. Moreover, a sensitivity calculation had been performed in order to study the dependences of the statistical model calculations on nuclear inputs. It was found, that both the (p,γ) and (p,n) cross section data can be described better with a modified proton optical potential (mod. JLM) than with the standard (JLM) potential [4]. Previously measured reaction cross sections at this mass and energy range [5,6] had been also compared with the calculations using this potential [3] and better agreement was found.

As a continuation of this work the cross section of ^{85}Rb(p,n)^{85}Sr reaction has been measured at ATOMKI using the Van de Graaff and cyclotron accelerators. The energy range of the proton beam was between 2.2 and 4.0 MeV covered with 200 keV steps. The reaction cross section has been determined using the activation technique i.e. by measuring the γ radiation following the β decay of the reaction products. More details about the experiment can be found in [7]. Figure 1. shows the measured

astrophysical S factor of the ^{85}Rb(p,n)^{85}Sr reaction and the results of the statistical calculations using as input the standard JLM [4] and the previously introduced modified JLM potential [3]. This independently confirms the conclusions drawn from the previously measured proton-induced cross sections of Germanium isotopes [3].

Moreover, we have also shown that it is possible to determine the astrophysical reaction rates for the ^{85}Rb(p,n)^{85}Sr and for the ^{85}Sr(n,p)^{85}Rb reactions from the measured cross sections despite of the negative reaction Q value.
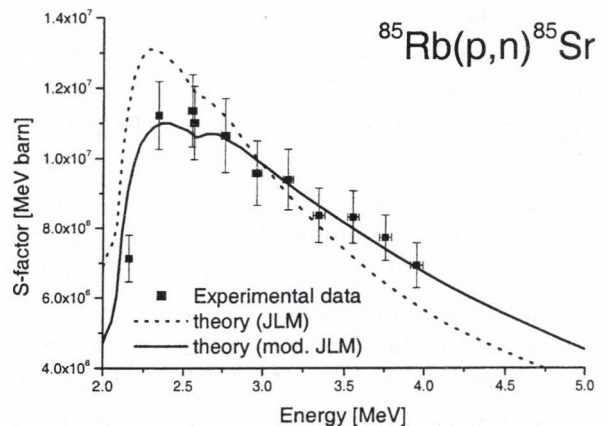

Figure 1. Measured and calculated S-factor of the investigated reaction. The lines correspond to Hauser-Feshbach model calculation using the NON-SMOKER code with different proton optical potenials.

a) Universität Basel, CH-4056 Basel, Switzerland

[1] S.E. Woosley and W.H. Howard, Astrophys. J. Suppl. 36, (1978) 285.

[2] W. Rapp *et al.*, Astrophys. J. 653 (2006) 474.

[3] G.G. Kiss *et al.*, Phys. Rev. C76 (2007) 055807.

[4] J.P. Jeukenne *et al.*, Phys. Rev. C16 (1977) 80.

[5] Gy. Gyürky *et al.*, Phys. Rev. C64 (2001) 065803.

[6] Gy. Gyürky *et al.*, Phys. Rev. C68 (2003) 055803.

[7] G.G. Kiss *et al.*, submitted to Phys. Rev. C

2.6 Study of the band structures in ^{104}Pd

D. Sohler, G. Berek, J. Timár, J. Molnár, A. Algora, Zs. Dombrádi, J. Gál, A. Krasznahorkay, L. Zolnai, P. Joshi[a], K. Starosta[b], D.B. Fossan[c], R. Wadsworth[a], P. Bednarczyk[d], D. Curien[e], G. Duchene[e], A. Gizon[f], J. Gizon[f], D.G. Jenkins[a], T. Koike[g], E.S. Paul[h], P.M. Raddon[a], G. Rainovski[i], J.N. Scheurer[j], A.J. Simons[a], C. Vaman[b], A.R. Wilkinson[a]

During the past years, beside the A~130 mass region, chiral candidate twin bands have been found also in odd-odd and odd-mass rhodium isotopes with A~100. The role of tri-axial deformation of the core in degeneracy of chiral band doubling has been pointed out in ^{102}Ru and ^{103}Rh [1]. More recently, a study of ^{106}Ag has revealed that gamma softness has marked implications for the phenomenon of nuclear chirality [2]. In order to further examine this effect on the stability of chiral geometry we studied the band structures of ^{104}Pd, the core nucleus of ^{106}Ag.

High-spin states in ^{104}Pd have been studied through the ^{96}Zr(^{13}C,5n) reaction at beam energies of 51 and 58 MeV, using the EUROBALL IV γ-ray spectrometer. The γ rays were measured in coincidence with charged particles detected by the DIAMANT array in order to eliminate the contaminants from the stronger (^{13}C,xn) reaction channels. A total of $\sim 2 \times 10^9$ triple- and higher-fold coincidence events were stored among which $\sim 4.5 \times 10^8$ belonged to the ^{104}Pd reaction channel. On the basis of the analysis of $\gamma\gamma\gamma$-coincidence data, several new high-spin bands have been established. The ground state band has been extended up to $E_x \sim 12$ MeV with $I^\pi = (26^+)$, while the previously published negative-parity bands have been extended up to $E_x \sim 11$ and ~ 9 MeV with $I^\pi = (23^-)$ and (20^-), respectively. The theoretical interpretation of the experimental results obtained is in progress.

a) Department of Physics, University of York, York, YO10 5DD, UK

b) NSCL, Cyclotron Laboratory, Michigan State University, East Lansing, MI 48824-1321, USA

c) Department of Physics and Astronomy, SUNY, Stony Brook, New York, 11794-3800, USA

d) GSI, Darmstadt, Germany

e) IReS, 23 rue du Loess, Strasbourg, 67037, France

f) LPSC, IN2P3-CNRS/UJF, F-38026 Grenoble-Cedex, France

g) Department of Physics, Tohoku University, Sendai, Japan

h) Oliver Lodge Laboratory, Department of Physics, University of Liverpool,Liverpool L69 7ZE, UK

i) Faculty of Physics, St. Kliment Ohridski University of Sofia, BG-1164 Sofia, Bulgaria

j) Université Bordeaux 1, IN2P3- CENBG - Le Haut-Vigneau BP120 33175, Gradignan Cedex, France

[1] J. Timár *et al.*, Phys. Rev. C 73, 011301 (2006)

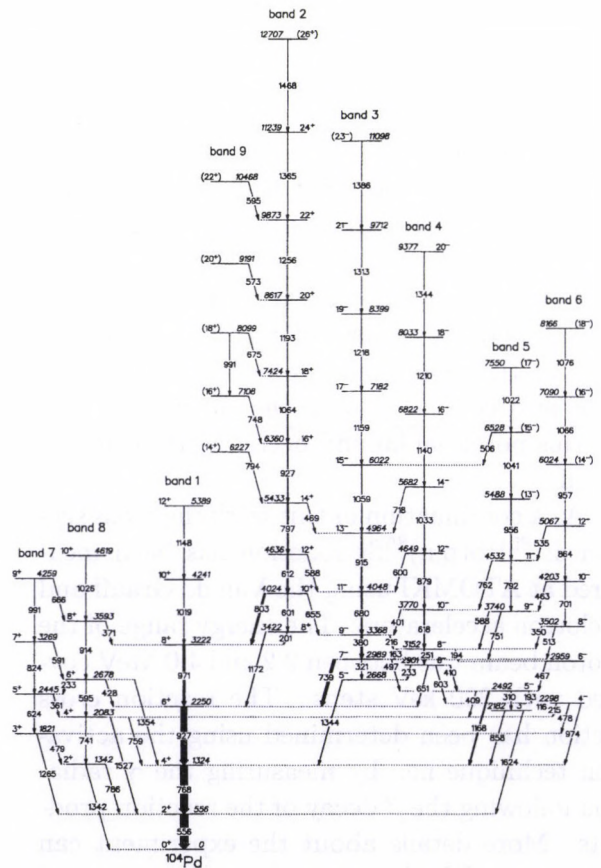[2] P.Joshi *et al.*, Phys. Rev. Lett. 98, 102501 (2007)

Figure 1. The level scheme of ^{104}Pd obtained in the present work.

2.7 Search for chirality in ^{109}Ag

J. Timár, B.M. Nyakó, G. Berek, J. Gál, G. Kalinka, A. Krasznahorkay, J. Molnár, L. Zolnai, S.M. Mullins[a], R.A. Bark[a], E.A. Gueorguieva[a], F.S. Komati[a], J.J. Lawrie[a], T. Malwela[a], S.H.T. Murray[a], J.F. Sharpey-Schafer[a], P. Joshi[b], R. Wadsworth[b], J.N. Scheurer[c], K. Juhász[d], S.M. Maliage[e], T.M. Ramashidza[e], P. Vymers[e], C.M. Petrache[f], G.K. Mabala[g],

The existence of nuclear chirality is one of the most intriguing questions of contemporary high-spin nuclear structure studies. Rotational doublet-band candidates for chiral structures have been observed mostly in two regions of the nuclear chart: around ^{134}Pr, and around ^{104}Rh. In this second region chirality in the Rh isotopes are rather well studied, chiral doubling have also been observed in ^{100}Tc, however, results obtained for chirality in the studied Ag nuclei (^{105}Ag and ^{106}Ag) look rather contradictory. Thus, it is interesting to study these doublet bands in the nearby higher-mass Ag nuclei.

Figure 1. Level scheme of ^{109}Ag obtained in the present experiment.

In order to search for a chiral-candidate partner band to the yrast $\pi g_{9/2}\nu(h_{11/2})^2$ band in ^{109}Ag, high-spin states of this nucleus have been studied using the ^{96}Zr(^{18}O,p4n) reaction. The experiment was performed at iThemba LABS using 8 Clover detectors of the AFRODITE array and the DIAMANT charged-particle array to detect the γ-rays and the charged particles, respectively. Altogether $\approx$140 million $\gamma\gamma$-coincidence events were collected. Approximately 10 million events of them correspond to the reaction channel producing ^{109}Ag. No chiral candidate partner band has been found to the $\pi g_{9/2}\nu(h_{11/2})^2$ band with this statistics, however, the level scheme could be extended by several new levels and γ-transitions.

A preliminary level scheme of ^{109}Ag obtained from the ongoing data analyzis is shown in Fig. 1.

a) iThemba LABS, P.O. Box 722, Somerset West 7129, South Africa

b) Department of Physics, University of York, York, YO10 5DD, UK

c) Centre d Etudes Nucléaires deBordeaux-Gradignan, F-33175 Gradignan, France

d) Faculty of Informatics, University of Debrecen, Hungary

e) Department of Physics, University of Western Cape, Private Bag X 17, Bellville 7535, South Africa

f) INFN and Dipartimento di Fisica, Università di Camerino, via Madonna delle Carceri, I-62032 Camerino, Italy

g) CARST, Yunibesity Ya Bokone-Bophirima, Private Bag X2046, Mafikeng 2735

2.8 Alpha capture reaction of ^{113}In in the p-process energy range

C. Yalçın[a], R. T. Güray[a], N. Özkan[a], S. Kutlu[a], Gy. Gyürky, Zs. Fülöp, G. G. Kiss, Z. Elekes, J. Farkas, E. Somorjai

The p-process is one of the least studied nucleosynthesis processes. Due to the lack of experimental data most p-process nucleosynthesis simulations rely on an extensive use of the Hauser Feshbach model for predicting the relevant reaction rates (e.g. [1]). While the Hauser Feshbach cross section predictions for proton capture on intermediate mass nuclei typically agree well within a factor of two with the observed data [2,3,4], there seem to be considerable discrepancies between the predicted and observed alpha capture cross sections. This is underlined by the first results of alpha capture measurements in this mass range with the goal to probe the reliability of the Hauser Feshbach approach for p-process studies [5,6,7]. This has been interpreted as caused by insufficiencies in the choice of the alpha potential for the Hauser Feshbach calculations and considerable effort has been spent in investigating improved alpha potential parameters [8,9,10].

^{113}In(α,γ)^{117}Sb reaction cross section measurements are being performed at the MGC cyclotron accelerator at energies between 8 MeV and 12 MeV using the activation method. The reaction product ^{117}Sb is relatively long-lived with half-life of 2.8h. The induced activity can be determined through the measurement the characteristic gamma decay transitions of 158keV by using HPGe detector at ATOMKI.

In order to determine target homogeneity and target stability we made test targets from natural indium. The targets were prepared by evaporating natural indium onto thin (d = 2.4μm) Al foil. The Al foil was placed 4.5 cm above the crucible in a holder defining a circular spot with a diameter of 12mm on the foil for In deposition. This procedure made it possible to determine the target thickness by weighing. The weight of the Al foil was measured before and after the evaporation with a precision better than 5μg the indium number density could be determined from the difference.

A test irradiation was made at 12.427MeV energy with a natural indium target. Although the natural indium contains 4.29% ^{113}In, we were able to see clear peak (Eγ=158 keV) coming from ^{113}In(α,γ)^{117}Sb reaction. The obtained spectrum is in Figure 1. For the experiment, targets will be prepared by evaporating highly enriched (93.1%) ^{113}In onto thin Al foil. Thus 158keV peak will be about 22 times more intense at the same energy. This work is in progress.
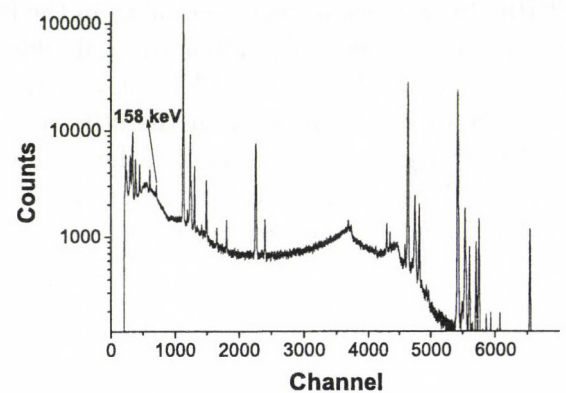

Figure 1. Measured spectrum from natural indium target for test.

a) Kocaeli University, Phys. Dept., 41380, Kocaeli, Turkey.

[1] T. Rauscher, F.-K. Thielemann, At. Data Nucl. Data Tabl. 75 (2000) 1.

[2] S. Sauter, F. Käppeler, Phys. Rev. C 55, (1997) 3127.

[3] S. Harissopoulos et al., Phys. Rev. C 64 (2001) 055804.

[4] F. Chloupek et al., Nucl. Phys. A652 (1999) 391.

[5] E. Somorjai et al., Astron.&Astrophys. 333 (1998) 1112.

[6] W. Rapp et al., Phys. Rev. C 66, (2002) 015803.

[7] N. Özkan et al., Phys. Rev. C, 75(2), (2007) 025801.

[8] P. Mohr, Phys. Rev. C 61, (2000) 045802.

[9] W. Rapp et al., Phys. Rev. C 68 (2003) 015802.

[10] P. E. Koehler et al., Phys. Rev. C 69 (2004) 015803.

2.9 Search for band termination in ^{121}Xe

G. Berek, B.M. Nyakó, J. Timár and the HLHD collaboration[a)]

The high-spin states of ^{121}Xe have been studied, using the ^{64}Ni(^{64}Ni,α3n) nuclear reaction, in order to identify terminating bands in this nucleus. The EUROBALL γ-ray spectrometer and its ancillary charged-particle detector, DIAMANT, were used to collect gamma–particle coincidence events (for experimental details see Ref. [1]). The data were sorted into $\gamma\gamma$- and $\gamma\gamma\gamma$-coincidence matrices by requiring the detection of one α particle.

The level scheme of ^{121}Xe, as shown in Fig. 1, was constructed using the triple-coincidence relations and the energy and intensity balances of the γ-ray transitions. The level spins and parities were deduced from transition multipolarities derived from measured DCO-ratios and linear polarisations. Most of the excited states

known from previous studies [2] were confirmed and some of the previously known bands have been extended to higher spins.

Configuration-dependent cranked Nilsson-Strutinsky-type calculations [3] were performed to help the interpretaion of high-spin states observed in ^{121}Xe and the identification of terminating states. This work is in progress.

a) see A. Al-Khatib *et al.*, ATOMKI Ann. Rep. (2006) 13.,

[1] B. M. Nyakó *et al.*, Acta Physica Polonica B36 (2005) 1033.,

[2] J. Timár *et al.*, J. Phys. G 21 (1995) 783., and references therein

[3] A. V. Afanasjev, D. B. Fossan, G. J. Lane, and I. Ragnarsson, Phys. Rep. 322 (1999) 1.

Figure 1. The observed level scheme of ^{121}Xe
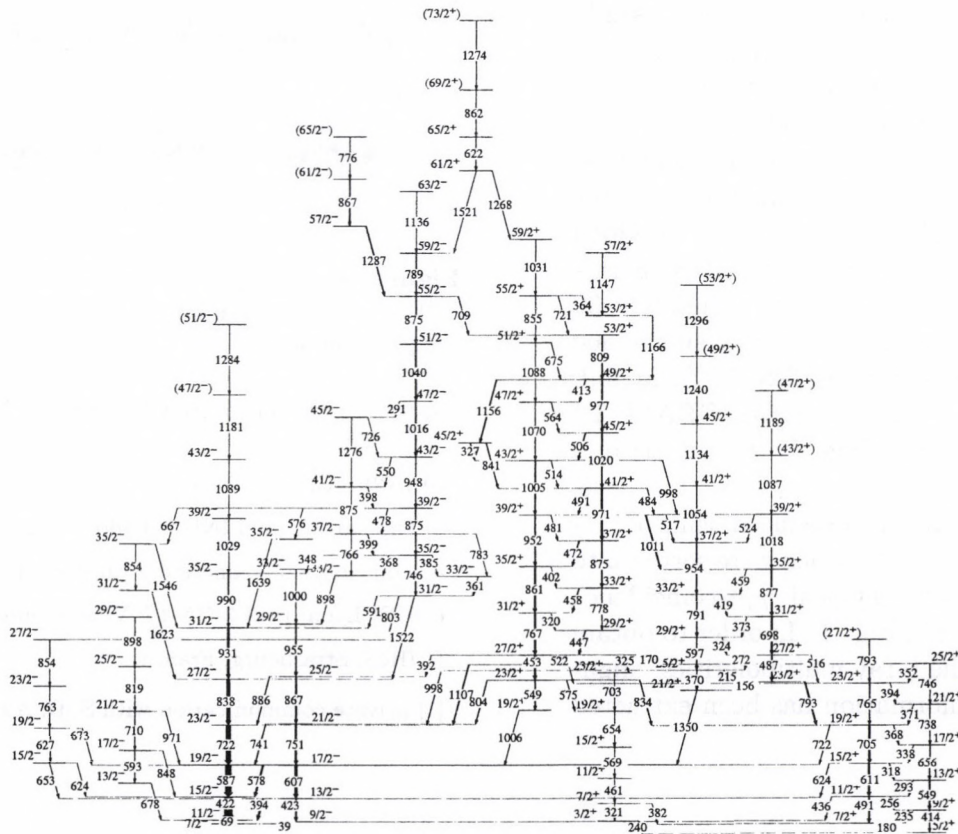
2.10 Rotational band structure in ^{132}La

J. Timár, D. Sohler, I. Kuti, G. Berek, B.M. Nyakó, L. Zolnai, Zs. Dombrádi, E.S. Paul[a], A.J. Boston[a], C. Fox[a], P.J. Nolan[a], J.A. Sampson[a], H.C. Scraggs[a], A. Walker[a], J. Gizon[b], A. Gizon[b], D. Bazzacco[c], S. Lunardi[c], C.M. Petrache[c,d], A. Astier[e], N. Buforn[e], P. Bednarczyk[f], N. Kintz[f]

Spontaneous formation of chirality is a possible explanation for the doublet $\Delta I=1$ rotational bands observed recently in several odd-odd nuclei in the $A\approx130$ and $A\approx105$ mass regions. This scenario is in good agreement with the predictions of Tilted Axis Cranking calculations. However, the most recent results obtained from lifetime experiments for ^{132}La, and ^{134}Pr seem to contradict the chiral interpretation of the doublet bands in these nuclei because the derived B(E2) values are considerably different for the two bands in the doublets. On the other hand, recent theoretical investigations revealed that in some special forms of nuclear chirality the equality of the B(E2) values for the two partner bands may not be necessary [1]. Therefore, it is important to further study these nuclei both experimentally and theoretically in order to find new features that may be characteristic for nuclear chirality.

Rotational bands in ^{132}La were studied using the ^{100}Mo(^{36}S,$p3n$) reaction at a bombarding energy of 160 MeV. The beam was provided by the Vivitron accelerator at IReS, Strasbourg, with an intensity of approximately 30 enA. The target was made of a single 500 μg/cm^2 self-supporting, enriched ^{100}Mo foil. γ rays were detected by the EUROBALL IV spectrometer. Approximately 1.5×10^9 triples coincidence events were collected. The level scheme of ^{132}La has been deduced using $E_{\gamma 1} - E_{\gamma 2} - E_{\gamma 3}$ triples events which were sorted into RADWARE cubes. Typical $\gamma\gamma\gamma$-coincidence spectra are shown in Fig. 1. In order to obtain information on the γ-ray multipolarities, angular correlation information has been extracted from the coincidence data. The linear polarization of the strongest γ-rays were also measured using the 24 clover detectors as Compton polarimeters. The analysis of the data is in progress. According to the preliminary results the level scheme of ^{132}La could be extended by new levels and γ transitions, which may help in assigning configuration to some of the rotational bands.
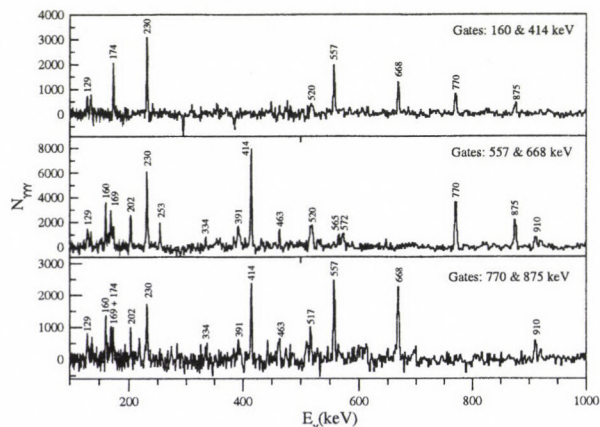
Figure 1. Sample $\gamma\gamma\gamma$-coincidence spectra of ^{132}La obtained in the present work. γ-ray energies are given in keV.

a) OLL, Univ. of Liverpool, Liverpool, United Kingdom

b) IN2P3-CNRS, Grenoble, France

c) Dip. di Fis. and INFN, Padova, Italy

d) University of Camerino, Camerino, Italy

e) IPN Lyon, IN2P3-CNRS, Villeurbanne, France

f) IReS, Strasbourg, France

[1] private communication with S. D. Almehed

2.11 Systematic study of EC decays in the ^{146}Gd region relevant for a Monoenergetic Neutrino Beam Facility

M.E. Estevez[a], A. Algora, B. Rubio[a], J. Bernabeu[a], E. Nacher[a], D. Cano[b], A. Gadea[c], J.L. Tain[a], L. Batist[d], K. Burkard[d], J. Döring[d], M. Gierlik[d], W. Hüller[d], R. Kirchner[d], I. Mukha[d], C. Plettner[d], E. Roeckl[d], J.J. Valiente[e]

The quest of non-zero neutrino mass has been one of the most exciting problems of the last years in physics, given that its evidence puts the Electroweak Theory of the Standard Model under scrutiny. Flavour mixing is a related problem that still needs deep understanding: if the last unknown mixing [U_{e3}] is non-zero, the possibility is open for Charge Conjugation-Parity violation in the lepton sector, which opens a window for new physics. For these topics to be studied, it will be desirable to have an intense tuneable neutrino source, that is, a pure monochromatic neutrino beam.

A monochromatic neutrino beam can be created using accelerated nuclei that decay through electron capture (EC) in a storage ring with long straight sections [1]. The EC process is a two-body problem, so the neutrino energy is well defined, provided mainly one state is populated in the daughter nucleus. Tunning the energy of such beam and detecting the emergence of new flavour in a detector far away can make possible precise measurements of the neutrino oscillation parameters. We have made a systematic study of possible candidates for such a facility in the Gd region and found that certain nuclei of interest were already measured in some of our ealier TAS (Total Absorption Spectroscopy) experiments. For example, ^{152}Yb could be a good candidate as its half-life is small (3.1 s).

The experimental data presented here were obtained during an experiment performed at GSI in 2001. This measurement was performed at the On-Line Mass Separator. This facility provided a high yield of rare earth nuclei around ^{146}Gd. In the measurements, a TAS detector which has both the high intrinsic efficiency and good geometry coverage needed in these studies, was used. The experiment was optimized for the study of ^{152}Tm decay [2], but separated isobaric chain of mass A=152 included also ^{152}Yb, which was produced via the reaction ^{96}Ru(^{58}Ni,2p)^{152}Yb at 4,53 MeV/u (beam energy at the target).

We are presently in the phase of analysing the data. A coincidence between the X ray of an element produced in the EC process and the γ cascade produced in the consequent de-excitation is required in order to separate the EC component of each decay in the TAS spectrum. This is done for each contaminant nucleus of the decay chain, separating their contributions. In Fig. 1 the black line represents the gamma spectra measured by TAS gated by the X rays of Yb's daughter Tm. The grey line is produced by gating on Tb X rays, one of our major contaminants. The ^{152}Er contaminant α-decays to ^{148}Tb ($T_{\frac{1}{2}}$=1h) which is present in all our data as a peak at 620 keV and must be substracted. With the present analysis we aim to demonstrate that the decay of ^{152}Yb proceeds mainly to a single state at 482 keV excitation energy in ^{152}Tm.
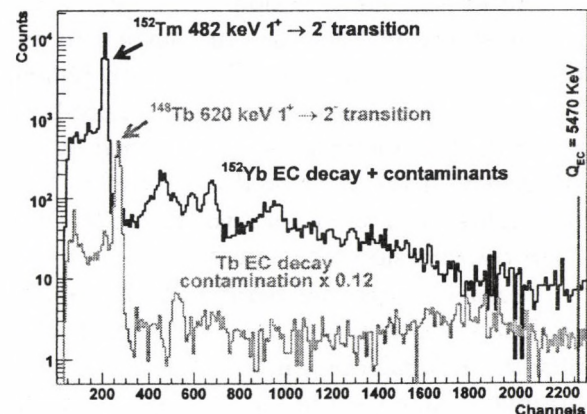

Figure 1. TAS spectra in coincidence with X rays.

a) IFIC, (CSIC-UV), Valencia, Spain,

b) CIEMAT, Madrid, Spain,

c) INFN, Legnaro (Padova) Italy,

d) GSI, Darmstadt, Germany,

e) University of Surrey, Surrey, United Kingdom

[1] J. Bernabeu *et al*, JHEP12(Dec.2005)014

[2] E. Nacher, PhD Thesis, UV, Spain (2004)

2.12   Searching for fission resonances in ^{232}U

L. Csige, M. Csatlós, T. Faestermann[b], Z. Gácsi, J. Gulyás, D. Habs[a], R. Hertenberger[a], M. Hunyadi, A. Krasznahorkay, R. Lutter[a], H.J. Maier[a], P.G. Thirolf[a], H.-F. Wirth[b]

According to recent calculations the depth of the third minimum for U isotopes is predicted to be much deeper than previously believed [1]. Calculations performed in Ref. [1] predicts actually two deep third minima for different values of the reflection-asymmetry.

In our most recent experiment the fission probability of ^{232}U was measured as a function of the excitation energy, using the ^{231}Pa(^{3}He,df) reaction in order to get information about the fission barriers of ^{232}U. The experiment was performed at the Tandem accelerator of the Maier-Leibnitz Laboratory (MLL) at Garching with ^{3}He beam at energy of E=38.1 MeV. The kinetic energy of the ejectiles was analysed by a Q3D magnetic spectrometer set to 35°. Fission fragments were detected by a position sensitive avalanche detector (PSAD) allowing for a detection of the fission fragment angular correlation with respect to the recoil axis ($\Theta_R = 0° - 100°$) with a solid angle coverage of 10% of 4π.

The experimental fission probability spectrum is shown in Fig. 1a). In contrast to our previous results obtained so far for ^{234}U [2] and ^{236}U [3] sharp resonance structure has not been observed. This may partly be explained by the asymmetry of the inner and outer fission barrier heights which does not favor the occurrence of the transmission resonances.

In order to get the parameters of the fission barrier from the measured fission probability JWKB calculation was performed with parametrization used in [4]. Our results on the fission barrier with the deduced parameters are shown in Fig 2. Isotropy of the measured angular distribution (Fig. 1b) indicates the energy interval of subbarrier fission as well as the height of the outer barrier which also supports our previous results.

a) Ludwig Maximilians Univ., München, Germany

c) Technische Univ. München, Garching, Germany
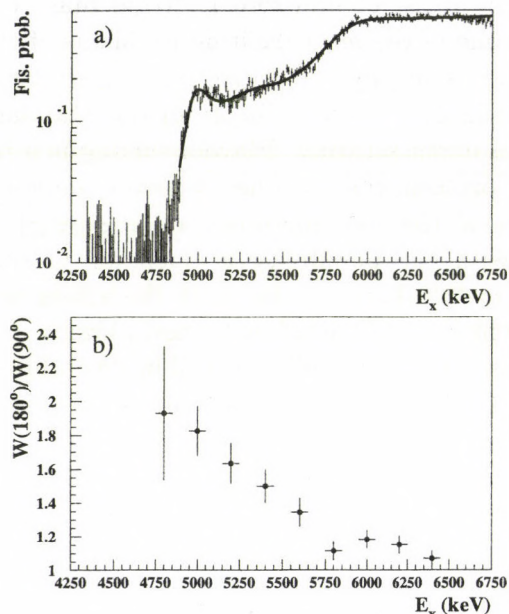
Figure 1. a) Fission probability spectrum with JWKB calculation b) Experimental angular distribution in the function of the excitation energy.
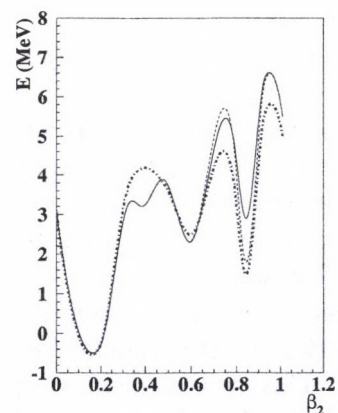
Figure 2. Triple-humped fission barrier of ^{232}U calculated by Cwioc (continuous line) and present work (dashed line).

[1] S. Cwiok *et al.*, Phys. Lett. **B322**, 304. (1994)

[2] A. Krasznahorkay *et al.*, Phys. Lett. **B461**, 15. (1999)

[3] M. Csatlós *et al.*, Phys. Lett. **B615**, 175. (2005)

[4] B. Bhandari *et al.*, Phys. Rev. **C39**, 917. (1989)

2.13 Study of the fission barrier parameters of ^{233}Th

M. Csatlós, L. Csige, T. Faestermann[b], J. Gulyás, D. Habs[a], R. Hertenberger[a], A. Krasznahorkay, H.J. Maier[a], P.G. Thirolf[a] T. Tornyi and H.F. Wirth[b]

From the detailed study of the hyperdeformed states in ^{234,236}U isotopes, we obtained new insight into the fission barrier landscape in the actinide region and shed light on the depth of the third potential energy minimum [1]. In the case of ^{231,233}Th isotopes Blons et al.[2] observed hyperdeformed resonances, claiming the existence of only a shallow third minimum. The fission probability they obtained from the ^{232}Th(d,pf) reaction at $E_d = 13$ MeV is shown in Fig. 1.
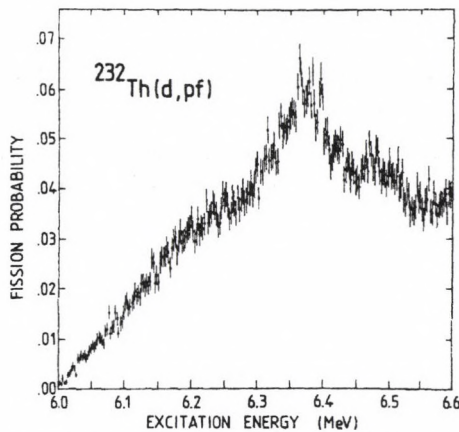
Figure 1. Fission probability of ^{233}Th measured by Blons et al.[2] in the (d,pf) reaction at $E_d = 13$ MeV.

In order to derive more accurate values for the barrier heights and to deduce the depth of the third minimum for ^{233}Th, in our latest experiment we measured the fission probability of ^{233}Th and the angular distribution of the fission fragments following the ^{232}Th(d,pf) reaction using the deuteron beam of the Munich Tandem accelerator at an energy of 14 MeV. A 70 μg/cm^2 thick ^{232}ThO$_2$ target deposited on a 22 μg/cm^2 thin carbon backing was used. The kinetic energy of the proton ejectiles was analysed with a Q3D magnetic spectrometer set at $\Theta_L = 139.2°$ relative to the beam axis, covering a solid angle of 10 msr. The position of the analyzed particles in

the focal plane was measured with a position-sensitive light-ion focal plane detector with individual cathode strip readout of 890 mm active length. Fission fragments were detected by two-position sensitive avalanche detectors (PSAD) constructed at ATOMKI, covering a total solid angle of 2.5 sr. The energy resolution was determined by measuring the low-lying states of ^{233}Th. Taking into account the long-term stability of the Tandem accelerator, the overall energy resolution in the high excitation energy region was 7 keV. The measured fission probability is shown in Fig. 2.
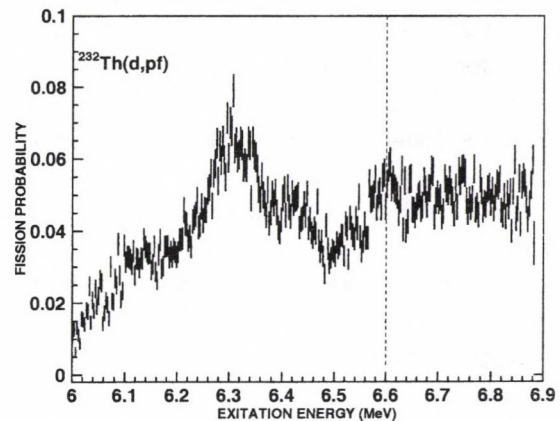
Figure 2. Fission probability of ^{233}Th measured at $E_d = 14$ MeV.

The vertical dashed line marks the upper limit of the excitation energy range measured by Blons et al. [2]. Comparing the present results with the previous ones, a more pronounced shoulder below 6.2 MeV is observed in the new experiment. A more careful analysis of the angular distribution of fragments is presently in progress in order to understand the differences between the two measurements.

a),b) LMU, TU München, Germany.

[1] M. Csatlós et al., Phys. Lett. B615 (2005) 175 and citations therein

[2] J. Blons et al., Nucl. Phys. A414 (1984) 1, A477 (1988) 231.

2.14 New simple form for phenomenological nuclear potential

P. Salamon[a) and T. Vertse[a)

A simple form is introduced for phenomenological nuclear potential as an alternative of the popular Woods-Saxon (WS) form

$$V^{WS}(r) = -\frac{V_0}{1 + e^{\frac{r-R}{a}}}, \qquad (1)$$

which has an infinite range in contradiction with the short range property of the nuclear forces. Therefore the WS shape is cut to zero at a certain finite R_{max} distance:

$$V_{tr}^{WS}(r) = \begin{cases} V^{WS}(r) & , \text{if } r < R_{max} \\ 0 & , \text{if } r \geq R_{max} . \end{cases} \qquad (2)$$

Due to the sharp truncation the function $V_{tr}^{WS}(r)$ has a discontinuity and its derivative does not exists at $r = R_{max}$. Another inconvenient feature of the truncated WS potential is that the distribution of the broad resonant poles does depend on the value of R_{max}. Since in the majority of the publications the R_{max} values are not specified therefore the position of the broad resonances might be quite uncertain. In order to cure the deficiencies of the WS form we approximate it with a combinations of new finite forms like:

$$f_\rho(r) = \begin{cases} -e^{\frac{r^2}{r^2-\rho^2}} & , \text{if } r < \rho \\ 0 & , \text{if } r \geq \rho , \end{cases} \qquad (3)$$

This form is continuous everywhere and its derivatives of all orders disappear at $r = \rho$.

$$V^{new}(r) = c_0 f_{\rho_0}(r) + c_1 f'_{\rho_1}(r) = V(r, c_0, c_1, \rho_0, \rho_1) . \qquad (4)$$

In order to get the best fit of the new potential to the central WS term we minimize the integral

$$\int_0^{\rho_>} [V(r, c_0, c_1, \rho_0, \rho_1) - V_{tr}^{WS}(r)]^2 dr , \qquad (5)$$

as function of the new parameters, where $\rho_> = max\{\rho_0, \rho_1\}$. The parameters of the WS potential: V_0, R, a and R_{max} are kept fixed during the minimization procedure.

We observed [1] that a typical WS form can be approximated reasonably well with the new form in Eq.(4) with four adjustable parameters. From the new parameters c_0 resembles to V_0 and ρ_1 resembles to R. The range ρ_0 of the new potential takes over the role of the cutoff radius of the WS potential, although its value is much smaller than R_{max}. The difference $\rho_0 - \rho_1$ correlates with the a diffuseness of the WS form.

For a matching distance $R_m \geq \rho_0$ the pole position is independent of R_m. If we use the new form the range of the nuclear interaction is defined unambiguously in contrast to the WS form.

If we complement the new potential with a spin-orbit term in Eq.(6) the single particle spectra of the WS and the new forms are very similar. This is true not only in the bound state region but in the resonant region as well.

$$V_{so}^{new}(r) = -\frac{c_{so}}{r c_0} 2(\vec{l} \cdot \vec{s}) \frac{dV(r)}{dr} . \qquad (6)$$

The sequence of the single particle levels of a WS potential with realistic parameters can be reproduced reasonably well with the new potential in which even the positions of the broad resonances are free from uncertainties.

Therefore we suggest to use the form in Eq.(4) as a new finite range potential instead of the truncated Woods-Saxon form.

a) University of Debrecen, Faculty of Informatics, H-4010 Debrecen, P. O. Box 12, Hungary

[1] P. Salamon, T. Vertse, Phys. Rev. C, submitted

2.15 Shell correction and function approximation

P. Salamon[a], A.T. Kruppa

The prediction of nuclear masses is of fundamental importance for nuclear science. Despite the great progress of self-consistent models the so called macroscopic-microscopic method remains one of the most important tool for mass calculation. The macroscopic part of the binding energy is described by the finite range liquid drop model. The microscopic part consist of the shell and pairing energy. For the description of the shell energy Strutinsky introduced two methods. In the first method one averages over the single particle spectrum and in the second method the average is over the particle number. The second method was never widely used. Recently a new type of averaging over the particle number space have been introduced [1]. This new formalism is very simple however the mathematical foundation of it is very incomplete. The basic ingredient of the shell correction in particle number space is the function approximation which is a standard part of the mathematical science. Our aim was to investigate the performance of different and mathematically well established methods in the context of the shell correction calculations.

For a given mean field potential the single particle energies are e_i. The total energy is $E(N) = \sum_{i=1}^{N} e_i$. We may consider this relation as the definition of an unknown one variable function $E(\cdot)$. The function $E(\cdot)$ is given only at discrete points. From the pairs $(N, E(N))$ one has to construct a function $\tilde{E}(\cdot)$ which approximate the unknown $E(\cdot)$. It is easy to construct an interpolating function but we want a smooth approximation which describes the average behavior of $E(\cdot)$. The shell correction for a given particle number N is given by $E(N) - \tilde{E}(N)$. In [1] the smooth part of the energy is of the form $\tilde{E}(N) = \sum_{N'} C_{N'} E(N') \exp(-(N-N')^2/\gamma^2)$. This approximation is similar to the Gaussian kernel

method of the mathematics. The rigorous theory is the Tikhonov regularization, where the unknown coefficients $C_{N'}$ are determined by minimizing $\sum_{N'} (E(N') - \tilde{E}(N'))^2 + \lambda ||\tilde{E}||_{\mathcal{H}}$. The value of the regularization parameter λ determines the 'degree' of the approximation. Interpolation corresponds to $\lambda = 0$. The Figure shows the input data pairs of $(N, E(N))$ and two smoothed binding energy curves. One of them gives overfitting (similar to interpolation). The single particle energies were calculated using a potential for ^{226}Os. We are currently working on the problem how to choose the regularization parameter properly. An another branch of approaches is the iterative regularization methods (conjugate gradient, minimal residual, Landweber-Friedman). Presently we are also investigating how they perform in the shell correction method.
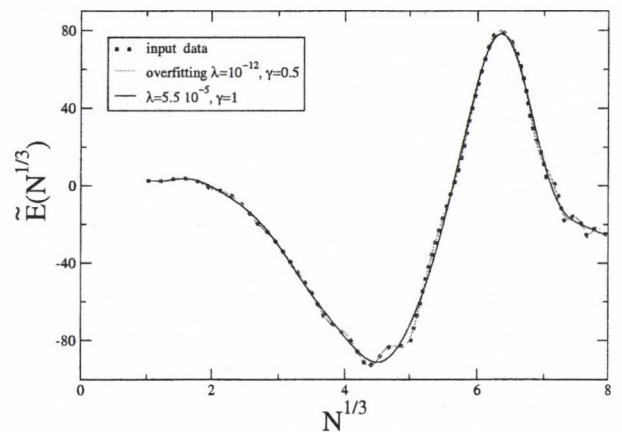
a) University of Debrecen, Faculty of Informatics, H-4010 Debrecen, P.O. Box 12, Hungary

[1] K. Pomorski, Phys. Rev. C., 70, 044306 (2004)

3.1 A new experiment for the existence of the left-right asymmetry in outer s-shell photoionization

T. Ricsóka, S. Ricz, Á. Kövér, K. Holste[a], A. A. Borovyk, Jr.[a], S. Schippers[a], D. Varga and A. Müller[a]

In the electromagnetic interaction parity is conserved, i.e., all processes are invariant under a mirror transformation of the coordinate system. However, in the last years we observed a left-right asymmetry in the double differential cross sections of the outer s-shell photoelectrons ionized by linearly polarized synchrotron radiation [1]. The left-right asymmetry parameter A_{LR} was determined from [1]:

$$A_{LR} = \frac{\sigma_L - \sigma_R}{\sigma_L + \sigma_R}, \qquad (1)$$

where σ_L and σ_R are the cross sections for photoelectron emission to the left (L) and to the right (R) hand sides, respectively, with respect to the photon propagation direction (see Fig. 1 in Ref. [1] for further details).

In order to verify our previous observation [1] a series of measurements were carried out to study the left-right asymmetry parameters for the following s-shells of noble gas atoms: He 1s, Ne 2s, Ar 3s and Xe 5s. The aim of present investigation was to test whether the left-right asymmetry parameters depend on the photon source.

The experiment was carried out at the beamline BW3 of the DORIS-III storage ring. The linear polarization of the photonbeam was monitored by recording the angular distribution of Ne 2s photoelectrons. A polarization degree of 100 % was found. The emitted electrons were analyzed with a newly built ESA-22 type [2] electron spectrometer of the Institute for Atomic and Molecular Physics (Giessen). This electron energy analyzer is capable of measuring the complete angular range of emitted electrons simultaneously (15°- 345° with 15° steps). Therefore, the confidence in the pattern of the angular distribution is very high. Any instabilities in the photon flux or in the density of the target atoms produce the same effect at all angles.

At the exit of the analyzer the energy an-alyzed electrons were counted by 22 channeltrons covering an angular range of 10° each. Their relative efficiencies were determined by measuring the angular distribution of the Ar $L_3 - M_{2,3}M_{2,3}$ $^2D_2$ diagram Auger line at 203.3 eV kinetic energy. All spectra were normalized to this Auger electron line. Photoelectrons ejected from the outer s-shells were collected at the same kinetic energy (E_{kin}) in order to ensure equal conditions for the measurements of Auger electrons and photoelectrons.
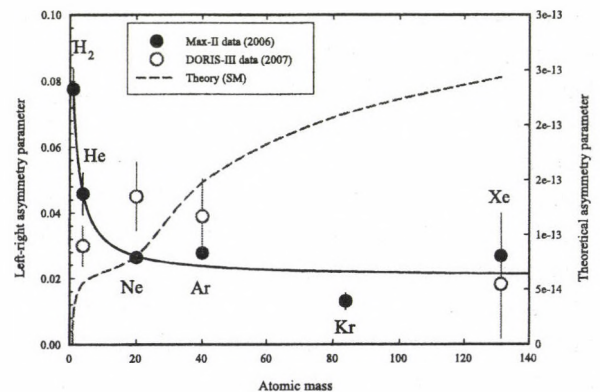
Figure 1. The experimental and theoretical s-shell left-right asymmetry parameters as a function of the atomic mass for H_2 molecule and for the noble gases from He to Xe. The solid circles show the measurement from Ref. [1] (the solid line is drawn to guide the eye) and the open circles are the present data. The dashed line and right hand scale denote the theoretical estimation of the left-right asymmetry parameters.

Figure 1. shows the comparison between our previous (solid circles) [1] and present (open circles) experimental left-right asymmetry parameters as well as the calculated one (dashed line and right hand scale). The theoretical estimation is based on the parity violation by the weak interaction through the exchange of a Z_0 boson between atomic nucleons and electron shell [1]. The figure shows a very good agreement between the two experi-

mental data sets. The definite non-zero asymmetry parameters suggest the breakdown of space inversion symmetry in photoionization. The present measurements confirm strongly our statement from Ref. [1] that the observed left-right asymmetry cannot originate from the weak interaction. It can be seen that the order of magnitude and the Z-dependence of the calculated data are in contradiction with both measurements. Another explanation was suggested in Ref. [1]. Namely, if the photon package is extremely short in the case of synchrotron radiation and the phase difference between the carrier-envelope and the VUV photon is constant, left-right asymmetry (or virtual parity violation) may exist similarly to the ultra short laser light-atom interactions observed by Paulus et. al. [3]. The good agreement between the two experimental data sets means that the time structure and phase difference between the carrier-envelop and the photons are same for both synchrotrons (Max-II in Lund, Sweden and DORIS-III in Hamburg, Germany) which is inconceivable.

In conclusion, a left-right asymmetry has been observed in photoionization created by linearly polarized synchrotron radiation. The experimental left-right asymmetry parameters were determined for photoelectrons ejected from the outer s-shells of noble gas atoms He, Ne, Ar and Xe. The present observation together with our previous one [1] strongly indicates that the left-right asymmetry is a result of a real physical process and cannot be interpreted as an instrumental effect.

Both experimental asymmetry data sets do not increase with increasing nuclear mass. This behaviour and the order of magnitude of the measured effect do not agree with the theoretical predictions for parity violation by the weak interaction (see Fig. 1.). Present non-zero left-right asymmetry parameters refute the interpretation of the breakdown of space inversion symmetry with a few cycle VUV photon package. It is hard to believe that two different synchrotrons and beamlines exhibit exactly the same carrier-envelopes, phase differences and time structures of the photon pulses.

The present results cannot be explained with existing models and experiments for the breakdown of atomic space inversion symmetry. Further experimental work is needed to investigate the behavior of the left-right asymmetry in more detail. We hope to stimulate theoretical research into the origin of the observed puzzling effect.

a) Institute for Atomic and Molecular Physics, Justus-Liebig University, D-35392 Giessen, Germany

[1] S. Ricz, T. Ricsóka, Á. Kövér, D. Varga, M. Huttula, S. Urpelainen, H. Aksela and S. Aksela, New J. Phys. **9**, 274 (2007).

[2] S. Ricz, Á. Kövér, M. Jurvansuu, D. Varga, J. Molnár, and S. Aksela, Phys. Rev. A **65**, 042707 (2002).

[3] G. G. Paulus, F. Grasbon, H. Walther, P. Villoresi, M. Nisoli, S. Stagira, E. Priori and S. De Silvestri, Nature **414**, 182 (2001).

3.2 Ionization of the hydrogen atom in intense ultrashort laser fields

S. Borbély[a], K. Tőkési, L. Nagy[a]

The ionization of the atomic hydrogen by intense ultrashort laser pulses is studied theoretically. The calculations were performed applying quantummechanical and classical approaches. The classical calculations were done within the framework of the classical trajectory Monte-Carlo (CTMC) method, where the Newton's classical nonrelativistic equations of motions are solved [1] numerically when an external sine-square enveloped electromagnetic field is included.

Treating the problem quantummechanically, the solution of the time dependent Schrodinger equation (TDSE) of our system is searched in the following form

$$\Psi(t) = \int d\vec{k} c(\vec{k}, t) \Psi_V(\vec{k}, t), \qquad (2)$$

where $\Psi_V(\vec{k}, t)$ are the Volkov wavefunctions. This approach transforms the TDSE into momentum space

$$\frac{\partial}{\partial t} c(\vec{q}, t) = -\frac{i}{(2\pi)^3} \int d\vec{s} c(\vec{s} + \vec{q}, t) \times$$

$$\times \quad e^{-\frac{i}{2} \int_0^t dt' \vec{s}(\vec{s} + 2\vec{q} + 2\vec{A}(t'))} \int d\vec{r} V(\vec{r}) e^{i\vec{s}\vec{r}} \quad (3)$$

where the equation for the expansion coefficients is solved iteratively. In the first iteration step the Coulomb potential, $V(\vec{r})$ is neglected and the obtained approach is identical with the Volkov model. Using the Volkov solution in the right hand side of the Eq. (3) the first order solution was derived.

The double differential ionization probabilities as a function of ejection energy and ejection angle were calculated using CTMC, Volkov and first order model for different laser pulse parameters. At a large scale all three models predicts the same probability distributions. In each approach the electrons are ejected with maximum probability along the polarization vector $\hat{\varepsilon}$.
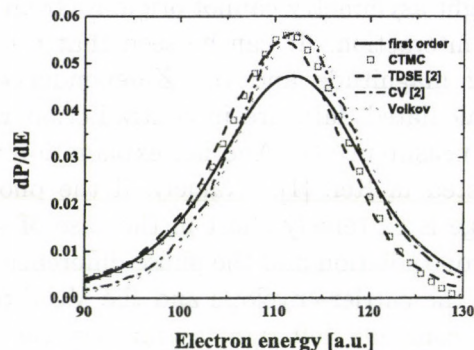
Figure 1. The spectrum of the photoelectrons for a laser pulse with duration of 3 a.u. and with intensity of $E_0 = 10$ a.u.

The spectrum of the photoelectrons was obtained from the ionization probability density by integrating over the ejection angles. The results given by our models was also compared with results provided by the Coulomb-Volkov(CV) model and by the numerical solution of the TDSE [2]. On Fig. 1. a good agreement is observed between the TDSE and CTMC curves, which confirms the classical nature of the over the barrier ionization. The agreement between the first order and TDSE results is also good and it is better then the agreement between the TDSE and other quantum models (CV, Volkov).

a) Babeş-Bolyai University, Faculty of Physics, 400084 Cluj, Kogalniceanu str. nr. 1, Romania

[1] K. Tőkési, G. Hock, Nucl. Instr. Meth. B **86**, 201 (1994).

[2] G. Duchateau et. al., J. Phys. B: At. Mol. Opt. Phys. **32**, L571 (2000)

3.3 Influence of the Coulomb interaction on the ionization of the hydrogen atom by intense ultrashort laser pulses

S. Borbély[a], K. Tőkési, L. Nagy[a]

The ionization of the hydrogen atom in intense laser field is studied theoretically employing quantummechanical and classical models. Classical calculations were performed within the framework of the classical trajectory Monte-Carlo (CTMC) method and the obtained results are considered to be the "exact" ones. For quantummechanical calculations the Volkov and the first order models were used. The main difference between them is that in the Volkov model the Coulomb interaction between the ionized electron and the residual ion is neglected. The comparison of the first order and Volkov results allow us to study in details the influence of the Coulomb interaction during the laser pulse.
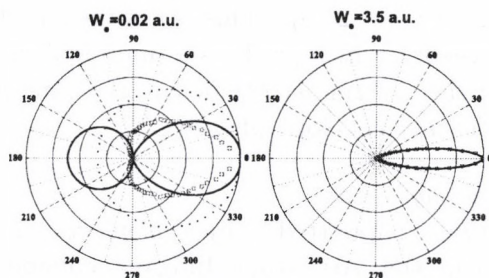
Figure 1. The angular distribution of the electrons ejected with a given energy (W_e) for a laser pulse with duration of 5 a. u. and with intensity of 1 a. u. Solid line - first order; Dotted line - Volkov; Squares - CTMC.

The angular distribution of the electrons ejected at given energies is studied in details. At low ejection energies (see Fig. 1.) big discrepancies are observed between the first order and Volkov distributions. The observed discrepancies diminishes and disappears at higher ejection energies, which indicates that during the ionization the electrons with high ejection energies are less influenced by the Coulomb interaction then the electrons with low ejection energies. This can be explained using a simple intuitive picture presented on Fig. 2. The

electrons with high ejection energy have their momentum in the initial state in the same direction as the net momentum transfer leading to a trajectory, with a very small portion close to the core where the Coulomb potential has a significant influence. On the other hand the electrons with lower ejection energies have a momentum in the initial state, which leads in the opposite direction of the net impulse transfer. In this way the low energy electrons need to "go around" the core, leading to a trajectory, which has a long portion close to the core, where they can be influenced significantly by the Coulomb interaction.
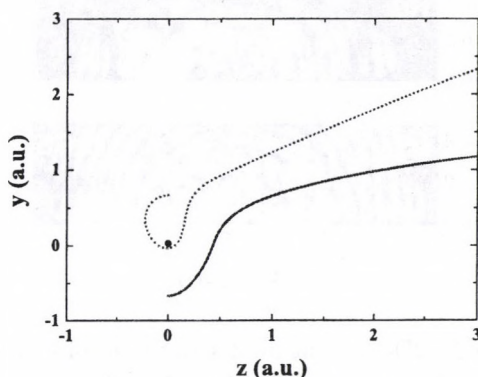
Figure 2. Two possible electron trajectories during the ionization corresponding to electrons with high (Solid line) and low (Dotted line) ejection energies.

a) Babeş-Bolyai University, Faculty of Physics, 400084 Cluj, Kogalniceanu str. nr. 1, Romania

39

3.4 Beyond the strong field model in atomic single photoionization

D.G. Arbó,[a,b], J.E. Miraglia,[a,b], M.S. Gravielle,[a,b], P.A. Macri,[c], V.D. Rodriguez,[b], K. Tőkési, K. Schiessl,[d] E. Persson,[d] J. Burgdörfer[d]

We investigate the effect of the Coulomb potential of the atomic core on the dynamics of the detached electron for single ionization by strong short-laser pulses. In the present work, we make use of a time-dependent distorted-wave theory, the Coulomb-Volkov (CV) approach [1], which allows us to consider the effect of the remaining core at the same level of approximation. In this way, we can probe the effect of the core potential on the dynamics of the detached electron.
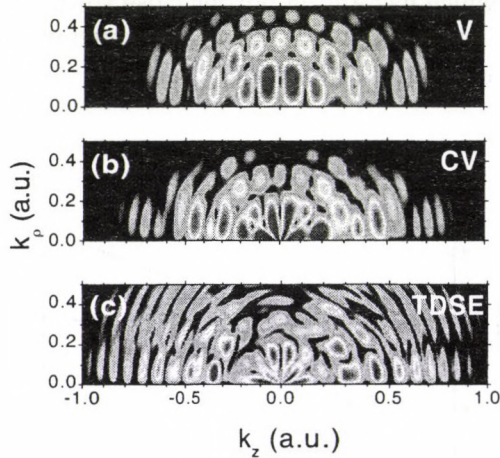
Figure 1. 2D-momentum distributions of emitted electrons from H. Laser wavelength 910 nm, intensity 5x1013 W/cm2 and duration 10 fs. (a) Volkov (SFA), (b) Coulomb-Volkov, and (c) ab initio calculations.

We compare CV and the standard Volkov (V) approximation with full numerical results of the time-dependent Schrödinger equation (TDSE) [2]. The V model is not adequate to resemble the full electron emission momentum spectrum, i.e., the near-threshold interference structure [fig. 1(a)] [2-4] and the cusp of the transverse momentum distribution [fig. 2(a)]. In turn, as the distorted final state in the CV theory includes the distortion introduced by the Coulomb potential, it reproduces the low-energy interference pattern [fig. 1(b)] as also the cusp in the transversal momentum distribution [fig. 2(a)].
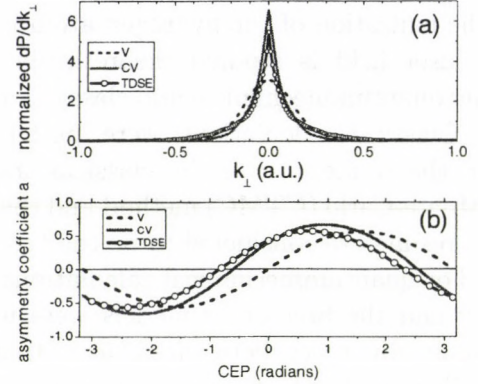
Figure 2. (a) Transversal momentum distribution, (b) asymmetry parameter as a function of the CE phase.

A study of the momentum distributions for zero carrier-envelope phase shows that the CV theory accounts also for the backward-forward asymmetry [fig. 2 (b)]. This is not the case for the V theory, which predicts a sinusoidal function of the asymmetry coefficient as a function of the carrier-envelope phase (CEP).

a) Institute for Astronomy and Space Physics, IAFE, CC67, SUC. 28 (1428) Buenos Aires, Argentina

b) Department of Physics, FCEN, University of Buenos Aires, Argentina

c) Departamento de Física, Universidad Nacional de Mar del Plata, 7600 Mar del Plata, Argentina

d) Institute for Theoretical Physics, Vienna University of Technology, A-1040 Vienna, Austria

[1] P.A. Macri, et al., J. Opt. Soc. Am. B 20, 1801 (2003); V.D. Rodriguez, et al., Phys. Rev. A 69, 053402 (2004).

[2] D.G. Arbó et al., Phys. Rev. Lett. 96, 143003 (2006).

[3] A. Rudenko et al., J. Phys. B 37, L407 (2004).

[4] C.M. Maharjan et al., J. Phys. B 39, 1955 (2006).

40

3.5 Emission of electrons in atomic single ionization by sudden momentum transfer: Quantum and classical distributions

D.G. Arbó[a], K. Tőkési

We investigate the electron emission from hydrogen atom in the framework of a sudden momentum transfer (Δp). We calculate the various distributions of emitted electrons both quantum mechanically, by solving the time-dependent Schrödinger equation (TDSE) and classically, using a classical trajectory Monte Carlo (CTMC) method [1].
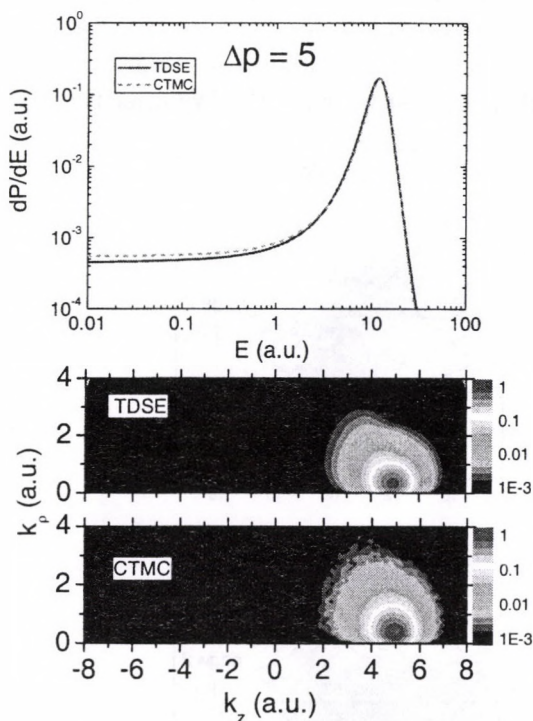

Figure 1. Up: Energy distribution of emitted electrons. Down: 2D-momentum distributions. The net momentum transfer is $\Delta p = 5$ a.u.

We show that the energy and the doubly-differential momentum distributions look quite alike in TDSE and CTMC approaches (see Fig. 1). In both cases the energy distribution possesses a maximum at $E = (\Delta p)^2/2$, and the momentum distribution has a maximum at $\Delta p = 5$ along the momentum transfer direction, as expected [2]. Discrepancies are found for small Δp, where the classical total ionization probabilities are smaller than the quantum one and the distributions are different. Despite the

quantum-classical correspondence for the 2D-momentum distributions, the maximum of the quantum partial population is at lower angular momentum than that of for classical one. This is due to the discrepancy between the classical and quantal initial spatial distribution (Fig. 2).
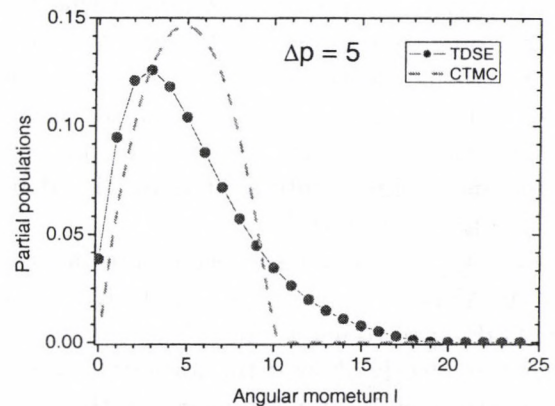
Figure 2. Angular momentum of emitted electrons calculated both quantum-mechanically (TDSE) and classically (CTMC).

We also investigate the sudden momentum transfer using the Coulomb-Volkov approximation (CVA) [3]. We observe that the CVA is appropriate for the quantal description of various distributions of emitted electrons by a sudden momentum transfer.

a) Institute for Astronomy and Space Physics, IAFE, CC67, SUC. 28 (1428) Buenos Aires, Argentina

[1] D.G. Arbó et al., Phys. Rev. Lett. 96, 143003 (2006).

[2] D.G. Arbó et al., Phys. Rev. A 60, 1091 (1999).

[3] P.A. Macri, et al., J. Opt. Soc. Am. B 20, 1801 (2003); D.G. Arbó et al., Phys. Rev. A 77, 013401 (2008).

3.6 Observation of the two-electron cusp in atomic collisions: Evidence for strong electron-electron correlation

L. Sarkadi and A. Orbán

In this report we present experimental data for a process when two electrons with velocity vectors equal to that of the projectile are emitted from collisions. By observing the two-electron cusp the study of the threshold phenomenon for two-electron break-up is possible. It is a particulary interesting question whether the outgoing charged projectile can attract the two repulsing electrons so strongly that the two-electron cusp is formed. If it is so, a further question arises: Are the two electrons correlated in the final state as it is predicted by the Wannier theory [1]?

The experiments have been done at the 1 MeV VdG accelerator of ATOMKI using our TOF spectrometer [2]. The first measurements clearly showed the formation of the two-electron cusp and signature of the electron correlation in 200 keV He^0+He collisions [3]. These promising results motivated us to carry out the experiment at 100 keV beam energy where the coincidence count rate is still reasonable but the energy resolution is better. For an acceptable data acquisition time we improved our data acquisition and data processing system for triple coincidence measurements. In Fig. 1a we present our measured relative fourfold differential cross section (FDCS) that shows strong electron correlation. For a comparison, in Fig. 1b we displayed the contour plot for *uncorrelated* electron pair emission. These latter data were synthesized artificially, generating the energies of the electron pairs from two independent double coincidence experiments. In both figures the distributions are characterized by two ridges. In Fig. 1b the ridges are perpendicular straight lines ($E_1 = E_2 = .13.6$ eV). As a result of the correlation, the ridges in Fig. 1a are distorted in such a way that they have a joint straight-line section following the line $E_1 + E_2 = 27.2$ eV. This means that the electron pairs in the vicinity of the cusp maximum are emitted with a center-of-mass velocity equal to that of the projectile.

The two-electron emission from a moving center strongly suggests the picture of formation of quasi-stationary low-lying two-electron continuum states around the projectile. On the basis of this picture the observed strong energy correlation can be explained by an angular correlation of 180° in the projectile-centered reference system: The correlation between the low- and high-energy emission in the laboratory system corresponds to that between backward and forward emission in the projectile frame. This result is consistent with the Wannier theory.
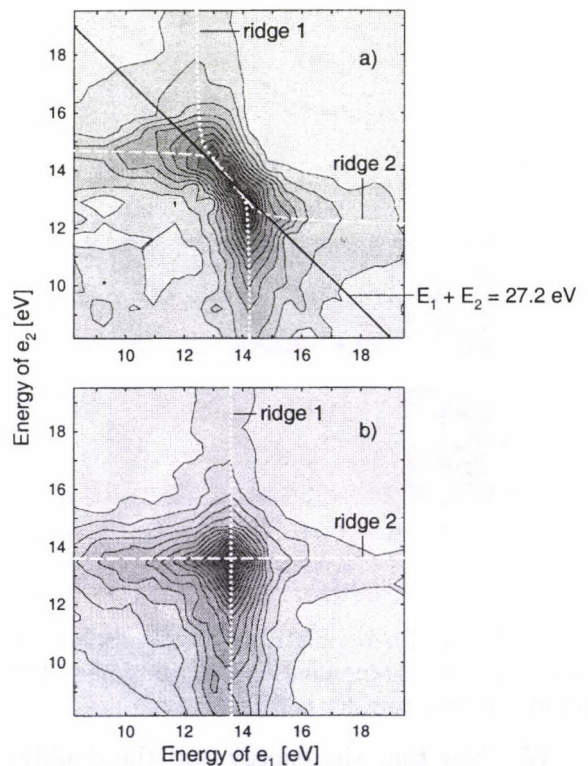

Figure 1. Contour plots of FDCS as a function of the electron energies obtained at 0° in 100 keV He^0+He collisions. Part (a): Measured FDCS. Part (b): FDCS for uncorrelated electron emission.

[1] G.H. Wannier, Phys. Rev. 90 (1953) 817.

[2] L. Sarkadi and A. Orbán, Meas. Sci. Technol. 17 (2006) 84-90.

[3] L. Sarkadi and A. Orbán, ATOMKI Annual Report (2006) 30.; L. Sarkadi and A. Orbán, Phys. Rev. Lett. (2008) in press

3.7 Search for multiple electron scattering sequences in simple systems

K. Tőkési, B. Sulik

Double differential spectra of electrons ejected in ion-atom or ion-solid collisions are in the focus of general interest for a long time. These spectra are relatively easy to measure, and they show many fine details relevant for the collisions dynamics. In the past decade special effort has been devoted to understand the high energy part of the electron spectra. Significantly enhanced emission of fast electrons far above the so-called binary encounter energy was observed in both ion-atom and ion-solid collisions [1,2]. In some cases, fast electrons have been identified from double, triple and quadruple scattering by the projectile and target cores [2]. The ejected electron gains energy in every encounter with the projectile in such processes. This mechanism is often referred to as Fermi-shuttle acceleration.

Most of the experiments were performed with dressed heavy projectiles and heavy target atoms, where the cross section is large enough for observing multiple scattering processes. No quantum calculations were possible at such complexity, only classical trajectory Monte-Carlo (CTMC) calculations have been performed for modeling these collisions [2]. Surprisingly, quantitative agreement has been found for many collision systems. Moreover, the analysis of the classical particle trajectories allows one to identify multiple scattering events in the classical sense.

The aim of this work is to study the process for simpler collision systems, which can be handled by both classical and quantum calculations. The relevant cross sections might be too small to be measured, but they can be identified and compared in classical and quantum calculations. In the present work, as a first step, we apply the CTMC method for 25

keV He^{2+} + H collisions at selected impact parameter (b) values. The first results, calculated differential ionization probabilities at $b = 0.05$ a.u, are shown in Fig. 1. The electron yield above 13.6 eV kinetic energy is expected to originate from multiple scattering. An additional feature is the predicted large enhancement of the electron yield at backward observation angles.
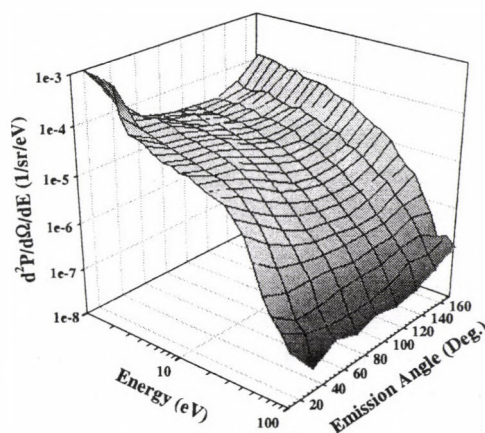
Figure 1. Double differential ionization probablility, $P(\theta, E)$, in collision between 25 keV He^{2+} and H at an impact parameter $b = 0.05$ a.u.

[1] S. Suarez et al., Phys. Rev. Lett. **77** (1996) 474; U. Bechtold et al., Phys. Rev. Lett. **79** (1997) 2034, G. Lanzano et al., Phys. Rev. Lett. **83** (1999) 4518.

[2] B. Sulik et al., Phys. Rev. Lett. **88** (2002) 073201; B. Sulik and K. Tőkési, Adv. Quant. Chem. **52** (2007) 253.

3.8 Ab initio molecular treatment of charge transfer processes induced by collision of C^{2+} ions with the OH radical

E. Bene, Á. Vibók[a], G.J. Halász[b], M.C. Bacchus-Montabonel[c]

Interaction of ionizing radiation with biological tissue can induce severe damage to DNA. Up to now, direct processes have been mainly considered, but, from a biophysical point of view, very important damage is caused by indirect processes, in particular, the action of ions on water molecules produces OH radicals which can then interact strongly with the biological medium. From the experimental point of view excitation and fragmentation processes have been mainly investigated, but charge transfer has been shown to be a complementary process [1,2].

In this work the charge transfer of C^{2+} ions in collision with the OH radical has been studied theoretically by means of ab initio quantum chemistry molecular methods followed by a semiclassical dynamical treatment in the $[0.1 - 0.35]$ a.u. collision velocity range. In this first step, the linear approach has been investigated, taking account of the influence of the variation of the distance r_{OH} of the target during the process.

The total cross-sections are presented in Figure 1 for the different geometries of the OH target. The results show clearly a regular increase of the cross-sections when the vibration coordinate is reduced from $r_{OH} = 2.0$ to $r_{OH} = 1.7$ a.u.. On the contrary, for the shorter OH distance $r_{OH} = 1.6$ a.u., there is a first decrease of the total cross-section at lower velocities before reaching the more regular variation previously observed. Such a distance corresponds to a very strongly constrained OH geometry and the collision with C^{2+} could lead to a strong and very rapid relaxation of the target.

Figure 1. Charge transfer cross-sections for the C^{2+} - OH system for the different geometries of the OH radical.

a) University of Debrecen, Department of Theoretical Physics, P.O. Box 5, H-4010 Debrecen, Hungary

b) University of Debrecen, Department of Information Technology, P.O. Box 12, H-4010 Debrecen, Hungary

c) CNRS et Université de Lyon, Laboratoire de Spectrométrie Ionique et Moléculaire, 69622 Villeurbanne Cedex, France

[1] M.-C. Bacchus-Montabonel, M. Łabuda, Y.S. Tergiman, J.E. Sienkiewicz, Phys. Rev A 72, 052706 (2005).

[2] M.-C. Bacchus-Montabonel, Y.S. Tergiman, Phys. Rev. A 74, 054702 (2006).

3.9 Double ionisation of He within the frame of independent event model

L. Gulyás, A. Igarashi[a), P. D. Fainstein[b) and T. Kirchner[c)

For those numerous collision processes, where the correlated motion of electrons are negligible, the independent event model (IEV) provides a simplified but realistic tool for the theoretical evaluation [1]. The IEV can also be invoked for investigating correlated mechanism as deviations between the confronted experimental and theoretical results might indicate the possible role of *e-e* interaction. It is obvious that an accurate evaluation of IEV probabilities and cross sections are very important in order to get the appropriate conclusion.

The accuracy of the IEV probabilities rely mostly on the evaluation of the one-electron transitions amplitudes that for a general case of ionisation can be obtained as [2]

$$a(\boldsymbol{\rho}) = \sum_{\mu=-\infty}^{+\infty} \sum_{lm} (-i)^{|\mu+\Delta m|} Y_l^m(\mathbf{k})$$
$$e^{-i\mu\varphi_e + i(\mu+\Delta m)\varphi_\rho} \int_0^\infty \eta d\eta J_{|\mu+\Delta m|}(\rho\eta) R_\mu^{lm}(\eta), \quad (4)$$

where $\boldsymbol{\rho} \equiv (\rho, \varphi_\rho)$ denotes the impact parameter, $\Delta m = m - m_i$ is the change of the azimuthal quantum number of the electron emitted with momentum vector $\mathbf{k}$. $R_{lm}^\mu(\eta)$, which is more often easier to evaluate than $a(\rho)$, is the partial transition amplitude as a function transverse momentum transfer $\boldsymbol{\eta} \equiv (\eta, \varphi_\eta)$. The sum over μ express the azimuthal variation of $R_{lm}(\boldsymbol{\eta})(= \sum_\mu e^{i\mu\varphi_\eta} R_{lm}^\mu(\eta, \varphi_\eta))$ correspond to the distortion effects of the projectile field on the ejected electron distribution.

In many applications of IEV a further approximation is implemented by replacing the $J|\mu + \Delta m|$ Bessel functions (in the above formula) with the simplest J_0 term (see [3] and references therein). This is a serious simplification as it completely modify the relative contribution of partial transition amplitudes and the distortion effects caused by the projectile.

This well seen in the figure, where the total cross sections for double ionisation (DI) of He by proton are presented. The DI cross section, within the framework of the IEV model, can be evaluated as

$$\sigma_{DI} = 2\pi \int_0^\infty d\rho\, \rho\, P_{He}(\rho) P_{He^+}(\rho), \quad (5)$$

where $P_X(\rho) = |a_X(\rho)|^2$ denotes the one-electron ionisation probabilities, respectively, for He and He$^+$ targets.
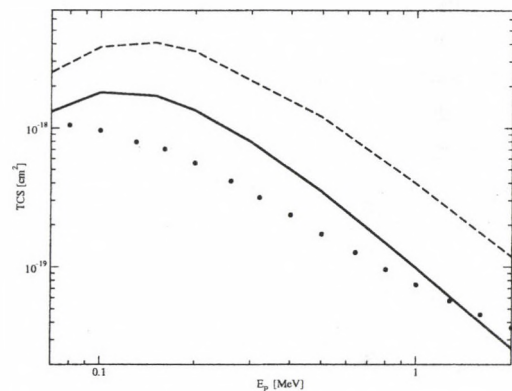

Figure 1. Total cross sections for double ionisation of He by proton impact evaluated within the frame of IEV. Solid line: present CDW-EIS calculation; dashed line: present CDW-EIS calculation with a change of all $J_{|\mu+\Delta m|}$ to J_0 in (4), (see ref. [4] for more details). • experimental data [5].

a) Dept. of Applied. Physics., Univ. of Miyazaki, 889-2192, Japan

b) Centro Atómico Bariloche, 8400 Bariloche, Argentina

c) Inst. für Theor. Phys., TU Clausthal, D-38678 Clausthal-Zellerfeld, Germany

[1] M. McCartney, J. Phys. B **bf 30** (1987) L155

[2] P. D. Faistein *et al*, J. Phys. B **bf 29** (1996) 1225

[3] M. Fiori *et al*, J. Phys. B **bf 39** (2006) 1751

[4] L. Gulyás *et al*, J. Phys. B **bf 41** (2008) 025202

[5] M. B. Shah and H. B. Gilbogy, J. Phys. B **bf 41** (1985) 899

3.10 Resonant Auger decay of 2p hole in argon induced by electron impact

M. Žitnik[a], M. Kavčič[a], M. Bučar[a], B. Paripás[b], B. Palásthy[b], K. Tőkési

By (e,2e) technique we study a well-known L-MM energy region of argon. For any electron impact energy, if energy loss is chosen properly by fixing one of the two electron detection energies, the continuous process of an outer shell electron ejection completely overlaps with the resonant Auger processes mediated by singly excited states $[2p]nl$ below the $L_{2,3}$ thresholds. In other word, the origin (the ionic state left behind) of the ejected electron which belongs to the continuous process is determined by the sum of its energy and the energy of the scattered electron provided the electron impact energy is known. Exactly the same final states then appear in the resonant Auger decay if the electron impact energy is properly chosen. It has been shown previously by non-coincidence measurement that resonance-continuum interference affects the relative line intensities in the resonant Auger spectra taken at different incoming photon energies [1]. Besides PCI effects also strong interference effects were found in the L-MM region of (e,2e) spectra if the energy deposited in the target was close to the L shell threshold [2]. This was attributed to the fact that the electron pair: fast scattered electron (≈ 740 eV) - Auger electron (≈ 200 eV) is not distinguishable from the electron pair emitted in a direct satellite-state ionization.

In our experiment the electron impact energy is reduced so that the energy of the scattered electron matches the energy of the (resonant) Auger electron at certain point in the spectrum. Now not only the final state pairs, but both electrons in each pair become indistinguishable. That way we could also study the state-to-state interference [3] where the resonant Auger electron from decay of a given resonance together with the scattered electron form an electron pair which can not be distinguished (at the same electron impact energy) from a pair generated by decay of another resonance; in this case, of course, the role of the scattered and the Auger electron are reversed

and the electrons must have different energies.

To the purpose we are using two highly efficient CMA spectrometers each with large acceptance angle (each 1.5% of the full solid angle) [4]. In figure we present three spectra recorded a) above the L_2 threshold, b) on the $[2p]_{3/2}3d$ resonance, and c) below the first resonant excitation.
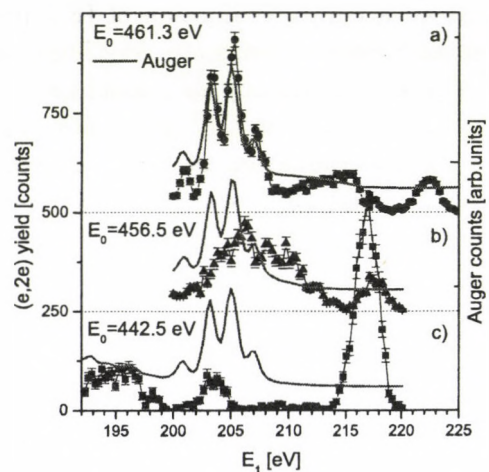

Figure 1. Argon spectra recorded at fixed detection energy E_2=209.6 eV at three different electron impact energies.

a) J. Stefan Institute, Jamova 39, P.O.B. 3000, SI 1000, Ljubljana, Slovenia

a) Dept. of Physics, University of Miskolc, 3515 Miskolc-Egyetemváros, Hungary

[1] R. Camilloni et al., Phys. Rev. Lett. **77**, 2647 (1996).

[2] D. K. Waterhouse and J. F. Williams, Phys. Rev. Lett. **79**, 391 (1997).

[3] J. P. van den Brink et al., J. Phys. B **22**, 3501 (1989).

[4] A. Kövér et al., Nucl. Instr. & Meth. A **373**, 51 (1996).

3.11 Ionization of neon by intermediate energy carbon ions

S.L. McLawhorn[a], L.H. Toburen[a], J.L. Shinpaugh[a], E.L.B. Justiniano[a], M. Dingfelder[a], K. Tőkési, B. Sulik, P. Sigmund[b], A. Schinner[c], C. Reinhold[d], D. Schultz[d]

During the past few years there has been increasing interest in ionization of atomic and molecular targets by intermediate-energy dressed and partially dressed ions. These systems are particularly challenging to describe theoretically owing to screening of the projectile nuclear charge by bound electrons, interactions of projectile electrons with target electrons, and the large number of possible exit channels. At ECU we have initiated measurements of the doubly-differential ionization cross sections, differential in ejected electron energy and emission energy, for carbon ions of different initial charge states with atomic and molecular targets. In this presentation we compare those results with calculations being conducted at several institutions. For this presentation we will focus on electron emission from neon following interactions with carbon ions with energies from 0.067 MeV/u to 0.35 MeV/u and incident charge states from C^+ to C^{3+}. Electron energies from 10 to 1500 eV are observed at emission angles from 20 to 120 degrees. The calculations separate the process into ionization of the target by the screened incident nucleus and the ionization of the target by the screened target nucleus. By summing these components in the rest frame of the target we can compare to the measured electron spectra. Figure 1 shows the single differential cross sections for ejection of electrons in C^+-Ne collisions. Note the small contribution from ionization of the projectile. As the energy increases the contribution from projectile ionization increases; likewise as the ion energy decreases that contribution decreases. The excellent agreement shown in Figure 1 provides confidence to our use of Bohr theory for this energy range for this target. Doubly-differential cross sections based on the Classical Trajectory Monte Carlo (CTMC) techniques are compared with measurements in Fig. 2 for electron emission at 30 degrees. Again, excellent agreement has been observed. We are currently exploring different incident charge states and will present those data at the meeting along with available theory.
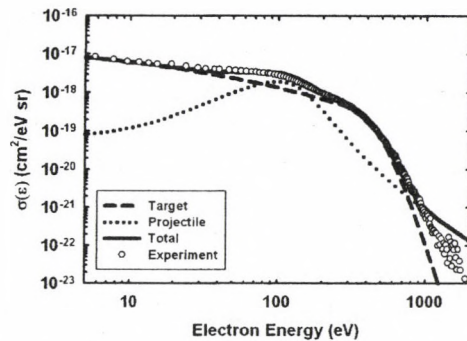

Figure 1. Single differential cross sections for 2.4 MeV C^+ on Neon. The lines are results of a Bohr calculations and the open symbols are measured cross sections.
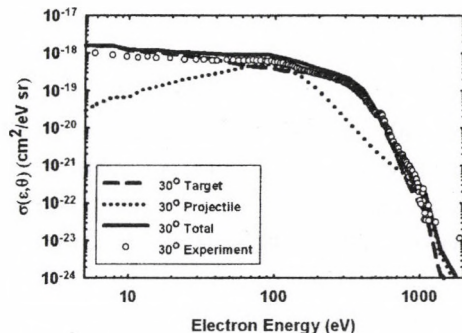

Figure 2. Doubly differential cross section for ionization of neon by 2.4 MeV C^+ ions. Lines are calculated with CTMC and the open symbols are from measurements.

3.12 Clusterization effects for resonances of the e^+-H system

J.Zs. Mezei, A.T. Kruppa, J. Mitroy[a], K. Varga[b]

The existence of low energy positron-hydrogen resonances have been demonstrated in a number of studies. These resonances are regarded as Feshbach resonances associated with the degenerate hydrogen (H) and positronium (Ps) thresholds. A positron moving in the field of an excited hydrogen atom experiences a dipole potential due to the degeneracy of the states. Similarly the proton experiences a dipole field due to the degeneracy of the excited states of the positronium atom.

In the present work [1] we have used the stochastic variational method (SVM) using explicitly correlated gaussian basis combined with the complex scaling (CS) method [2] to determine the energies and widths of a number of e^+-H resonances for $L = 0$ total angular momentum. In the calculation atomic units are used.

Besides the ease of determining the energies of the resonances another useful feature of complex scaling approach is that the resulting wave function is an L^2 function. This makes it possible to examine the structure of the resonance wave function or correlation function in detail.

The correlation function, $C(r)$ [1] at a given r is simply the probability of finding a given pair of particles a distance r apart. In the case of the (e^+, e^-, p) three-body system for the p-e^- and p-e^+ particle combinations, the correlation function is just the radial probability density.

In the Figure bellow the correlation functions of the pairs of the particles are shown in the case of the lowest lying resonance bellow the H($n = 2$) threshold ($E_{th} = -0.125$ a.u).

The p-e^- correlation function is similar to the same correlation function of the H($2s$) state. The difference between this two functions at small r distances is due to the degeneracy between H($2s$) and H($2p$) states. The closer view of the e^--e^+ correlation function re-

veals an additional degree of structure at small distances, a small bump near $R \approx 2a_0$ which is very similar to the correlation function of the Ps($1s$) state.
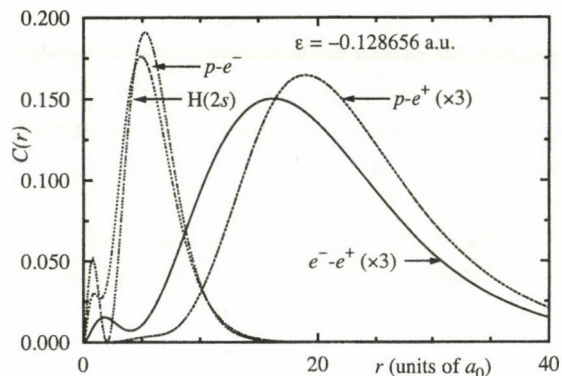

Figure 1. The correlation functions for the lowest energy resonance below the H($n = 2$) threshold. The p-e^- correlation function for the H($2s$) state is also shown. The e^+-e^- and p-e^+ correlation functions are multiplied by 3 to make the fine structures more visible.

The reason this occurs is due to the attractive electron-positron interaction. In accordance with the studies of positronic atom bound states there is a competition between the nucleus (residual part of the atom) and the positron to attach the most weakly bound electron, which give rises to clusterization effect.

a) ARC Center for Anti-Matter Studies, Faculty of Technology, Charles Darwin University, Darwin NT 0909, Australia

b) Vanderbilt University, Department of Physics and Astronomy, Nashville, TN 37240, USA

[1] K. Varga, J. Mitroy, J.Zs. Mezei and A.T. Kruppa, Phys. Rev A. **77** (2008) 044502.

[2] J.Zs. Mezei, A.T. Kruppa and K. Varga, Few Body Systems **41** (2007) 233.

---

[1]for the definition see [1]

4.1 Intrinsic plasmon excitation in total reflection X-ray photoelectron spectra of crystalline Ge

L. Kövér, W. Drube[a], I. Cserny, M. Novák and S. Egri[b]

Core photoionization of atoms in solids are accompanied by excitations causing energy loss of photoelectrons. With the appearance of the core hole, intrinsic excitations (shake, plasmon) can take place. During electron transport bulk or surface plasmons can be induced (extrinsic excitations). Multiple excitations are probable and interferences can appear among various excitations. The understanding of these processes yielding the energy loss part of the electron spectra, is important for deriving accurate electronic structure or chemical state information on the material studied.

In the present experiment a Ge (111) single crystal was used, cleaned by annealing and ion sputtering cycles, resulting in a clean and well-ordered surface as checked by surface sensitive photoemission and LEED. The high energy resolution measurements of the Ge core level photoelectron spectra were performed with the Tunable High Energy XPS instrument [1] at the BW2 beamline. The exciting photon beam was focussed onto the sample by a Si (111) monochromator. The angles of incidence for the photon beam were ~ 0.3° (*grazing incidence*) and 45° (*normal emission*) measured from to the sample surface. In Fig. 1 the Ge 2s photoelectron spectra, excited by 4600 eV photons in the *normal emission* and the *grazing incidence* geometries, are compared with the contribution from intrinsic plasmon excitations as predicted earlier by the simple Modified Hüfner (MH) model applied for a similar case *normal emission*, similar photon energy, polycrystalline Ge layer sample) [2].

A significant decrease of the inelastic background is observed in the case of the *grazing incidence* spectrum (Fig. 1) due to the suppression of the extrinsic excitations. However, the intrinsic loss contribution predicted by the simple MH model is less intense than the experimental spectrum taken under total external re-

flection conditions. An increase of the photon energy is expected to further decrease of the contribution from extrinsic losses due to the increase of the inelastic mean free path. The corresponding experimental spectra excited using 5280 eV indeed show a small change in this direction.
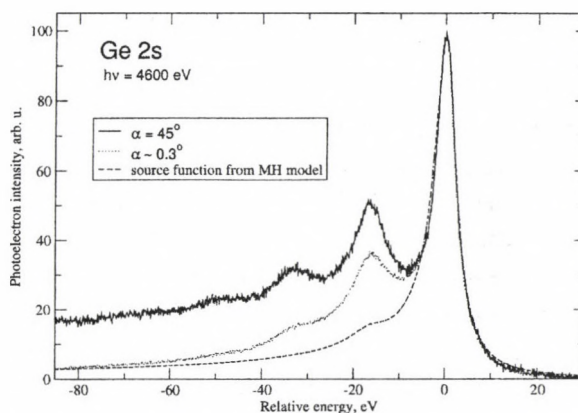

Figure 1. Comparison of the Ge 2s photoelectron spectra excited by 4600 eV energy photons from a Ge (111) single crystal using the normal emission (line) and grazing incidence (dots) experimental geometry, to the contribution of intrinsic excitations predicted earlier for "normal emission" (dashed line) [2]. The light incidence angle relative to the sample surface is denoted by α.

a) Hamburger Synchrotrostrahlugslabor HASYLAB at Deutsches Elektronen-Synchrotron DESY, Notkestrasse 85, D-22603 Hamburg, Germany

b) Department of Experimental Physics, Debrecen University, H-4026 Debrecen, Bem tér 18/a.

[1] W. Drube, T.M. Grehk, R. Treusch and G. Materlik, J. Electron Spectrosc. Relat. Phenom. 88-91, 683 (1998).

[2] M. Novák, L. Kövér, S. Egri, I. Cserny, J. Tóth, D. Varga and W. Drube, J. of Electron Spectrosc. Relat. Phenom. 163, 7 (2007).

49

4.2 Spatiotemporal Correlations of Earthquakes

J. Farkas and F. Kun[a]

An earthquake is the result of a sudden release of energy in the Earth's crust that creates seismic waves. At the present technological level, earthquakes of magnitude larger than three can be recorded all over the world. In spite of the apparent randomness of earthquake occurrence, long term measurements have revealed interesting scaling laws of earthquake characteristics: the rate of aftershocks following major earthquakes has a power law decay (Omori law); the magnitude distribution of earthquakes exhibits a power law behavior (Gutenberg-Richter law), furthermore, it has recently been pointed out that epicenters form fractal networks in fault zones (Kagan law) [1].

The theoretical explanation of earthquakes is based on plate tectonics: the earth's crust has been broken into plates which slowly move under the action of the flowing magma. Neighboring plates touch each other along ridges (fault zones) where a large amount of energy is stored in deformation. Earthquakes occur when the stored energy exceeds a material dependent threshold value and gets released in a sudden jump of the plate.

The Burridge-Knopoff (BK) model of earthquakes represents earth's crust as a coupled system of driven oscillators where nonlinearity occurs through a stick-slip frictional instability [2]. Laboratory experiments have revealed that under a high pressure the friction of rock interfaces exhibits a weakening with increasing velocity [3,4,5,6].

In the present project we extend recent theoretical studies of the BK model by taking into account a realistic velocity weakening friction force between tectonic plates. Varying the strength of weakening a broad spectrum of interesting phenomena is obtained: the model reproduces the Omori and Gutenberg-Richter laws of earthquakes, furthermore, it provides information on the correlation of earthquake sequences. We showed by computer simulations that the spatial and temporal correlations of consecutive earthquakes are very sensitive to the details of the friction force, i.e. in certain parameter regimes spatial correlations have a power law decay instead of the exponential form typically obtained with the classical Coulomb friction. Such correlations are very important for the development of forecasting techniques of earthquake occurrence [7,8].

a) Department of Theoretical Physics, University of Debrecen, Debrecen, Hungary.

[1] A. Corral, Phys. Rev. Lett. **92**, 108501 (2004).

[2] R. Burridge and L. Knopoff, Bull. Seismol. Soc. Am. **57**, 341 (1967).

[3] T. Mori and H. Kawamura, Phys. Rev. Lett. **94**, 058501 (2005).

[4] J. M. Carlson and J. S. Langer, Phys. Rev. Lett. **62**, 2632 (1989).

[5] Z. Olami, H. J. Feder, and K. Christensen, Phys. Rev. Lett. **68**, 1244 (1992).

[6] P. Bak, K. Christensen, L. Danon, and T. Scanlon, Phys. Rev. Lett. **88**, 178501 (2002).

[7] J. Farkas, *Computer simulation of earthquakes*, Master's Thesis, University of Debrecen, 2007.

[8] J. Farkas and F. Kun, *Spatial correlation in earthquake sequences*, in preparation.

Figure 1. Basic setup of the one-dimensional Burridge-Knopoff model. Blocks are attached to each other by non-linear springs. The system is driven by the upper plate which moves to the right at a constant speed. The blocks have a frictional contact with the ground plate and slide when the driving force on them exceeds static friction. A single sliding event can trigger an avalanche of slidings which is the analogue of earthquakes in the model [2].

4.3 Effect of network topology on the spreading of technologies

G. Kocsis and F. Kun[a]

Technological evolution of socio-economic systems has two major components: (*i*) *Innovation* New products, ideas, paradigms emerge as a result of innovations which are then tested by the market. (*ii*) *Spreading* Successful technologies spread over the system resulting in an overall technological progress. In the present project we study the spreading of new technological achievements, searching for the conditions of technological development. One of the key components of the spreading of successful technologies is the copying, *i.e.* members of the system adopt technologies used by other individuals according to certain decision mechanisms. Decision making is usually based on a cost-benefit balance so that a technology gets adopted by a large number of individuals if the upgrading provides enough benefits. The gradual adaptation of high level technologies leads to spreading of technologies and an overall technological progress of the socio-economic system. We proposed an agent based model for the spreading process of such technologies in which the interaction of individuals plays a crucial role [1].

Agents of the model use products of different technologies to collaborate with each other which induce costs proportional to the difference of technological levels. Additional costs arise when technologies of different providers are used. Agents can adopt technologies and providers of their interacting partners in order to reduce their costs leading to microscopic rearrangements of the system [1]. Starting from a random configuration of different technological levels a complex time evolution emerges where the spreading of advanced technologies and the overall technological progress of the system are determined by the amount of advantages more advanced technologies provide, and by the structure of the social environment of agents. When technological progress arises, the spreading of technologies in the system can be described by extreme order statistics [1,2].

We showed that the topology of social contacts of agents plays a significant role in the spreading of telecommunication technologies. To make the model more realistic we considered networks of agents with small-world and scale-free properties. Based on computer simulations we showed that a complex system of a large number of local communities is more favorable for the spreading of technologies than a fully interconnected one [2].

a) Department of Theoretical Physics, University of Debrecen
[1] G. Kocsis, J. Farkas, and F. Kun, Physica A **383**, 660 (2007).
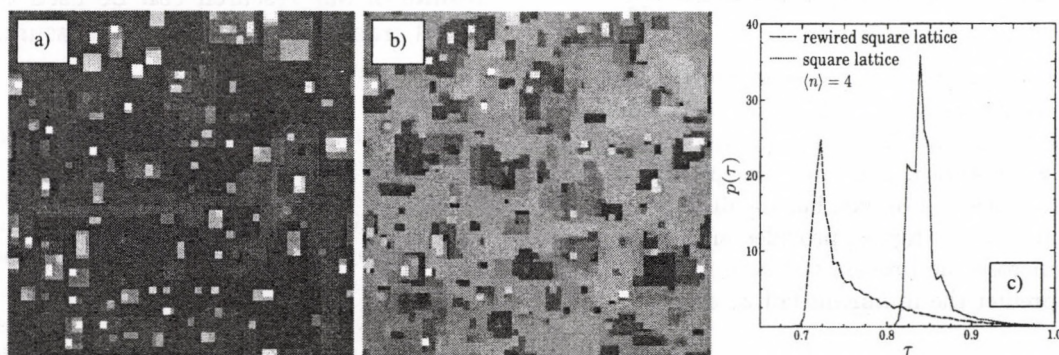[2] G. Kocsis and F. Kun, submitted to Physica A, 2007.

Figure 1. Final states of computer simulations starting from a random configuration (*a*) on a regular square lattice, and (*b*) on a small world network obtained by rewiring a square lattice . The color code indicates the technological level of agents. The polidispersity of the number of connections changes both the average and the scattering of technological levels. (*c*) Probability distribution of technological levels for the two simulations.

4.4 Crackling noise in strongly disordered materials

K. Kovács[a], F. Kun[a] and T. Vertse

Materials of high mechanical performance are often fabricated by embedding strong fibers in a relatively weak matrix. Under a constant or slowly increasing external load such reinforced composites undergo a damage process of gradual microcrack accumulation which then leads to localization and macroscopic fracture. The process of damaging can be followed experimentally by recording acoustic signals emitted by nucleating and growing cracks. This so-called crackling noise is a very important diagnostic tool in non-destructive fracture testing and can even be used to predict the imminent failure event. The goal of this project is to analyze the properties of crackling noise under realistic loading and material conditions with special emphasis on novel high performance materials.
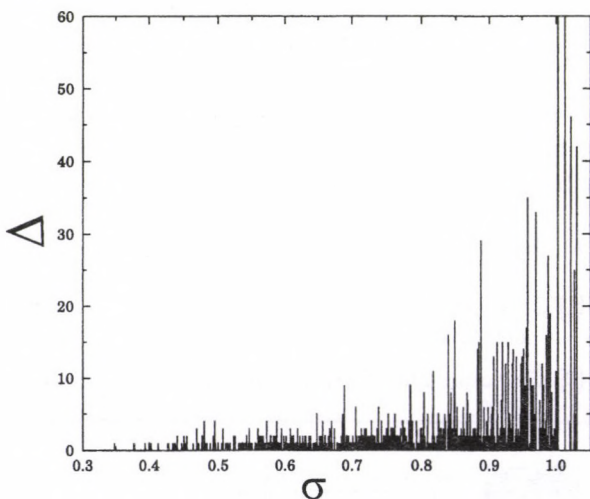
Figure 1. Under a slowly increasing external load σ bursts of local breakings occur in disordered materials. The burst size Δ has an increasing average with σ when approaching macroscopic failure. The size distribution of bursts, i.e. the distribution of peak heights in the figure, provides information about the microscopic process of fracture and can be used to predict the imminent failure event.

To capture the effect of disorder, recently several stochastic fracture models have been proposed such as the fiber bundle model (FBM) and lattice models of fuses, springs, and beam elements. Based on these models, analytic calculations and computer simulations revealed that macroscopic fracture of disordered materials shows interesting analogies with phase transitions and critical phenomena having several universal features independent of specific material details.

We showed by means of analytical calculations and computer simulations that the presence of two subsets of materials in the system with widely different mechanical strength (e.g. strong fiber-weak matrix) has a crucial effect on the characteristics of crackling noise [1,2,3]. We demonstrated that the fracture process of such two-component systems has two universality classes characterized by different distributions of the noise amplitudes. The distribution function has a power law behavior over a wide range of amplitudes but its exponent depends on the mixing fraction of the components. Astonishingly we found a critical fraction of the strong and weak components where the exponent of the burst size distribution switches from the well known mean field exponent of $\tau = 5/2$ to a significantly lower value $\tau = 9/4$. The transition is conditioned to disorder distributions where the macroscopic constitutive response of the system has a single maximum and an inflexion point, implying a novel universality class of composites. The results of our research can be used to understand crackling noise spectra measured by on-field monitoring systems [1,2,3].

a) Department of Theoretical Physics, University of Debrecen

[1] K. Kovács, R. C. Hidalgo, I. Pagonabarraga, and F. Kun, *Universality class of fiber bundles with strong heterogeneities*, accepted by Europhysics Letters, 2007.

[2] K. Kovács, R. C. Hidalgo, F. Kun, and I. Pagonabarraga, *Phase transition in a bundle of mixed fibers*, submitted to Physical Review E (2007).

[3] F. Kun, H. A. Carmona, J. S. Andrade, and H. J. Herrmann, *Universality behind Basquin's law*, accepted by Physical Review Letters, 2007.

5.1 Pop-in effect in Ge and Si coated single-crystalline Si

P.M. Nagy[a], K. Vad, A. Csik, E. Kálmán[a]

Silicon is one of the most important elements in contemporary times. Its central role in semiconductor industry makes all of its properties important. Consequently even its mechanical properties gain wide attention in the research community. Additionally, silicon shows a series of very interesting pressure-dependent phase transformations, drawing even more attention to this field [1-2]. More than twelve stable and metastable solid phases have been observed, which are arising at high pressure by increasing or decreasing hydrostatic stress. Nanoindentation or depth sensing indentation is often used for studying local mechanical properties, because it is in many cases the only method providing results from the small volume considered, and because of the simplicity of the test [3]. As result of the phase transformation caused by the pressure increase during loading of the indenter a discontinuity (a "pop-in" effect) can occur in the load curve, represented by a horizontal line (or an elbow), pointing to larger penetration depth. Similarly during unloading of the indenter a second discontinuity (a "pop-out" effect) can occur, represented by a horizontal line (or an elbow), pointing to shallower depths [1].

In this study single-crystalline silicon substrates covered by amorphous Si and Ge layer, produced by magnetron sputtering, were nanoindented by different types of indenter (Berkovich, cube corner and spherical indenters), to investigate the effect of these coatings on the pop-in and pop-out effects. It has been investigated 20-, 50-, 100-, 150 nm thick layers of amorphous Si and Ge in single- and in multiple load events. The impressions caused by the indentation were imaged by atomic force microscopy (AFM). Our experiments provide a consistent evaluation of the Young's modulus and hardness of the samples and consistent data on the exact shape of the indent impressions. The measured elastic modulus shows a slight decrease of both properties due to the softer top layer on the Si single crystal substrate, while the hardness values are decreasing with increasing coating thickness. Surprisingly small differences in measured elastic modulus and hardness of single crystalline Si substrates coated by an amorphous Si or Ge layer were found in our nanoindentation tests. We found several pop-in effects occurring during the tests, but no pop-out was connected to these events. The pop-in effect during a nanoindentation test connected to the phase transformation in Si single crystals is usually accompanied by a pop-out effect in the unloading arm of the same load curve. We did not found even a single pop-out occurring in our nanoindentations on coated Si substrates, but the pop-ins which we found occurred at lower loads, as expected. Also the depth increase in the pop-in is in most cases higher, than in uncoated Si. From these facts we can conclude that the pop-ins are probably caused by other factors than the expected phase transition. Investigating the indentation sites by AFM shows a pile-up around each indentation impression in the samples. These pile-ups are virtually decreasing the (measured) hardness by increasing the area carrying the load compared to the area calculated in the Oliver-Pharr evaluation.

a) Chemical Research Centre of HAS, Institute of Surface Chemistry and Catalysis, P.O. Box 17, H-1525 Budapest, Hungary

[1] J. Jang, M.J. Lance, S. Wen, T.Y. Tsui, G.M. Pharr, Acta Materialia 53 (2005) 1759

[2] T-H. Fang, W-J. Chang, C-M. Lin, Microelectronic engineering 77 (2005) 389

[3] J.B. Pethica, R. Hutchings, W.C. Oliver, Phil Mag 48 (1983) 593

5.2 Nanoscale effects in interdiffusion

Z. Erdélyi[a], G.A. Langer[a], A. Csik, D.L. Beke[a]

Diffusion on the nano/atomic scales in multilayers, thin films has many challenging features even if the role of structural defects can be neglected and 'only' the effects related to the nano/atomic scale raise. The most basic equations to describe the diffusion are Fick's equations. It is important to emphasize that the diffusion coefficient in Fick's equations is in general composition independent and Fick's classical equations do not include the stress effects, which can have important influence onto the diffusion especially on the nano/atomic scale. We illustrate that the continuum descriptions of the diffusion cannot be applied automatically on such short distances, the classical continuum approxi-mations (Fick's laws) cannot describe correctly the atomic movements [1-3]. They predict faster kinetics than the atomistic models and the interface shift is always proportional to the squareroot of the time. However, the kinetics can be even linear on the nano/atomic scale.

We have shown from computer simulations that Fick's laws violate on the nanoscale either in completely or restricted miscible systems. This is strongly related to the discrete character of the system on the nanoscale and to the highly neglected fact in the literature that the diffusion coefficients depend on the composition. As will be seen the composition dependence of D is very important and has very significant influence on the diffusion kinetics on the nano/atomic scales. It originates from the fact that usually the diffusion coefficients are different in an A and in a B matrix. Consequently in case of a real interface, which is not atomically sharp, i.e. there is a more or less intermixed region between the pure A and B matrixes, the diffusion coefficient changes continuously while e.g. an A atom diffuses from the pure A matrix into the pure B. This feature can be also called diffusion asymmetry.

We have also illustrated that in this case not only the composition profile develops highly asymmetrically but also the stress profile. Moreover, we have also seen that the stress effects usually slow down the intermixing process, and the slowing down is more pronounced in case of asymmetric diffusion. Computer simulations also have shown that on the nanoscale, for strongly composition dependent diffusion coefficients, diffuse interfaces can sharpen rather broaden in completely miscible binary systems during annealing independently of the different kind of stress effects considered. The stress effects influence only the timescale of the process. This phenomenon could provide a useful tool for the improvement of interfaces and offer a way to fabricate of e.g. better X-ray or neutron mirrors, microelectronic devices or multilayers with giant magnetic resistance. These phenomena predicted by computer simulations have been proved experimentally as well.

a) Dept. of Solid State Physics, Uni. Debrecen, P.O. Box 2, H-4010 Debrecen, Hungary

[1] Z. Erdélyi, D.L. Beke, P. Nemes, G.A. Langer, Phil. Mag. A Vol.79 (1998) 1757

[2] Z. Erdélyi, Ch. Girardeaux, Zs. Tőkei, D.L. Beke, Surf. Sci. Vol. 496 (2002) 129

[3] D.L. Beke, Z. Erdélyi, Phys. Rev. B Vol. 73 (2006) 035426

5.3 Photo- and thermally induced interdiffusion in Se/As$_2$S$_3$ nanomultilayers

V. Takáts[a)], *P. Nemec*[b)], *A. Csik, S. Kökényesi*[a)]

Few approaches are known for extending investigations of amorphous chalcogenide layers towards the nanostructures, but the nanolayered, superlattice-like structures are the most investigated. Inserting the light-sensitive amorphous layer between different barrier layers and changing the modulation period as well as the type of matrix (barriers) new effects are expected: enhanced interdiffusion, simple formation of solid solutions or stimulation of the solid-state reactions, crystallization and phase separation, a complex of related changes of optical and electrical parameters [1]. The enhanced interdiffusion in the a-Se/As$_2$S$_3$ nano-multilayers, that can be considered as model ones, results in the giant volume expansion, so other combinations of materials or the influence of the technology, real structure on the above mentioned effects should be analyzed. The method of vacuum evaporation of different components and cyclic deposition of nanometer-thick sub-layers onto the same substrate was usually used up to now, but serious problems can arise from the non-stoichiometry of the deposited components. The thermal evaporation technology is not always applicable for producing barrier layers (especially oxides, organics), while the best and simplest technology for amorphous chalcogenide multilayer fabrication must ensure the possibility of simultaneous deposition of chalcogenide and the barrier layers. One of the relatively new methods for thin films preparation is pulsed laser deposition (PLD) [2]. When compared with vacuum thermal evaporation, magnetron sputtering, chemical vapour deposition techniques, etc., the PLD has several advantages-relative simplicity of the process, often nearly stoichiometric transfer of target material to the films, easy control of the process by laser operating parameters.

In this work the effects of light- and thermally stimulated interdiffusion in Se/As$_2$S$_3$ nanomultilayers with modulation period of 6-9 nm fabricated by pulsed laser deposition and by the method of cyclic thermal evaporation (CTE) of the Se and As$_2$S$_3$ components were investigated by means of direct low-angle X-ray diffraction (LAXRD) measurements and by indirect methods of optical measurements. It was shown that we have developed the PLD method for preparing nanomultilayers from amorphous chalcogenides with improved structural characteristics (better periodicity and quality of interfaces) in comparison with thermal evaporation method. More pronounced nano-granular structure is characteristic for PLD samples but at the same time the interfaces are essentially sharpened, the periodicity and the initial blue-shift of the optical absorption edge are better in comparison with CTE samples. At the same time the important characteristics of stimulated changes of optical parameters remains the same as well as possibilities of applications for optical recording, formation of amplitude-phase and geometrical relief for optoelectronics. Such samples enables further investigations of the influence of structure formation at nano- and microscopic scale on optical parameters, diffusion and quantum size effects in amorphous structures.

a) Dept. of Exp. Phys., Uni. Debrecen, P.O. Box 2, H-4010 Debrecen, Hungary

b) Department of General and Inorganic Chemistry and Research Center, University of Pardubice, Legions Sq. 565, 53210 Pardubice, Czech Republic

[1] T. Wagner, S. Schroeter, T. Glasser, M. Vlcek, J. Non-Cryst. Solids 326-327 (2003) 500

[2] P. Nemec, J. Jedelsky, M. Frumar, M. Vlcek, J. Optoelectron. Adv. Mater. 7 (2005) 2635

5.4 Structural modifications induced in hydrogenated amorphous Si/Ge multilayers

C. Frigeri[a)], M. Serényi[b)], A. Csik, Z. Erdélyi[c)], D.L. Beke[c)], L. Nasi[a)]

Amorphous multilayers have applications in electronics and optics, e.g., for optical recording and solar cells. Optimization for such applications often requires the selection of appropriate pairs of materials and the creation of solid state solutions by interdiffusion. As a consequence, tailoring of the layer physical properties, like thickness, refractive index, electrical conductivity etc, is achieved. In the case of Si/Ge amorphous multilayers (MLs) the improvement of the physical properties is also accomplished by enriching them with hydrogen because H passivates the dangling bonds of Si and Ge that act otherwise as efficient electronic levels [1]. Hydrogen stability is of primary importance in order to avoid de-passivation of the dangling bonds. To optimize the amorphous layers properties one must also control the diffusion of the elements which is quite hard because at present the mechanisms of diffusion are not fully understood. Investigation of the overall thermal stability of these multilayers is thus of great interest for the interpretation of their operation and prediction of their lifetime.

In our previous works it was experimentally shown that in amorphous Si/Ge MLs the diffusion is very asymmetric because of the strong concentration dependence of the interdiffusion coefficient. In agreement with our calculations the silicon could enter into the germanium layer but germanium cold not diffuse into silicon. At the same time the initially sharp interface at the start of the process does not flatten but shifts consuming the Si layer. Calculation can show that with increase of the Si concentration the process of diffusion slows down at longer times. It was expected that in hydrogenated Si/Ge MLs hydrogen could affect diffusion of Si. However, it was seen that after a short annealing time significant structural changes occurred at the surface of the hydrogenated Si/Ge MLs (Fig. 1). This urged the study of the relationship between anneal-ing conditions and structural modifications in such samples. We can seen that the structural changes occurring as a function of the annealing conditions. Annealing changes the structure of the as-deposited multilayer except for the less severe conditions here applied (423 K for 22 h). For higher temperatures and/or times, the modifications consist of layer inter-mixing and surface degradation in the shape of bumps and craters. Besides craters the sample surface has bumped up in many places, which suggests that bubbles have formed inside the hydrogenated multilayers. Hydrogen should be mostly released from the amorphous Ge layers because of the lower binding energy of the Ge-H bond.

Figure 1. SEM image of the surface of a hydrogenated sample after heat treatment.

a) CNR-IMEM Institute, Parco Area delle Scienze, 37/A, 43010 Parma, Italy

b) MTA-MFA Institute, Konkoly-Thege ut 29-33, Budapest H-1121, Hungary

c) Dept. of Solid State Physics, Uni. of Debrecen, P.O. Box 2, H-4010 Debrecen, Hungary

[1] W. Beyer, U. Zastrow, J. Non-Cryst. Solids 206 (2000) 266

5.5 Energy Loss Spectra of Iron

M. Novák, R.J. Bereczky, Z.M. Zhang[a] Z.J. Ding[b] J. Tóth, D. Varga, K. Tőkési

The quasi-elastic Monte Carlo approach was used to simulate the path length distribution of the backscattered electrons from the Fe sample. Iron loss spectra were simulated at the primary electron energies between 500 eV and 4000 eV [1] where the reduced partial intensities for surface and bulk excitations were applied. The simulated and measured Fe loss spectra are shown in Fig. 1. The contributions of single surface, single bulk and the sum of these two modes are also shown. We found a good agreement between the simulated and the measured Fe loss spectra above 1500 eV. A sharp edge can be observed in the measured loss spectra in the 50-60 eV energy loss range correspondingly to the Fe 3p ionization edge. Since the optical model dielectric function [2] cannot accurately describe the sharp ionization edges using Drude-Lorentz line shapes, we observed deviation between the measured and simulated spectra in this energy range.

Acknowledgements
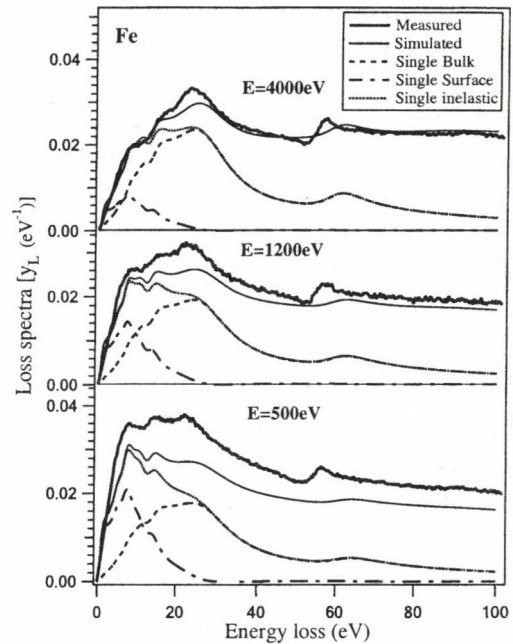
Figure 1. Comparison of the measured and simulated loss spectra using the bulk and surface energy loss distribution at different primary electron energies. The primary incident electron angle was 50° and the observation angle was 0° with respect to the surface normal of the sample.

a) Dept. of Astronomy and Applied Physics, Uni. of Science and Technology of China, 96 Jinzhai Road, Hefei, Anhui 230026, P.R. China

b) Hefei National Laboratory for Physical Sciences at Microscale and Dept. of Physics, Uni. of Science and Technology of China, 96 Jinzhai Road, Hefei, Anhui 230026, P.R. China

[1] M. Novák, R.J. Bereczky, Z.M. Zhang, Z.J. Ding, J. Tóth, D. Varga, K. Tőkési, Surf. Interf. Anal. (2008) in press.

[2] C.J. Tung, Y.F. Chen, C.M. Kwei, T.L. Chou, Phys. Rev. B49 (1994) 16684.

5.6 Preliminary result on the analysis of Late Bronze Age metals

G. Sánta[a], I. Uzonyi

The main event of the complex cultural changes during the transition from Middle to Late Bronze Age was the appearance of Tumulus culture in the Danube-Tisza region. In this period people rose mounds (tumuli) above their graves made from stone and soil. According to our present knowledge we believe that the ethnically inhomogeneous Tumulus culture was made homogenous by commerce (especially bronze commerce).

Depots were typical of the final period of Middle Bronze Age called Koszider-phase. During the tumulus period the practice of hiding depots came to its end, bronze objects were put into graves. Therefore, it would be important to analyze the relation between the Koszider and Tumulus metallurgy. The main question to be answered is the following: were the trade connections and exchange of goods discontinued during the time of cultural changes?

Examination of archaeological finds is carried out usually by typological methods which provide information on the attire fashion and funeral rite of cultures. The inherent capability of analytical techniques makes it possible to draw conclusions on the provenance of metals, thus facilitating to establish the contemporary trade routes. The metal finds from the southern part of the Great Hungarian Plain has not been investigated yet, though it would be important from the point of view of Tumulus culture. The main question is whether there is any noticeable change between the metallurgical craftsmanship of the consecutive eras. Therefore, it is important to determine the composition of the used raw materials, their sources, as well as the applied manufacturing technologies.

For the characterization of archaeological bronze finds both conventional X-ray fluorescence (XRF) method and micro proton-induced X-ray fluorescence (micro-PIXE) techniques are applied. The first one serves for the determination of the bulk composition of samples while the second one for the characterization of microstructure, namely, the lateral distribution of elements (fig. 1). In this case we use our special experimental-setup with two Si(Li) X-ray detectors installed at our scanning nuclear microprobe facility. It allows the determination of elements in the C-U atomic number range [1] with typically 10-100 ppm detection limits.

In the future we intend to analyze hundreds of archaeological bronze finds in order to build a comprehensive data base for this era and territory. It will help to classify objects, determine workshops and applied metallurgical techniques. The recent trace elements in the finds may be characteristic for the minefield of the raw materials thus possibly allowing the determination of trade routes of ores. This work was supported by the EU co-funded Economic Competitiveness Operative Programme GVOP-3.2.1.-2004-04-0402/3.0.
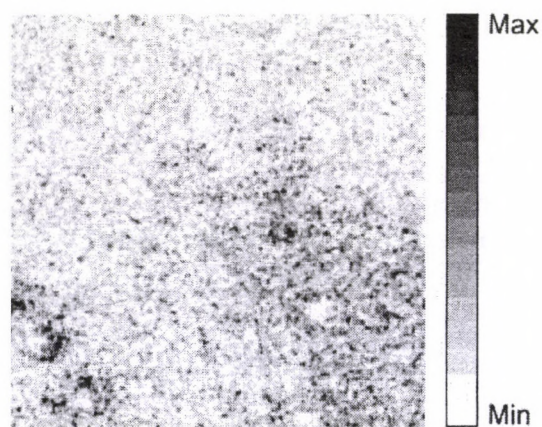
Figure 1. Lateral concentration distribution for Sn in a bronze sample (scan size: 2 x 2 mm^2). The heterogeneity is a typical characteristic of archaeological objects.

a) University of Szeged, Szeged, Hungary

[1] I. Uzonyi et. al, NIM B 181 (2001) 193.

[2] I. Uzonyi, Gy. Szabó, NIM B 231 (2005) 156.

5.7 Guiding of Charged Particles Through Insulating Nanocapillaries: Comparison Between Ions and Electrons

B. Stix[a], S. Pleschko[a], K. Schiessl[a] K. Tőkési, C. Lemell, B. Solleder, and J. Burgdörfer

Following the first experimental observation of guiding of slow highly-charged ions (HCI) through insulating nanocapillaries by Stolterfoht et al. [1], recent experiments have found guiding of electrons with energies of several hundred eV [2]. Guided transmission through an array of Al_2O_3 capillaries could be observed for angles of incidence as large as about 11°. In this contribution we present new simulations for the guiding of slow HCI through mylar capillaries which are based on a classical trajetory Monte Carlo simulation of the projectiles inside the insulating nanocapillaries [3]. The dependence on the capillary diameter is investigated and compared with the experiment. Furthermore, first results for electron guiding will be presented. Although experimental observations appear similar for electrons and HCI, the detailed mechanism of interaction with an insulating surface is considerably different. For an HCI, almost full neutralization takes place upon impact, leading to a depostion of charge on the surface. On the other hand, electrons impacting grazing incidence on an insulator have a considerable probability of being elastically backscattered. Additionally, secondary electron emission (SEE) with a SEE coefficient of $\delta \approx 1$, leads to charge-up of opposite polarity, clearly different from the case of positively charged projectiles. We analyze the interaction of grazing incidence electrons with a surface of amorphous Al_2O_3 as starting point for a simulation of electron trajectories inside a nanocapillary by the means of a Monte Carlo (MC) technique [4]. Differential backscattering distributions and SEE yields are obtained. Fig. 1 shows a simulated energy spectrum of grazing incidence electrons scattered from a Al_2O_3 surface. Such a spectrum with significant traces of inelastic processes is in clear contrast to scattering of HCI on a surface, indicating that qualitatively different processes are involved in electron guiding.
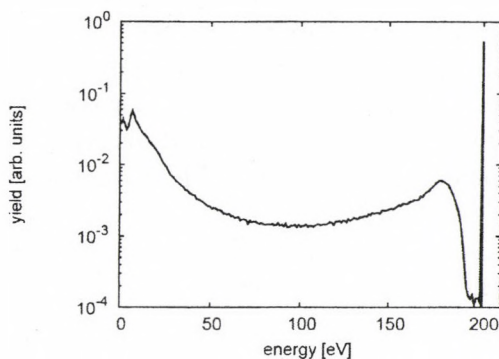
Figure 1. Energy spectrum of grazing incidence ($\theta_{in} = 2°$) electrons with an energy of 200 eV scattering at a surface of Al_2O_3.

These results serve as input for scattering of projectile trajectories in a nanocapillary. Preliminary results show considerable transmission for large angles of incidence as well as relatively broad angular distributions of the transmitted projectiles which can be traced back to multiple scattering of the projectiles. In this model transmission can be achieved even without charge-up of the internal capillary walls, however with a smaller transmission coefficient.

a) Dept. of Astronomy and Applied Physics, Uni. of Science and Technology of China, 96 Jinzhai Road, Hefei, Anhui 230026, P.R. China

[1] N. Stolterfoht et al., PRL **88**, 133201 (2002).

[2] A. R. Milosavljević et al., PRA (2007) in press.

[3] K. Schiessl et al., Phys. Rev. A **62**, 042902 (2005).

[4] D. Varga et al., Surf. Interf. Anal. **38**, 544 (2006).

5.8 XPS Analysis of Nano Thin Films on Substrate

S.F. Mao[a], Z.M. Zhang[b], K. Tőkési, A. Csik, D. Varga, J. Tóth, R.J. Bereczky, Z.J. Ding[a]

X-ray photoelectron spectroscopy (XPS) has been a conventional surface analysis tool. In recent years quantification of nano film thickness with XPS has been discussed. Considering the fact that the analysis rely only on the peak intensity, it would lead a great uncertainty. Therefore a universal analysis strategy has been proposed by Tougaard [1] when an exponential in-depth distribution is supposed. This algorithm can be applied for the determination of the in-depth concentration distribution within the outermost few nanometers of the surface.

In this work, we propose a more elaborate and convenient algorithm for quantification of the thickness of the nano films on the substrate [1]. The alternative method is based on the relation between the kinetic energy of photoelectrons generated in a film and the film thickness. The XPS spectrum is formed by overlapping the emission spectra from different generation depths of signal electrons; these electrons suffer energy losses during their travel to the surface. Therefore, the deeper depth layer will give more contribution to the spectrum intensity at lower kinetic energies. Although the total intensity of the spectrum increases with the film thickness, the thicker film would have more intensive inelastic background at certain energy, E, when the signal peak intensity is normalized. A relationship between background intensity and the film thickness may thus be derived [2]. As a test, a W/SiO2 overlayer sample was investigated. Theoretical evaluation of the spectra is compared with the experimental result (see Fig. 1). We found, that our method estimate the film thickness with reasonable well.
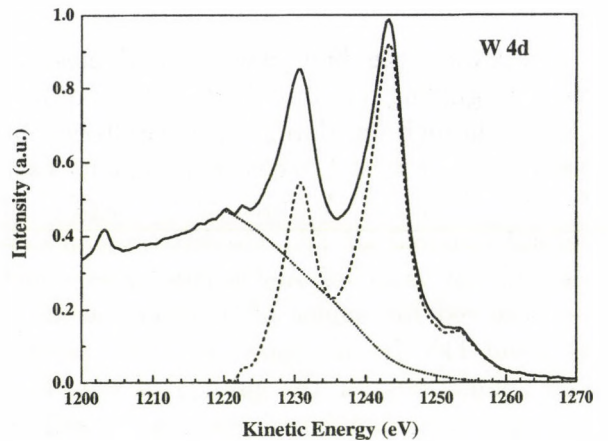
Figure 1. XPS spectrum of W 4d peak measured from a W(3 nm)/SiO2 sample in the direction normal to the surface (solid line). Dotted line is the Tougaard background. The dashed line represents the background subtracted XPS peak.

a) Hefei National Laboratory for Physical Sciences at Microscale and Dept. of Physics, Uni. of Science and Technology of China 96 Jinzhai Road, Hefei, Anhui 230026, P.R. China

b) Dept. of Astronomy and Applied Physics, Uni. of Science and Technology of China 96 Jinzhai Road, Hefei, Anhui 230026, P.R. China

[1] S. Tougaard, Surf. Sci. 216 (1989) 343.

[2] S.F. Mao, Z.M. Zhang, K. Tőkési, A. Csik, J. Tóth, R.J. Bereczky, Z.J. Ding, Surf. Interf. Anal. (2008) in press.

5.9 XPS study of Co-Cr-Mo and Ni-Cr-Mo dental alloys treated in artificial saliva

J Tóth and L. Crăciun[a]

Importance of the usage of non-allergic alloys Co-Cr-Mo relative to the more allergic Ni-Cr-Mo alloys well known in the field of biomedical science. The aim of the present study was to compare the surface layers by XPS (Al K_α X-ray excited Photoelectron Spectroscopy) method from the point of view of corrosion and passivation of the mentioned alloys.

Sample preparation were made in Bucharest in a NIPNE cooperation: Co-Cr-Mo and Ni-Cr-Mo discs of diameter of 8 mm with a thickness of about 1.3 mm were treated in artificial saliva solutions. XPS measurements were made in Debrecen in ATOMKI by a home made electron spectrometer [1] based on a hemispherical analyzer in fixed retardation ratio mode using the retardation ratios of k=4 for survey scan and k=8 ($k=E_{kinetic}/E_{pass}$) for more detailed narrow scan spectra. In this way the relative energy resolution was 0.125 % at k=4 and 0.0625 % at k=8, respectively. Survey and detailed XPS spectra were taken as a function of depth of a few times 10 nm measured from the top surface by the help of Ar^+ ion etching (AG21 ionsource, VG Microtech). Elemental composition and chemical states were studied. The angle of incidence of the ions were 40 degrees relative to the surface normal of the specimen to increase the ion sputtering yield and the same time to decrease the matrix effects caused by the ion beam, that is as much as possible to decrease the preferential sputtering. The data evaluation was made by a home-made computer software of EWA [2]. The XPS peak components of different chemical states of Cr and the relative

atomic concentrations of the different components (oxide and metal) were determined from the peak area of XPS using the Voight peak shape. The survey scan spectra showed not only the main components of the alloys, but the chemical components characteristic for the chemical treatment of the alloys, like Na, Cl, etc. The main conclusions are: the Cr was in the form of Cr^{3+} in the top surface. The metal to oxide ratios from Cr 2p XPS spectra vs. Ar^+ etching for all the samples changed very much. The other two main components of the alloys, Co and Ni were in metallic form except in the as received spectra. As a function of the alloy composition and the saliva solution treatment (time, temperature, concentration of NaCl, etc.) the Cr-oxide layer thickness changed dramatically.

a) "Horia Hulubei" - National Institute for Physics and Nuclear Engineering, 077125, MG-6 Magurele, Bucharest, Romania

[1] L Kövér, D. Varga, I. Cserny, J. Tóth and K. Tőkesi, Surf. Interf. Anal. 19 (1992) 9.

[1] J. Végh, *EWA: A spectrum evaluation program for XPS/UPS*. ECASIA 95. 6th Eu. Conf. on Appl of Surf. and Interf. Anal. Montreux, Switzerland, October 9-13, 1995. eds: H.J. Mathieu, B. Reihl, D. Briggs, Chichester, etc, John Wiley and Sons (1996) pp679

5.10 Investigation of organic thin layers (iron-porphyrin complex) prepared by spin-coating method with ion beam analytical techniques

R. Huszánk, A. Simon

Nowadays, keep increasing interests in metalloporphyrin complexes because of their considerable importance in numerous fields such as biochemistry, medical science and catalysis. As a consequence of the diverse photophysical and photochemical properties of these compounds, they are used in photovoltaic devices, sensors, and photodynamic therapy. The porphyrin derivatives, for example a kind of free base porphyrin (H_2TPPS, tetrakis(4-sulfonatophenyl)porphyrin) or its metallo-complexes with iron(II) or iron(III) ions have very high molar light absorption [1,2]. The different functional groups linked on the prophyrin macrocycle or coordinated to the central atom has effect to the spectral properties of the whole molecule. This kind of behaviour make these kind of compounds applicable to, for example, as a chemical sensing base material.
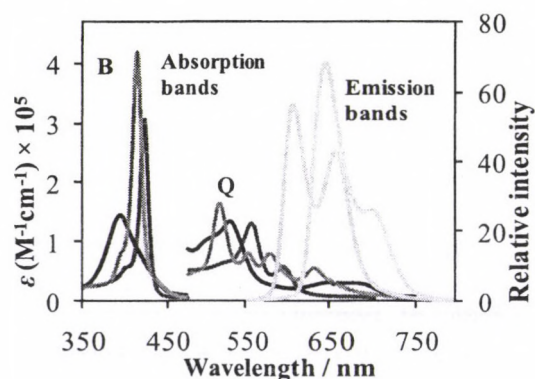
Figure 1. The absorption spectra of Fe^{III}TPPS (blue line), H_2TPPS (grey line) and Fe^{II}TPPS (red line), and emission spectra of Fe^{II}TPPS (yellow line) and H_2TPPS (purple line). For colour figure see the online version: http://www.atomki.hu/ar2007/

In ATOMKI we prepared thin layers by spin-coating technique with the porphyrin complex's chloroform solution (c=0.014 M/dm^3). To optimize the thin layer preparation method and to investigate the layer properties we use Rutherford-backscattering spectrometry (RBS) and Elastic Recoil Detection Analysis (ERDA) techniques. In addition, we use profilometry technique as well.
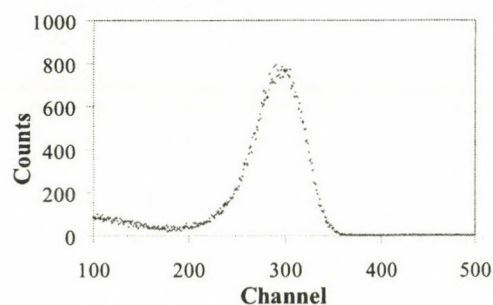
Figure 2. The ERDA spectrum of the iron(III)-porphyrin spin-coated on Si substrate (RPM=1000 1/min, 1.6 MeV He^+ beam, detecting angle 30°, tilt angle 80°)
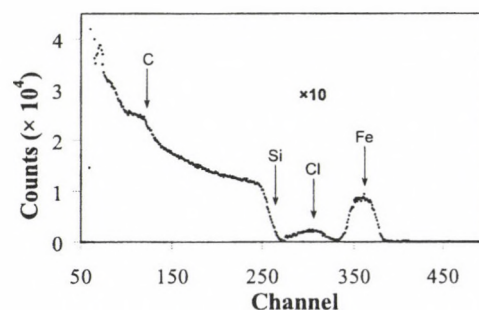
Figure 3. The RBS spectrum of the iron(III)-porphyrin spin-coated on Si substrate (RPM=1000 1/min, 1.6 MeV He^+ beam, detecting angle 135°)

An ERDA and RBS spectrum of the thin porphyrin complex (Fe^{III}TPPCl) layer on a Si substrate prepared at our laboratory is shown on Fig. 2. and 3. According to our measurements the layer thickness is 35 nm.

[1] R. Huszánk, O. Horváth, Chem. Comm. 2005, 224.

[2] O. Horváth, R. Huszánk, Zs. Valicsek and Gy. Lendvay, Coord. Chem. Rev., 2006, 250, 1792.

6.1 A 6-yr record of stable isotope ratios of hydrogen and oxygen and temperature correlation of $\delta^{18}O$ in precipitation from Eastern Hungary

Zs. Szántó, I. Futó L. Palcsu, G. Vodila

Investigation of past environmental changes might be possible only if we understand the isotopic systematic of modern precipitation using precipitation-linked stable isotope proxies or models. The apparent temperature coefficient $\Delta\delta^{18}O/\Delta T$ is important because it is used to calculate some paleotemperature changes, and because it is a basis for validating the accuracy of GCMs. In principle, three relationships can be observed between the isotopic composition of precipitation and local surface air temperature [1]: (1) a spatial relation between the long-term averages of $\delta^{18}O$ (δ^2H) of precipitation and the local air temperature for different stations; (2) a temporal relation between short-term (seasonal) changes of $\delta^{18}O$ (δ^2H) and temperature for a single station or group of stations and (3) a temporal relation between long-term changes in $\delta^{18}O$ (δ^2H) and temperature at a certain location.

The isotopic composition of hydrogen and oxygen of the monthly precipitation from Eastern Hungary was analyzed in samples collected during a monitoring period from the beginning of 2001 to the end of 2006. At the same time an event-based sample collection and data analysis were also performed.

During the studied period, the $\delta^{18}O$ values varied from 3.9 to -21.3‰ and the δ^2H values from 2.0 to -176.3‰. The composite monthly isotopic ratios of oxygen and hydrogen yield a regression line $\delta^2H = 6.9\delta^{18}O - 4.1‰$ with a correlation coefficient of 0.92, while the LMWL calculated on event-based sample δ^2H and $\delta^{18}O$ values gives a regression line $\delta^2H = 6.6\delta^{18}O - 9.1‰$ with a correlation coefficient of 0.90. Both lines are close to the GMWL but show the effect of secondary evaporation. The highest δ^2H and $\delta^{18}O$ values were obtained during the summer months, whereas the lowest δ^2H and $\delta^{18}O$ values were recorded during autumn and winter.

Time series of δ^2H and $\delta^{18}O$ values for individual samples, amount-weighted monthly average δ^2H and $\delta^{18}O$ values and deuterium excess for Debrecen (47,52997° Northern latitude, 21,63916° Eastern longitude) and Ebes (47,47051° Northern latitude, 21,49042° Eastern longitude) precipitation were calculated and the temporal relationship between monthly $\delta^{18}O$ and the mean monthly surface air temperature (MMT), and the mean monthly precipitation temperature (MMPT) respectively were determined.

Observational data have displayed a good correlation of $\delta^{18}O$ with air temperature, which validate the temporal (but not the spatial) isotope approach. The slope of $\delta^{18}O$ vs. temperature varied between 0.34‰°C^{-1} and 0.32‰°C^{-1}. The temperature coefficients obtained in case of MMPTs instead of MMTs suggest that fine-scale weather observations are needed for accurate calculations and realistic modeling of GCMs. Mean temperature over a time interval actually has little to do with precipitation because most of the time there is no precipitation or precipitation is rarely distributed uniformly throughout a particular time interval, therefore caution should be used in any quantitative (or even qualitative) interpretation of $\delta^{18}O$ or δ^2H paleorecords.

GCM: General Circulation Model
GMWL: Global Meteoric Water Line
LMWL: Local Meteoric Water Line

[1] K. Rozanski, L. Araguas-Araguas, R. Gonfiantini, (1993), Isotopic patterns in modern global precipitation. In: Climate Change in Continental Isotopic Records, Geophysical Monograph: 78, American Geophysical Union, USA, 1-36.

6.2 Field experiment on excess air formation in the riverbank of Danube

L. Palcsu, Z. Major, L. Papp[a], W. Aeschbach-Hertig[b]

Excess air is a contribution to the gases dissolved in groundwater in addition to the solubility equilibrium component, formed by partial or total dissolution of air trapped during water level rises in the unsaturated zone. The amount of excess air can be quite large, mainly if the water level increase is significant. The first aim of this field experiment carried out in September 2007 during a flood (Fig. 1/b) occurred along the Danube River has been to demonstrate that the excess air formation can be detected and studied under natural conditions when the groundwater level is rising.
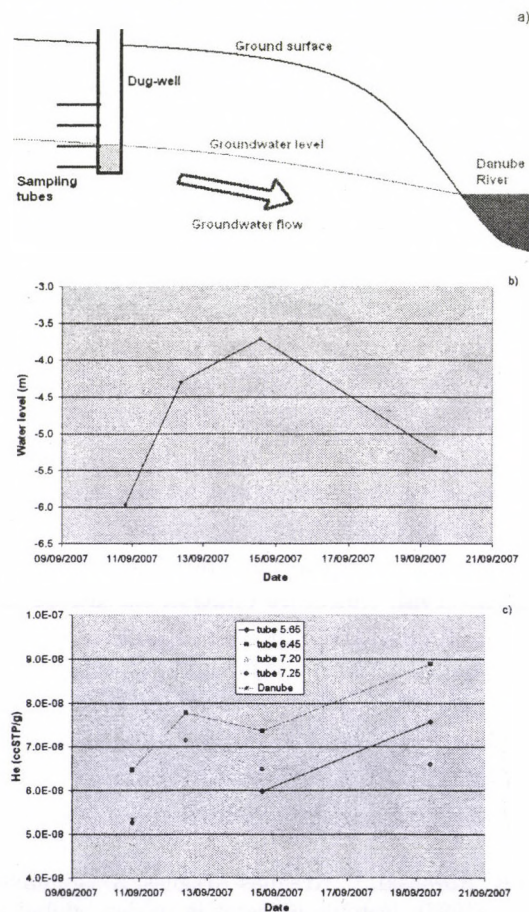
Figure 1. a) Schematic cross section of the study site **b)** Water level rising in the dug-well **c)** Helium concentration during the sampling period

The study site is located in the riverbank of Danube River, the dug-well is at around 30 m from the riverbed (Fig. 1/a). The whole area is composed of fluvial sand. Separated water samples can be taken from the sampling tubes. Each sampling tube represents a certain depth. The horizontal groundwater flow velocity is supposed to be around 10 m/day (or at least this magnitude), that of course depends on the level difference between Danube and the groundwater.

Helium and neon concentrations have been measured from the water samples. What we can see from these noble gas data is a probable correlation between groundwater level and excess noble gas concentrations. He and Ne are correlating providing evidence that the excess components are of same origin. However, the helium excess is usually larger than that of neon that means there has to be non-atmospheric components of helium, such as terrigenic and tritiogenic. The R/Ra ratios are generally higher than one clearly showing tritiogenic ^{3}He in the water. Having a look at Fig. 1/b-c, it can be observed that there is a relatively good relation between groundwater rising and the excesses of the noble gases.

From this sampling campaign, we can conclude that this kind of field experiment does make sense. Further noble gases have to be measured, and more information has to be gained regarding to the local hydrological behaviour. Nevertheless, a few fascinating things have appeared: 1) Contrary to our expectations, the highest noble gas excess was at the depth of 6.45 m, and not at 7.25 m. 2) While the groundwater level was sinking after 14th September, none of the water samples contained less noble gas, rather more. As if the water level had been rising further. Explanations can be that the water might have been flowing along different flow paths, additionally the excess gas dissolution had occurred somewhere farther from the dug-well, and then the water body was flowing towards the dug-well.

a) University of Debrecen, Debrecen, Hungary

b) Institut für Umweltphysik, Heidelberg, Germany

6.3 Improving helium and neon measurements for environmental water samples

L. Palcsu, Z. Major

The analysis of dissolved noble gas concentrations in groundwater has proven to be a reliable method to determine quantitative palaeotemperatures and water ages. The aim of instrumental and methodological improvements in the noble gas laboratory is to achieve a reliable accuracy of mass spectrometric noble gas measurements for environmental water samples.

To interpret the dissolved noble gases in water as noble gas temperature, excess air component and $T/^3$He age with low error, it is necessary to achieve a very precise measurement of noble gases. Therefore, the accuracy of each noble gas measurements should be around 1 % or better.

In the noble gas laboratory tritium measurements of environmental water samples have been performed since 1998 that is based on a VG 5400 noble gas mass spectrometer. The VG 5400 is an all-metal, statically operated, double focused, 90° sector field mass spectrometer with 57 cm extended geometry.

In 2007 a new cryosystem was installed that makes possible the quantitative collection of gas samples. It also contributes to the purification and separation of the different noble gases. As a new measurement, helium and neon measurements have been developed for environmental water so far. The sample preparation and the measurement technique were worked out in summer 2007. Measurements are calibrated with air aliquots. Moreover, fast calibration procedure has been initiated. After each noble gas measurement a pure helium as well as neon aliquot is admitted to the mass spectrometer and measured so that the instability of the mass spectrometer can be corrected for. Air equilibrated water samples have been prepared under well know circumstances (T = 23.5 °C, p = 0.987 atm), hence the expected concentrations are $4.372 \cdot 10^{-8}$ ccSTP/g for helium and $1.779 \cdot 10^{-7}$ ccSTP/g for neon (ccSTP: cubic centimeter at standard temperature and pressure). Stability and reproducibil-

ity measurements for helium and neon have been performed on ten identical water samples taken into copper tubes. The standard deviation of the ^{4}He and ^{3}He measurements were 0.5 % and 1.2 %, whilst the measured data were varying within the range of ±1 % and ±3 % around the average (Fig. 1). The standard deviation of the neon measurements were 1.5 %.
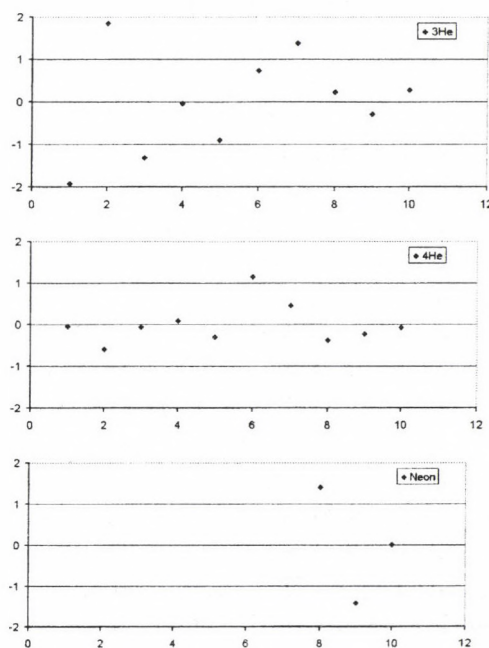
Figure 1. Deviation of different noble gas measurements from the average (X-axis: number of measurements, Y-axis: deviation in %).

These precisions are better for than expected, but seems to be too high for neon, although the accuracy is extremely good. The average of the measured concentrations is $4.379 \cdot 10^{-8}$ ccSTP/g for helium and $1.795 \cdot 10^{-7}$ ccSTP/g for neon, that are tiny different from the expected values.

We have been further working on the analytical development of noble gas measurements for a few months. We have started developing a new measurement for the heavier noble gases dissolved in water samples. Argon, krypton and xenon measurement will hopefully be worked out in spring 2008.

6.4 Hourly variation of elemental components of urban aerosol in Debrecen

Zs. Kertész, E. Dobos, Z. Szoboszlai and I. Borbély-Kiss

With the use of accelerator based PIXE elemental analysis technique and statistical methods, systematic investigation of aerosol samples have been performed in the Institute of Nuclear Research of the Hungarian Academy of Sciences for 20 years determining the elemental composition, size distribution, seasonal and long term time variation, sources and lung deposition probabilities of atmospheric aerosol characteristic to the east-Hungary region.

In continuation of this research we observed the short-term time variation of the elemental components in spring and in autumn 2007, at the end and the beginning of the heating season. We studied the changes in the elemental concentrations, their periodicity, correlation with other elements and meteorological parameters.

The sampling was done with a PIXE International streaker sampler, which enables a time-discrete record of fine (PM2.5) and coarse (PM10-2.5) size fractions. Sampling campaigns were carried out in the garden of the Atomki on 10-16 April and 10-19 October.

Elemental concentration data ($Z > 12$) with 2h time resolution were determined on the two size fractions. Statistical evaluation and source determination were carried out with the positive mass factorization method developed for aerosol source characterization by US EPA.

Six sources of the urban aerosols were identified: 2 types of soil - loess and sand - biomass burning, sulfate originating form long range transport processes, an unknown source enriched with chlorine and heavy metals origi-nating form traffic.

The hourly contribution of some sources for the week 12-19 October is presented on figure 1. In the time trend of soil and heavy metals a periodicity can be observed: the peaks in the morning and in the evening of working days fall together with traffic rush hours. Peaks of biomass burning appear during nights and mornings indicating its origin of domestic heating. Several emission episodes were also detected. Such an episode is presented on figure 2 with a few-hours long increase in the concentration of Cu, Cl and Pb. The shape of the peak suggests industrial origin.

The higher resolution in time makes the source characterization more efficient and more accurate. It allows the identification of local emission and long-range transport episodes. The short-time variation of urban aerosol combined with meteorological data and with mass size distribution serves as a basis to reach a better understanding of the aerosol sources and receptor areas, to follow the evolution of aerosol, and to make a better estimate on the health impact.

[1] Zs. Kertész et al., X-ray Spectometry (2008) 37, 107-110
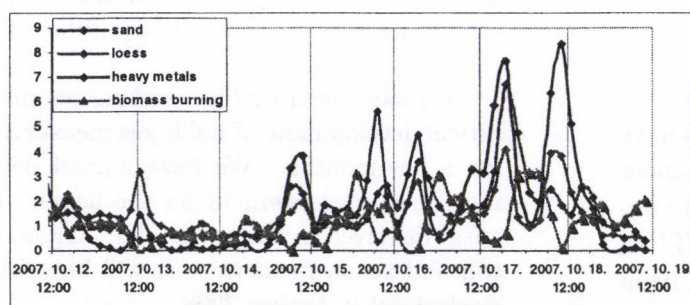
Figure 1. Contribution of sources during 12-19 October, 2007.
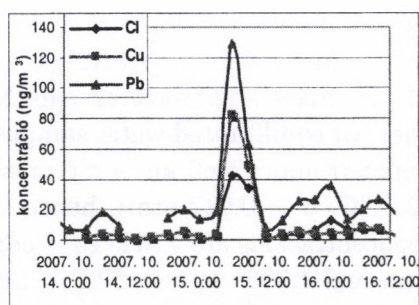
Figure 2. Emission episode.

6.5 Elemetal mass size distribution of the Debrecen urban aerosol

Zs. Kertész, Z. Szoboszlai E. Dobos, and I. Borbély-Kiss

Size distribution is one of the basic properties of atmospheric aerosol. It is closely related to the origin, chemical composition and age of the aerosol particles, and it influences the optical properties, environmental effects and health impact of aerosol.

As part of the ongoing aerosol research in the Group of Ion Beam Applications of the Atomki, elemental mass size distribution of urban aerosol were determined using particle induced X-ray emission (PIXE) analytical technique.

Aerosol sampling campaigns were carried out with 9-stage PIXE International cascade impactors, which separates the aerosol into 10 size fractions in the 0.05-30 μm range. Five 48-hours long samplings were done in the garden of the Atomki, in April and in October, 2007. Both campaigns included weekend and working day samplings.

Basically two different kinds of particles could be identified according to the size distribution. In the size distribution of Al, Si, Ca, Fe, Ba, Ti, Mn and Co one dominant peak can be found around the 3 m aerodynamic diameter size range, as it is shown on Figure 1. These are the elements of predominantly natural origin.
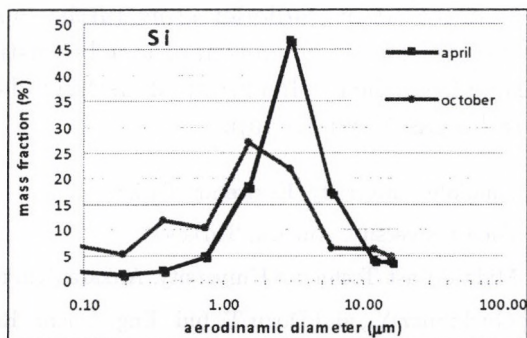
Figure 1. Mass size distribution of Si

Elements like S, Cl, K, Zn, Pb and Br appears with high frequency in the 0.25-0.5 mm size range as presented in Figure 2. These elements are originated mainly from anthropogenic sources. However sometimes in the size distribution of these elements a 2nd, smaller peak appears at the 2-4 μm size ranges, indicating different sources.
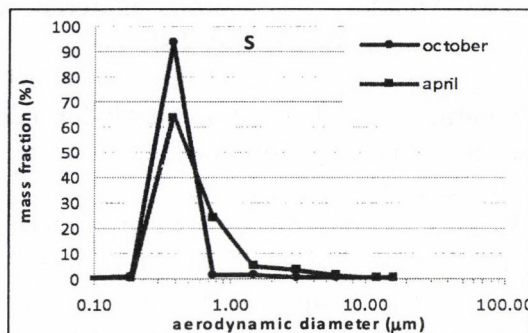
Figure 2. Mass size distribution of S

Differences were found between the size distribution of the spring and autumn samples. In the case of elements of soil origin the size distribution was shifted towards smaller diameters during October, and a 2nd peak appeared around 0.5 μm. A possible explanation to this phenomenon can be the different meteorological conditions. No differences were found between the weekend and working days in the size distribution, however the concentration values were smaller during the weekend than the other days.

The elemental mass size distribution provides information about the origin and sources of aerosol particles, and with emphasis on the $PM_{2.5}$, serves as an input parameter for the determination of lung deposition probabilities by stochastic lung model calculation. This calculation together with short-term time variation enables us to give a more precise health impact of the urban aerosol.

[1] Zs. Kertész et al., X-ray Spectometry 37 (2008) 107

7.1 The ^{11}C-radioisotopic study of methanol conversion on V-MCM-41; the influence of methyl iodide on the transformation

É. Sarkadi-Pribóczki, Y. Gucbilmez[a], A. Solmaz[b], S. Balci[b], F. Szelecsényi, Z. Kovács and T. Dogu[c]

The MCM-41 mesoporous material has Lewis and even Brønsted acid sites to produce dimethyl ether with some hydrocarbons, while over metal modified MCM-41 mostly formaldehyde and dimethoxy methane (i.e. methylal) or methyl formate are produced.

In present experiments V incorporated basically mild acid sites of MCM-41 was prepared by low temperature direct synthesis. The V-MCM-41 has enough main active Lewis sites (by V-) to form formaldehyde and also light Brønsted acid sites to let the adsorbed formaldehyde eliminate and afterwards, with methanol, to form dimethoxy methane in non-oxidative environment.

This V-MCM-41 has been tested by ethanol conversion in non-oxidative environments [1] too and diethoxy methane as main product was detected. In present work the methanol conversion, as well as the methanol co-reaction with methyl iodide are studied from the same V-MCM-41 sample using ^{11}C-technique. The ^{11}C-labelled radioactive methanol has been already applied for determination of methanol conversion rates on Cu-modified MCM-41 [2].

The V-MCM-41 was prepared by direct hydrothermal synthesis method. The adsorption rate of ^{11}C-methanol and, after the reaction, the desorption rate of the remaining ^{11}C-derivatives on catalyst were continuously detected by gamma detectors. The derivatives were analyzed by radio-gas chromatography (gas chromatograph with FID coupled on-line with a radioactivity detector).

Both dimethyl ether and hydrocarbon formation are also in slight degrees according to weak Lewis and Brønsted acidities. Since the conversion was carried out without added oxygen gas, only the frame oxygen can take part into catalysis.

In presence of non-radioactive methyl iodide, the radioactive methanol is converted to radioactive methyl iodide on V-MCM-41. The radio-GC analysis confirmed that the iodide-induced change of the reaction performance was reversible i.e. the radioactive methyl iodide was regenerated to non-radioactive methyl iodide again. The iodides bound to a part of the Brønsted acid sites decreasing the acidity of catalyst, and those even bound to V-cation. This can be a reason that the methanol conversion selectivity to dimethoxy methane decreased while the conversion selectivity to radioactive methyl iodide increased.

Considering the results of the radioactive experiments, the methyl groups of methanol and methyl iodide can be created and bound to free iodide to recompose methyl iodide from methanol. The results show that only methyl iodide can be produced this way but the methanol can not be formed on V-MCM-41.

Two great advantages of this radiolabelling method: the ^{11}C-methanol adsorption-desorption rates on catalyst can be continuously detected by radiodetectors furthermore the methyl group of methanol can be distinguished from the methyl group of methyl iodide by radio-gaschromatograph.

a) Anadolu University, Eskisehir, Turkey

b) Gazi University, Ankara, Turkey

c) Middle East Technical University, Ankara, Turkey

[1] Gucbilmez Y., and Dogu.T, Ind. Eng. Chem. Res. 45, 3496 (2006).

[2] Sarkadi-Pribóczki É., Kumar N., Salmi T., Kovács Z. and Murzin D. Yu., Cat. Letters 114, 17 (2007).

7.2 Production possibility of ^{51}Mn via ^{nat}V(^{3}He,x)^{51}Mn nuclear process for combined positron emission tomography and magnetic resonance imaging studies

F. Szelecsényi, K. Suzuki[a], Z. Kovács and K. Mukai[a,b]

It is very difficult to quantify the uptake kinetics and bio-distribution of magneto-pharmaceuticals in humans using MRI (Magnetic Resonance Imaging). The well-know PET (Positron Emission Tomography) technique, however, could give a solution to this problem in the case of those MRI contrast agents that are based on manganese as paramagnetic contrast enhancer. Luckily manganese has a proper radioisotope, namely the ^{51}Mn ($T_{1/2}$= 46.2 min, β^+ = 97%) [1], which can be easily employed (in the form of ^{51}Mn-labelled contrast agents) for PET studies.

Recently, for the production of this radioisotope proton and deuteron induced nuclear reactions were suggested using natural and enriched Cr targets, respectively [2,3].

In this work we studied the ^{nat}V(^{3}He,x)^{51}Mn nuclear processes in detail from their respective threshold energies up to 40 MeV.

For natural vanadium, the ^{51}V(^{3}He,3n)^{51}Mn reaction (natural isotopic composition of ^{51}V: 99.75%) forms the majority of the required radioisotope. The cross-sections were measured by the conventional stacked-foil method. Two stacks containing 10 and 8 pieces of thin natural V foils were irradiated in external collimated ^{3}He beams of the AVF-930 isochronous cyclotron of NIRS. Thin copper and titanium foils served as energy degraders. The activations lasted for 1 h with a beam current of 100 nA. The activity of the irradiated samples was measured without chemical separation by using the usual gamma-ray spectroscopy. Since the ^{51}Mn has a very weak gamma-line at 749 keV ($I\gamma$=0.265%) [1] its activity was measured via decay curve analysis of the annihilation peaks.

We also measured the excitation functions of those reactions which form the major radio-contaminants i.e. ^{52m}Mn ($T_{1/2}$=21.1 min, $E\gamma$=1434.068 keV($I\gamma$=98.3%)) and ^{52}Mn ($T_{1/2}$= 5.591 d, $E\gamma$=744.223 keV ($I\gamma$=90%), $E\gamma$=935.538 keV ($I\gamma$=94.5%)) [1]. The excitation function curve of the ^{nat}V(^{3}He,x)^{51}Mn nuclear process shows one maximum of about 40 mb at about 30 MeV. The maximum cross-sections of the ^{nat}V(^{3}He,x)^{52m}Mn and ^{nat}V(^{3}He,x)^{52}Mn processes are about 55 (at about 14.5 MeV) and 85 mb (at about 14.5 MeV), respectively.

As far as we know, the present measurements describe a first systematic study of the above processes up to 40 MeV.

Based on the results of the present measurements, thick target yields were also calculated for the production of ^{51}Mn, ^{52m}Mn and ^{52}Mn up to 40 MeV. We also evaluated the optimum production circumstances both for the targets and the applicability circumstances of the product.

According to the results, the ^{nat}V(^{3}He,x)^{51}Mn route seems to be useful for practical production purposes in the energy range of 23→50 MeV.

a) Molecular Probe Group, Molecular Imaging Center, National Institute of Radiological Sciences, Chiba, Japan

b) Ion Beam Group, The Japan Steel Works, Yokohama, Japan

[1] WWW Table of Radioactive Isotopes http://ie.lbl.gov/toi

[2] A.T.J. Klein, F. Rösch and S.M. Qaim, Radiochim. Acta 88, 253 (2000).

7.3 Energetic change of the primary quinone in photosynthetic reaction center: mutation, delayed fluorescence and model calculations (Theses of the Ph.D. dissertation)

L. Rinyu

Photosynthesis is one of the basic metabolic processes of living organisms. Photosynthesizing species (bacteria, algae and higher class plants) convert the energy of light into other forms of free energy (redox potential, electrochemical potential of ions and protons and phosphate-potential) which are directly suitable either to cover the energy need of the vital processes of the cell or to storage.

In reaction center (RC) protein of photosynthetic bacteria, electron transfer is initiated upon light excitation from the excited bacteriochlorophyll dimer (P) to the secondary quinone (Q_B) via bacteriopheophytine (Bph) and the primary quinone (Q_A). In *Rhodobacter sphaeroides* purple bacteria, both quinones are ubiquinone-10, but due to the different protein environment, their electrochemical properties is highly different. Whereas Q_A makes one-electron chemistry, Q_B can be doubly reduced to form hydroquinone, Q_BH_2 by uptake of two protons. Q_BH_2 subsequently leaves the RC and is replaced by an oxidized quinone from to membrane pool. The semiquinones are important intermediates in the quinone reduction cycle of the RC. The redox midpoint potentials of the Q/Q^- redox pairs (E_m) are also different: the Q_A/Q_A^- has 60 mV more negative potential than the Q_B/Q_B^- couple (pH 8) to make the (interquinone) electron transfer favorable. For fine tuning of the midpoint redox potentials of the quinones, the protein assures appropriate steric and electrostatic environment.

The most important aim of this study was the design and production of reaction center mutants in the binding pocket of the primary quinone to investigate the effect of the amino acids of the protein and lipids of the membrane on the thermodynamics of the primary quinone. The first priority was the determination of the absolute free energy gap between the P* and the $P^+Q_A^-$ states in wild type and mutant reaction centers by comparison of the intensities of prompt and delayed fluorescence emitted by the primary donor of the reaction center. By use of the values of the free energy gaps, I calculated the *in situ* midpoint redox potential of the Q_A/Q_A^- redox couple in the mutants and the wild type and compared these values with each other. Based on the available data of reaction center structures I gave a possible explanation to the substantial change in E_m of Q_A in case of mutants.

The available X-ray structures of reaction center make possible to calculate the thermodynamic properties of the mutants with computer simulations. Using docking simulations in wild type and mutant reaction centers, I calculated the binding free energies of the quinone and semiquinone molecules to the Q_A packet and estimated the midpoint redox potential of the Q_A/Q_A^- redox couple. Additionally, by use of the free energy perturbation method, I modeled the reductions process of the primary quinone molecule in wild-type and mutant reaction centers.

With the application of cardiolipin (diphosphatide-glycerol) as a model-lipid, I investigated the interaction between the reaction center protein and the lipid environment. I described how it affects to the charge-recombination process and how it influences the free energy level of the charge couple ($P^+Q_A^-$) relative to the free energy level of the excited primary donor.

With the investigation of the delayed fluorescence emission of the reaction center embedded into membrane fragment (chromatophore) I gave further information about the effects of reaction center proteins and lipid membranes on the energetic properties of Q_A. In addition to these studies, I characterized the complex kinetics of the decay of delayed fluorescence emitted by chromatophore and also gave a description of the new fastest kinetic component.

7.4 NANODERM: Quality of skin as a barrier to ultra-fine particles

Á.Z. Kiss, T. Bíró[a], G. Czifra[a], I. Juhász[b], Zs. Kertész, B. Kiss[b], Z. Szikszai, B.I. Tóth[a], J. Hunyadi[b]

The EU5 project carried out by a consortium of 12 European universities and research institutes under the leadership of the Faculty of Physics and Geosciences, University of Leipzig started in 2003 and ended with the publication of its final report in 2007. The main goal of the project was to get quantitative information on the penetration of ultra-fine particles in all strata of skin, on their penetration pathways as well as on their impact on human health. Details of the project can be found on the following website:
http://www.uni-leipzig.de/~nanoderm.

The Hungarian team was lead by the Department of Dermatology, University of Debrecen, who provided human skin grafted on SCID (Severe Combined Immune Deficiency) mice as a suitable model for studying particle penetration. In the Institute of Physiology, University of Debrecen, the cellular effects of the nanoparticles were assessed. The ATOMKI group performed ion beam analytical investigations using proton induced x-ray emission and scanning transmission ion microscopy techniques to determine the particle distribution on porcine, SCID graft and human skin samples on which various nanoparticle (TiO$_2$) formulations including commercially available sunscreens were applied. Several pre-treatments of the skin were tested, too. The skin samples were cryofixed native specimens, reducing considerably the possibility of creating artefacts.

Results

Titanium was only detected in the stratum corneum for healthy skin. Penetration to layers consisting of living cells was not observed. No diffusion profile was present therefore we conclude that the penetration takes place through mechanical action. Deep penetration into hair follicles was also observed, but not into vital tissue. Clearance is expected via desquamation and sebum excretion respectively for corneocyte layers and hair follicles. In conclusion, the NANODERM group does not expect any harmful effects of sunscreens containing ultra-fine particles on healthy skin. On the other hand, micronised titanium-dioxide particles are internalized by melanocytes and fibroblasts in cell culture. Particles disturb cell viability and proliferation as well as keratinocyte differentiation.

Outlook

Although this EU project has ended, there are still several questions to be answered. In view of the cellular effects, we are currently investigating the penetration of nanosized particles into skin with impaired barrier function. Long term exposure studies are also required.

a) University of Debrecen, Dept. of Physiology

b) University of Debrecen, Dept. of Dermatology

Publications by authors or co-authors from ATOMKI:

[1] Zs. Kertész *et al.*, NIM B 231 (2005) 106-111

[2] Zs. Kertész *et al.*, NIM B 231 (2005) 280-285

[3] P. Auger *et al.*, NIM B 231 (2005) 292-299

[4] J. Lekki *et al.*, NIM B 260 (2007) 174-177

[5] B. Kiss *et al.*, Exp. Dermatol. 2008 Feb 27
    (in press, available online)

8.1 Status Report on Cyclotron Operation

Z. Kormány, P. Kovács, I. Szűcs, I. Ander, F. Tárkányi

The operation of the cyclotron in 2007 was concentrated to the usual 9 months; January, July and August were reserved for maintenance and holidays. The overall working time of the accelerator was 2951 hours; the time used for systematic maintenance was 343 hours. The breakdown periods amounted to 43 hours last year. The cyclotron was available for users during 2565 hours. The effectively used beam-on-target time is summarized in Table 1.

Table 1. Statistics of the irradiation time (beam-on-target) for different research groups

Projects	Hours	%
Nuclear spectroscopy	151	14.2
Nuclear astrophysics	465	43.8
Radiation tolerance test	214	20.2
Medical isotope production	96	9.0
Thin layer activation (TLA)	50	4.8
Target technology	85	8.0
Total	**1061**	**100**

The summer shutdown period was extended by one week this year to complete a major maintenance task in the vacuum chamber of the cyclotron. The septum electrode of the electrostatic deflector had been in operation for over 7 years and it started showing some early signs of deterioration. As a preventive action we decided to replace it by a new one.

A new ion source head manufactured and assembled in our workshop was also installed during the summer maintenance period. Both installations were successful; the new septum electrode provides even slightly better extraction efficiency than the usual value and beam intensities produced by the new ion source are well in accordance with the specifications.

8.2 Activities at the Van de Graaff Accelerator Laboratory

L. Bartha

During 2007 the beam time of the VdG-1 machine amounted to 1450 hours. The accelerator delivered proton (68.2 %) and ^{4}He$^+$ (31.8 %). The ion beams were used for low energy atomic physics (548 hours, 37.8 %) and nuclear physics (896 hours, 61.8 %) experiments. Machine tests required 6 hours (0.4 %) beam time.

The 5 MV Van de Graaff machine was operating for 1421 hours during this period. Proton (78.75 %), ^{4}He$^+$ (7.88 %) and ^{14}N$_2^+$ (13.37 %) particles were accelerated. The beam time was distributed among different research subjects as shown in Table 1.

Table 1. Time distribution among different research activities at VdG-5

Field	Sign	Hours	%
Atomic physics	AP	141	9.92
Nuclear physics	NP	103	7.25
Nuclear astrophysics	NAP	138	9.72
Analytical studies	IBA	628	44.19
Micromachining	MM	336	23.64
Machine tests	MT	75	5.28
Total		**1421**	**100**

Improvements

During the year the following reconstruction works had been carried out on the 5 MV VdG machine:

- The supporting column side holder clips of potential divider chain members had been velded to the column torus rings to avoid fall down of the resistors.
- We ran out of the original charging belt of he machine. As manufacturing of such size of charging belts stopped, it had been replaced by a new type of belt, made originally as transporter belt for food-industrial application.

Type of the new belt: E 8/2 U0/U2 MT-NA WHITE FDA

Manufacturer/supplier: Siegling Hungária Kft, H-1044 Budapest, Megyeri út 8.

- The old charging belt had been charged on the inner side, against a counter-electrode placed at the opposite side of the belt. The inner side of the new belt is a plain carcass, which cannot be charged, thus the old charging system had been changed. At the new system the driver pulley acts as a counter-electrode and the charging brush is placed in front of that part of the pulley, where the belt lays on it. The pulley had been insulated from the ground, and grounded through an ammeter. That meter measures the upcharge current. To avoid erosion effects of the charging current going through the bearings of the pulley, a short circuiting bridge composed of a carbon brush and a slipping ring had been constructed.

- The old worn-out tungsten brushes had been replaced by stainless-steel brushes, made also for food-industry. Type of the brush: ABL100005-K1.

Body: Aluminium, bristle material: Bekinox twisted, visible bristle height: 15 mm, body length: 1000 mm. We cut it into two 500 mm pieces.

Manufacturer/supplier: Mink-Bürsten, August Mink KG, Autenbachstrasse 24-30, 73035 Göppingen, Germany.

The new upcharge brush is fed by as low as 4 kV charging voltage. The collector brush is placed against a traditional counter-electrode and about 250 μA current can be collected by it with ease.

At the installation of the new belt the inner equipotential bars had been left out. As a result of the new charging system, the energy stability improved and the terminal ripple significantly decreased. Both this fact and the lowered Bremsstrahlung due to the well running oil-free vacuum-system contributed to safe operation of the accelerator up to 4 MV terminal voltage.

8.3 Activities in the Electron Cyclotron Resonance (ECR) Laboratory

S. Biri

It is a tradition in our institute that the staffs of the accelerators write short reports about the activities in the current year. These non-scientific reviews are actually statistics in the institute Annual Report showing the delivered beams and beam-times for each research. The electron cyclotron resonance (ECR) ion source (ECRIS) has been operating since 1997 and 2003 was the first year when we distributed its operation time among the users. Between 2003 and 2007 the yearly operation time was around 500...600 hours. From this year we decided to follow the example of the other accelerators (Cyclotron and the Van de Graaff generators). In this paper we give a short summary on the activities took place in the ECR Laboratory in 2007 (and is planned to do it in every Annual Reports in the subsequent years).

Since 2006 the ATOMKI-ECRIS has two operation modes [1]. The ECRIS-A is the original assembly to produce highly charged ion beams. The ECRIS-B configuration [2] forms large-size, low-charged plasmas for materials research and plasma investigations. In 2007 the ion source operated two months in the "B" mode (January and February) and 10 months in the "A" mode.

Table 1 summarizes the plasma and beam hours devoted for the research topics. Separated papers are published in this Report if remarkable results were achieved in any of these topics. More information and other details are in the homepage of the laboratory [3]. The terminology "beam-time" or "hour" however, is a little different from the other accelerators. A part of the experiments at the ECR ion source require the generation of plasma only and no beam extraction is necessary. The "Hours" in the table mean the time when a plasma was made in the plasma chamber. In most cases an ion beam was extracted so the ECRIS operated as a real accelerator. "Beam development" means our continuous time-consuming efforts with the goal to produce new plasmas and beams with better parameters: higher charge, higher intensity, better transport efficiency, wider ion choice, etc.

Table 1. Plasmas and beams produced in the ECR Laboratory in 2007. HCI means highly charged ion.

Research topic	Ion species	Hours	%
Ion guiding through nano-capillaries	Ne^{6+}, Ne^{7+} Ar^{8+}, Ar^{12+}	200	32
Fullerene research	C_{58}^{+}, C_{60}^{+} C_{58}^{2+}, C_{60}^{2+} Fe^{+}	100	16
Surface modification with HCIs	Ar^{8+}	30	5
X-ray spectroscopy	Kr^{15+} $Ar^{1+...16+}$	150	24
Beam development & maintenance	$O^{3+...7+}$ I^{14+}, C_{60}^{+} $Ar^{8+...16+}$ $Ne^{6+...9+}$	140	23
Total		**620**	**100**

Beyond the scientific research several technical developments improved the ability of the ion source. The plasma chamber (A-mode) was modified in order to avoid O-ring melting. The high voltage insulation was improved and now we can reach and use 30 kV acceleration voltage (the old top value was 20 kV). Two quartz windows were installed in the beam-line for on-line observing of the beam spot using web cameras. We successfully exceeded the old record for He-like Ar (Ar^{16+}) and now the new record is 7 nA at 10 kV terminal voltage.

[1] S. Biri, É. Fekete, I. Iván, and I. Gál: Transformation of the ATOMI-ECRIS into a Plasma Device, ATOMKI Annual Report 2006, pp. 72-73.

[2] GVOP-3.2.1-2004-04-0054/3.0.

[3] http://www.atomki.hu/atomki/ECR

8.4 Concept for processing of silicon check valves by proton beam micromachining

Cs. Dücső[a], I. Rajta, P. Fürjes[a], E. Baradács[b]

The increasing demand for chemical or biochemical microsystems, e.g. Lab-on-a-Chip inspires the development of integrable microfluidic components. In this work, we propose a novel approach for the formation of check valves by combining direct proton beam implantation with porous Si etching technique [1].

When implanting Si single crystal with high energy protons, defects are generated along the ion path resulting in locally increased resistivity. The damaged volume acts as a barrier against the current flow during the electrochemical etching process. Applying high implantation dose the current flow is locally inhibited, thereby the porous Si formation is locally ceased. This effect can be exploited in fabrication of 3D crystalline silicon (c-Si) structures by combining with the locally selective porous Si formation and dissolution. As the implantation energy determines the projection range of the ions, with appropriate selection of energy and dose of the ion microbeam, 3D structures can be formed in the Si crystal.

Two types of check valve structures were considered: the first group is called "horizontal". The membrane is attached to the flow channel at one of its side or by a reduced cross-section neck at the side. The flexible membrane is vertical to the surface but tilted with the sidewall of the channel by an angle of 30-60°. Therefore, flow from the two directions has different effect, may open the valve membrane more or close it, the valve works like a door. The SEM image of the "horizontal" structure is shown on Fig. 1.

In the "vertical" versions both the sidewalls and the membranes are attached to the bottom of the channel but there are no contacts at the sides. The membrane is not perpendicular, it has an angle of 40-60° to the bottom of the channel (see Fig. 2). The operation is similar to the other versions.

The feasibility of fabricating check valves by this method was proved both experimentally and by model calculations. In a 10-15 ohm cm substrate 1 μm or submicron proton beams of minimum 2 MeV energy and $\sim 10^{16}$ cm^2 dose is necessary for fabrication of the required structures.
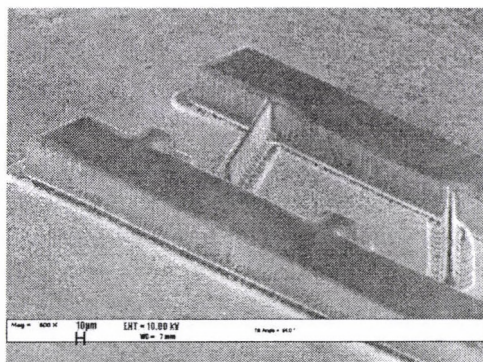
Figure 1. SEM views of the "horizontal" structures. The implantation energy is 2 MeV, proton dose is 2.4×10^{15} cm^2.
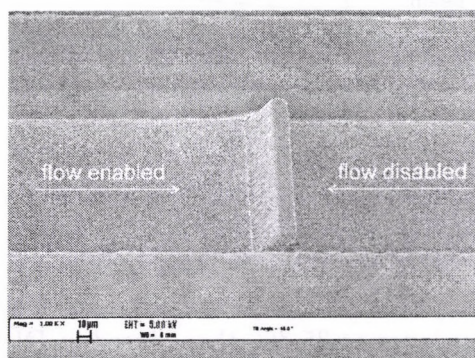
Figure 2. The "vertical" structure in a 30 μm deep channel. The tilt of the valve membrane is 43°.

a) Res. Inst. for Tech. Phys. &Mat. Sci, Budapest

b) Dept. of Environ. Phys., Uni. Debrecen

[1] Cs. Dücső *et al.* NIM B260 (2007) 409.

8.5 Polymer microcapillaries created by P-beam Writing

S.Z. Szilasi, I. Rajta, S. Sipka[a], B. Sulik, Z. Juhász, C. Cserháti[b]

PMMA sheets of 50 μm thickness were irradiated using a pattern of 10 μm diameter filled circles. The proton beam energy was 2 MeV, which have a penetration depth in PMMA of 64 μm. Figure 1. shows the energy loss of the ions as a function of depth in the sample. The energy deposition along the path is almost homogeneuos, the Bragg-peak is behind the sample. This ensures that the created microcapillaries will have smooth cylindrical walls. The ions were collected by a Faraday-cup behind the sample, which also served for charge normalization.
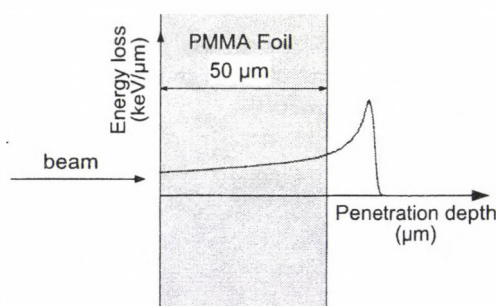
Figure 1. Energy loss of 2 MeV protons as a function of depth in 50 μm thick PMMA sample.

The produced samples were developed in GG-developer at 35 °C, then rinsed in DI water. The inside of the microcapillaries were rinsed by means of ultrasonic bath.

The samples were quality checked using optical and electron microsopes. It was concluded that the microcapillaries have the designed circular cross section, and the error (undeveloped or missing holes) is less than 2%. The transparency of the filters is 20% (hole area / total area). Fig. 2. shows a typical optical microscopy image.

Promising experiments have started in biological applications of these filters in the Laboratory of Immunology, 3rd Department of Internal Medicine, University of Debrecen, Medical and Health Science Center.
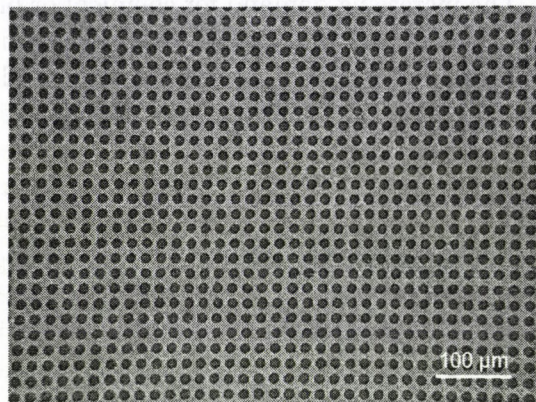
Figure 2. Optical microscopy image of the developed samples.

We are also going to study the ion-guiding properties [1] of the capillary arrays. Such experiments have been started recently in ATOMKI [2]. If they can efficiently deflect the highly charged heavy ions in a few degrees range, they are applicable for constructing small ion-focusing elements without power consumption in the keV ion-energy range.

a) Dept. Internal Med. 3, Uni. Debrecen

b) Dept. of Solid State Physics, Uni. Debrecen

[1] Stolterfoht N., Bremer J. -H., Hoffmann V., Hellhammer R., Fink D., Petrov A., Sulik B.: *Transmission of 3 keV Ne7+ ions through nanocapillaries etched in polymer foils: Evidence for capillary guiding*, Phys. Rev. Lett. 88 (2002)133201

[2] Mátéfi-Tempfli S., Mátéfi-Tempfli M., Piraux L., Juhász Z., Biri S., Fekete É., Iván I., Gáll L. F., Sulik B., Víkor Gy., Pálinkás J., Stolterfoht N.: *Guided transmission of slow Ne6+ ions through the nanochannels of highly ordered anodic alumina*, Nanotechnology 17 (2006)3915

8.6 Aqueous base developable: easy stripping, high aspect ratio negative photoresist for optical and proton beam lithography

M. Chatzichristidi[a)], I. Rajta, Th. Speliotis[a)], E. Valamontes[a)], D. Goustouridis[a)], P. Argitis[a)], I. Raptis[a)]

A variety of different photo resists are used for the fabrication of polymer and metal high aspect ratio structures. Among them SU-8, a chemically amplified negative tone photoresist is the mostly used. However, after processing the finished resist pattern (SU-8) is hardly removed from the substrate. In the present work the formulation and process optimization of a negative tone chemically amplified photoresist (TADEP) is presented.

TADEP resist consists of epoxy (EP), partially hydrogenated poly(hydroxystyrene) (PHS) components and 1-(4-hydroxy-3-methylphenyl) tetrahydrothiophenium triflate as PAG. In particular the component relative concentration and the PAG molecule have been optimized towards the optimum absorption in the exposure spectrum as also the dissolution rate of the uncrosslinked regions. In addition the PAB step has been studied towards the optimum conditions in terms of resist adhesion.

The proton beam exposures were performed on the nuclear microprobe facility at ATOMKI. The proton energy was 2 MeV, the beam was focussed down to $\sim$3 μm spot size and the beam current used was in the 5-60 pA range. The scan size was typically 1000 μm and the beam step size was 1 μm. The fluence was 300 nC/mm^2.

The thermal processing steps (Post Apply Bake (PAB), Post Exposure Bake (PEB)) were carried out on a levelled hot plate. The development was performed in AZ726 MIF (0.26N TMAH) at room temperature in stirring mode. Before the nitrogen drying, the samples were rinsed in deionized water.

Electroplating was carried out at a temperature controlled bath at 50 °C by using a solution consisting of nickel sulfate, nickel chloride, boric acid, ferrous sulfate and saccharin and a constant current density of 40 mA/cm^2. Stripping of the crosslinked regions was performed using acetone in an ultrasonic bath (Branson 2200, frequency of 47 kHz $\pm$ 6%). The resist structures are totally removed, despite the fact the width of the polymer structures was very small compared to the width of the complementary metallic ones.

The TADEP resist owns two significant advantages over the SU-8: the dissolution of the uncrosslinked areas in IC standard aqueous developers and the easy stripping in acetone by the assistance of ultrasonic bath. By using the TADEP resist 1.5 μm wide very long lines were printed, by UV lithography, in an 11 μm thick film, providing an aspect ratio of 7. These structures were transferred, by electroplating followed by resist stripping, into thick Ni film. In addition first experiments with Proton Beam Writing showed an aspect ratio of 8, most probably limited by the rather large beam diameter used [1].

a) IMEL, NCSR "Demokritos", Athens, Greece

[1] Microsyst Technol, in press.

8.7 Ion guiding and losses in insulator capillaries

Z. Juhász, B. Sulik, Gy. Vikor, S. Biri, É. Fekete, I. Iván, F. Gáll, K. Tőkési, S. Mátéfi-Tempfli[a], M. Mátéfi-Tempfli[a], E. Takács[b], J. Pálinkás[b]

Not long ago it was discovered that insulating capillaries can guide slow ions [1], so that the ions avoid close contact with the capillary walls and preserve their initial charge state. This phenomenon did not only give a new puzzle for theoreticians but opened the way for new possible applications where ions are manipulated (deflected, focused and directed to different patterns on the irradiated media) with small capillary devices. The most important question for such applications is how large fraction of the ions can be guided to the desired direction.

It is already known that the ion guiding is due to the charging up of the inner capillary walls by earlier ion impact events. In tilted capillaries one side of the capillary walls charges up. This deflects the later arriving ions, so that some of them pass through the capillaries nearly parallel with respect to their axes. The angle where the transmission drops to $1/e$ of the direct transmission at $0°$ is the guiding angle, which characterize the guiding ability.

At $0°$ the ideal 100 percent transmission for the ions, which enter the capillaries, is reduced due to the mirror charge attraction and geometrical imperfections. These losses appear in the transmission for tilted capillaries with similar magnitude, since after the deflection region, which usually restricted to the close surroundings of the capillary openings, the guided ions pass through the rest of the capillaries as in non-tilted samples.

In our experimental studies [2] with Al_2O_3 capillaries we found that around 90 percent of the incoming ions are lost. To understand these significant losses, the effects of the mirror charge attraction and geometrical imperfections have been calculated classically. The mirror charge potential was taken from [3]. The model of the capillaries used in the calculations can be seen in Figure 1.
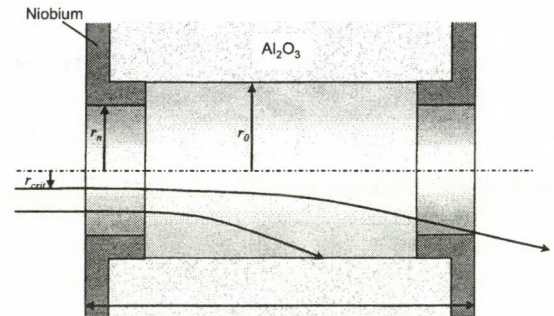
Figure 1. Capillary model with ion trajectories, r_n: radius of the capillary opening at the metallic layer, r_0: inner radius of the capillary, r_{crit}: critical starting distance from the axis from where ions can still pass the capillary.

The calculations have shown that the effects of mirror charge attraction and the angular distributions of the primary beam and the capillary axes can cause such large transmission losses. The very different transmission abilities measured in the different experiments for different materials can be explained by the different dielectric constant of the materials, the different beam properties and the different capillary angular distributions due to different preparation methods. Such simple calculations can significantly contribute to the understanding of the phenomenon.

a) Unité de Physico-Chimie et de Physique des Matériaux, Université Catholique de Louvain, Louvain-la-Neuve, Belgium

b) Dept. of Exp. Phys. Uni. Deberecen

[1] N. Stolterfoht *et al*, PRL **88** (2002) 133201-1.

[2] S. Mátéfi-Tempfli *et al*, Nanotech. **17**, 3915 (2006)

[3] K. Tőkési *et al*, Phys. Rev. A **64**, 042902 (2001).

8.8 Response of a few LaBr$_3$ scintillation detectors to high energy γ-rays

A. Vitéz, D. Balabanski[a], M. Csatlós, M. Ciemala[b], G. Georgiev[c], J. Gulyás, A. Krasznahorkay, M. Kmiecik[b], A. Lefebvre-Schuhl[c], R. Lozeva[c,d], A. Maj[b], S. Lalkovski[e], J.-M. Daugas[f]

LaBr$_3$:Ce scintillators are attracting particular interest for γ-spectroscopy due to their excellent time and energy resolutions. Motivated by Giant Resonance studies and neutron-skin thickness measurements, in this work we tested the energy resolution and efficiency of 1"x1", 1.5"x1.5" and 2"x2" crystals for γ-rays up to 17.6 MeV.

At low energies the resolution and efficiency were measured using standard ^{60}Co and ^{152}Eu γ-ray emitters, which were placed at 15 cm from the face of the detectors.

The measurements for the high energy region were performed with proton beams from the 5 MV Van de Graaf accelerator of ATOMKI using different (p,γ) reactions on ^{7}Li, ^{11}B, ^{27}Al, ^{23}Na, and ^{39}K targets in the similar way as we did previously in calibrating a Clover detector [1]. The detectors were set at 15 cm from the target and at 55° with respect to the beam direction, in order to minimize the effect of the different angular correlations. All targets were made by evaporation onto 0.1 mm thick Ta backings in vacuum. The thicknesses of the targets were varied between 10 - 75 μg/cm^2. Beam currents varied between 1 and 2 μA and the charge collection was continued till the statistical error for the high energy γ-rays becomes less than 5 %.

A typical gamma-spectrum for e.g. 2"x2" detector is shown in Fig. 1. Although the photopeak efficiency decreases at higher energy, this detector can still be used. Around 10 MeV it is comparable to the efficiency of e.g. an Euroball type Clover detector (with more than four times larger active volume [1]) in adding back mode. For energies above 15 MeV a larger LaBr3:Ce crystal would be required.

The relative energy resolution (FWHM) is shown as a function of the γ-ray energy in Fig. 2. It goes well below to 1 % at 10 MeV and reaches about 0.5 % at 17.6 MeV, which is the best for scintillation type detectors.
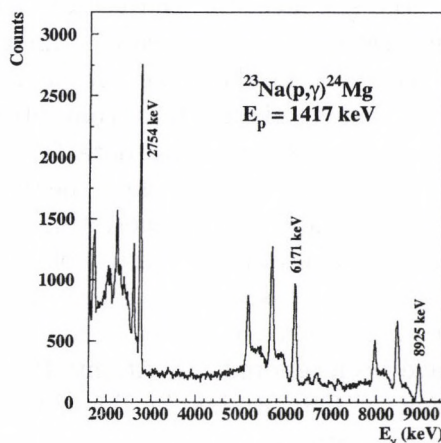
Figure 1. Response of a 2"x2" crystal to high energy γ-rays created in the ^{23}Na(p,γ) ^{24}Mg reaction. The intensity of the 3 radiation is approximately the same. The single and double escape peaks are nicely resolved.
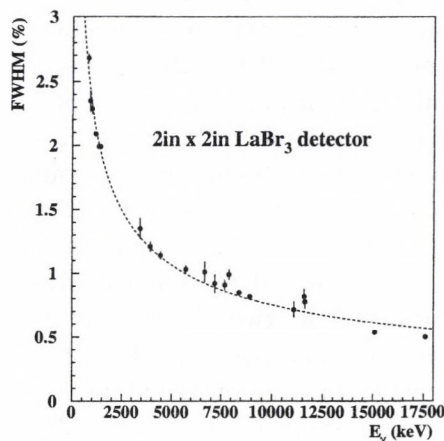
Figure 2. Relative energy resolution of a 2"x2" crystal as a function of the γ-ray energy. The dashed line shows the expected E$^{-1/2}$ behaviour.

a) INRNE-BAS Sofia, Bulgaria;

b) IFJ Krakow, Poland;

c) CSNSM Orsay, France;

d) IKS KU Leuven, Belgium;

e) University Sofia, Bulgaria;

f) CEN, Bruyeres-le-Chatel, France;

[1] Z. Elekes et al., NIM A503 (2003) 580.

8.9 Developments for ion-solid interaction studies: The commission of an electrostatic deflector unit

A. Orbán and S. Hagmann [a,b)]

Heavy ions for the first time have been used in cancer therapy at GSI, Darmstadt. The heavy-ion treatment of deep-seated tumors is more effective and in the same time less destructive for benign tissues than conventional photon therapy. Experimental data for electron production and transport along the trajectory of energetic heavy ions penetrating solids are required as input data for therapy plans. So far these plans are based on data provided by gas-phase experiments, in this way solid state effects have been ignored. In Atomic Physics Department of GSI studies in this direction are going on with use of a toroidal electrostatic electron spectrometer for ion-foil collisions. The spectrometer is equipped with a position sensitive multi channel plate (MCP) detector, used for electron detection in angular range between 0° and ±180°. In this way angular and energy distribution of electrons emitted due to ion-solid interaction is accessible.

Previous studies of the group raised questions about the non-linear operation of the detector. Determination of absolute cross sections assumes, among many other parameters, the knowledge of the detector performance. Furthermore, without detailed quantitative information about the MCP reliable analysis and interpretation of the two-dimensional electron spectra are also not possible. For the above reason we have commissioned and implemented an electron gun system as a tool for MCP test measurements at the beam-line X3 (UNILAC, the linear accelerator of GSI). For the calibration of the detector, the assurance of the same experimental conditions for ion- and electron beam experiments is of crucial importance. For this reason we also implemented a new electrostatic 90° quadrupole deflector which bends the electron beam into the beam channel X3 (Fig. 1). This development allows to have ion- and electron beam of the same trajectory without changing the set-up and breaking the vacuum. The electron deflector was designed to keep the optical properties of the beam which was achieved by the use of the additional lens

systems at the entrance and exit part of the deflector.
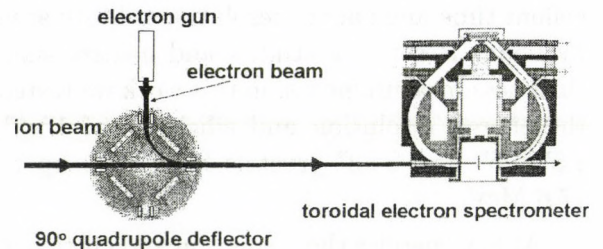
Figure 1. Scheme of the experimental set-up.

This new set-up will allow for the first time the analysis of electrons emitted in angular range between 0° and ±180° in collisions of solid targets with electron- and ion beam. As a first step we checked the properties of our electron beam (energy: 0.5 - 2 keV), analyzing it with the spectrometer. In Fig. 2 the size of the beam and the peak/background ratio indicates the satisfactory performance of the set-up.
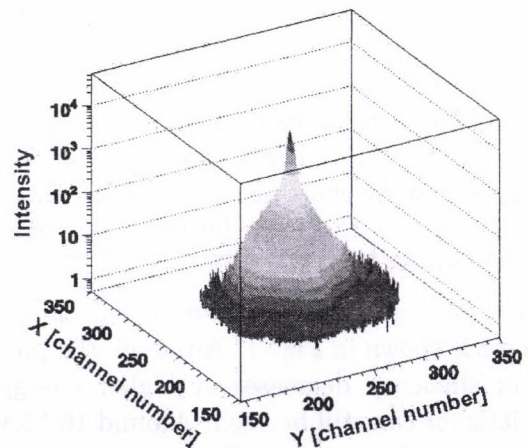
Figure 2. The image of an 1-keV electron beam on MCP analyzed by the spectrometer.

a) Gesellschaft für Schwerionenforschung, GSI, D-64291 Darmstadt, Germany

b) Institute für Kernphysik, University of Frankfurt, D-60438 Frankfurt, Germany

8.10 First beam tests at the isotope separator

M. Hunyadi, Z. Gácsi

Subsequent to the transportation of the sector magnet, vacuum system elements and electronic modules to Debrecen [1], the installation of the isotope separator involving the construction of a new ion source [2] and beam line were started in 2006 and completed in early 2007. The first isotopic beam of singly charged noble gas ions (Ne, Ar, Kr) was produced in April 2007 after the complete equipment became operational. The development of the ion source was then extended to the implementation of a vaporizer oven connected to the plasma chamber, which can provide ion beams formed of solid elements with melting points of approximately up to 500 °C. In the first test experiments on solid elements, sulphur and selenium vapors were ionized and extracted at 10-20 kV. Newly designed and constructed electrostatic ion-optical elements were employed to shape and guide the extracted beam, which then was momentum-separated by the high-dispersion 55° sector magnet. Separated beam currents were measured at a maximum of 40 μA.

Impinging of isotopic beams on sample surfaces was facilitated with the use of focussing and decelerator lenses to achieve appropriate conditions for soft-landing deposition below 100 eV and to avoid undesirable sputtering.

Fig. 1 presents a view of the ZnS screen placed at the end of the beamline, showing four of the stable selenium isotopes as isolated spots with intensities proportional to their natural abundances. To check the purity of selenium isotopes deposited on various substrates, Secondary Neutral Mass Spectrometry (SNMS) has been applied, and a mass spectrum obtained for a Se-80 sample is shown in Fig. 2. Evidently, the neighbours of a selected isotope were not contributing significantly at this moderate level of statistics, which resulted in an enrichment of approximately 97%, even for the least abundant isotopes.

Further development will focus on the improvement of various operational characteristics of the ion source, like temperature stability, ionization efficiency, plasma density concentration and vapour pressure regulation. A high performance ion source and beam guide system are a conceptual condition for most applications, and must form a suitable basis for optimizing further extensions of development.

Figure 1. Four of stable selenium isotopes incident on a fluorescent ZnS screen. Masses and natural abundances of isotopes are also indicated.
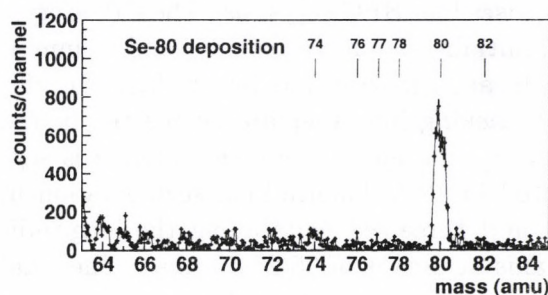
Figure 2. Mass spectrum of SNMS analysis obtained for Se-80 deposited on a tungsten plate.

[1] Z. Gácsi et al., Atomki Ann. Rep. 70 (2005)

[2] M. Hunyadi, Z. Gácsi, Atomki Ann. Rep. 76 (2006)

8.11 Study of the performance of a clover array for the DESPEC experiment

A. Algora, for the DESPEC Collaboration

The DESPEC experiment (DEcay SPECstroscopy) aims to study the decay properties of exotic nuclei produced in the future FAIR facility. A Ge array, adapted to the specific conditions of the Super FRS, is one of the key setups for this experiment. The collaboration is considering two possible setups for the Ge detector array. One possibility is to use an array of stacks of planar Ge detectors specifically designed for the DESPEC needs. An study of the planar setup was already discussed in our contribution to the annual report last year [1]. The other alternative is to use an array of "more" standard segmented Ge detectors of EXOGAM [2] or TIGRESS [3] type with a higher segmentation. The R&D phase of this project requires the realization of Monte Carlo(MC) simulations to evaluate the optimal setup for the future experimental facility.

The results obtained for the simulations of the proposed segmented clover setup are presented here. This setup consists of an array of 6 segmented clover detectors arranged around a focal plane of $260 \times 100 \times 40 \ mm^3$. Each clover comprises four HPGe crystals. The HPGe crystals, initially 60 mm in diameter and 90 mm in length, are cut with four flat surfaces for efficient packing into a square geometry. In the geometry considered here each crystal is segmented in 12 (a longitudinal segmentation in four and three segments along the longitudinal axis at depths of 25-25-40 mm). The total number of electronic channels of such an array is $6 \times 4 \times 12 = 288$.

The described clover geometry has been implemented using the MC code GEANT4 [4]. As in our previous work [1] the tracking code *mgt* developed by D. Bazzacco [5] for the AGATA collaboration was used to study the tracking properties of such an array. The results, presented in Table 1, correspond to the application of the *mgt* code to simulation data of centered, point-like monoenergetic gamma sources. The first column shows the energy of the emitted gamma rays. The second presents the maximum peak efficiency that can be obtained with the setup (as a total absorption spectrometer). The third column shows the peak to total ratio obtained in case the clover detectors are considered as detector units (add-back use). The fourth column shows the peak to total ratio obtained after the application of the tracking code for the full array. Finally, in the last column the efficiency of the tracking algorithm is given. As part of our work the effect of emission of gamma cascades on the tracking efficiency has also been studied. Similar results for the planar array were already presented in [1].

The next step of our work will be the study of the electrical pulses generated in the detectors in order to evaluate the performance of pulse shape analysis for the present setup. Different longitudinal segmentations are also under consideration.

Table 1. Results of the simulations for monoenergetic gamma rays (see text for details).

E MeV	Eff Peak	P/T Clov.	P/T Track.	Track. Eff.
0.10	37	88	91	98
0.25	28	67	76	95
0.50	20	49	59	96
1.00	15	38	47	94
2.00	10	29	34	92
5.00	6	16	17	76

[1] A. Algora *et al.*, Atomki Ann. Rep. 2006, p.20

[2] http://www.ganil.fr/exogam/

[3] H.C. Scraggs *et al.*, Nucl. Inst. Meth. A543 (2005) 431

[4] S. Agostinelli *et al.*, Nucl. Inst. Meth. A506 (2003) 250

[5] D. Bazzacco, The *mgt* code, unpublished

8.12 Production of single glass capillary

F. Turi, R.J. Bereczky and K. Tőkési

Investigations of the interactions of highly charged ions with internal surfaces recently become available due to the advances in the fabrication of microcapillaries. The first measurements were performed using metallic microcapillaries. Therefore the first theoretical descriptions pertained also to metallic microcapillaries and highly charged ions (HCI) which have proven to be quite successful in comparison with experimental data [1]. Later the investigations of HCI and insulator capillaries become also available and the unexpected charge particle guiding was discovered, i.e. the slow HCIs can able to pass through the capillary, keeping their initial charge states even though that the capillary axis is tilted with large angles compared with the direction of the incident beam [2,3]. In this case, the theoretical descriptions of the interaction between charged particles and insulator capillaries are far from being well understood. So far, a thin insulating foil with multitude of straight holes was used to study the the interaction between HCI and insulator capillaries. Therefore, for the accurate simulation of the ion trajectories, the collective effects due to the neighboring capillaries must be also taken into account. This causes an extremely hard and challenging task for theoreticians.

Therefore, for ideal and clear investigations, both experimental and theoretical, we produced single glass capillaries (see Fig. 1.). The capillaries were prepared by heating a straight glass tube made from pirex, and then it was stretched by pulling both ends with a constant force. The diameter of these capillaries are between 90 and 300 μm and we varied the ratio between the length and the diameter from 50 to 100. The individual capillary was fixed into an Al holder (see Fig. 2.). Thus, the capillary is stabilized and it can be used for our forthcoming experiments. We note, that avoiding the macroscopic charge-up during the transmission measurements, the capillary ends were covered by graphite.
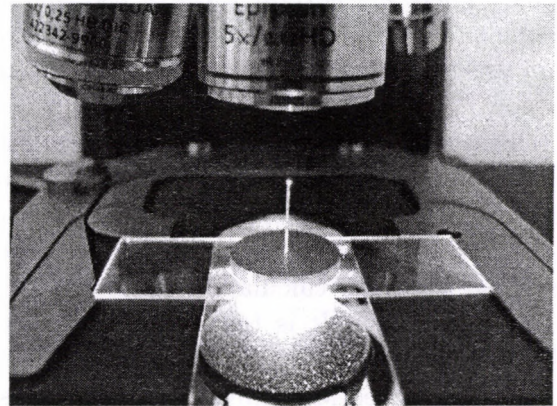
Figure 2. Photo of the fixed single glass capillary.

Figure 1. Optical micrograph of a single glass capillary.

[1] K. Tőkési, L. Writz, C. Lemell and J. Burgdörfer, Phys. Rev. A 64 (2001) 042902.

[2] N. Stolterfoht, J.H. Bremer,V. Hoffmann, R. Hellhammer, D. Fink,A. Petrov, B. Sulik, Phys Rev. Lett. 88 (2002) 133201.

[3] K. Schiessel, W. Palfinger, K. Tőkési, H. Nowotny, C. Lemell, J. Burgdörfer, Phys. Rev. A 72 (2005) 062902.

8.13 High performance computer code for molecular dynamics simulations

I. Lévay and K. Tőkési

Molecular Dynamics (MD) simulation is a widely used technique for modeling complicated physical phenomena. Since 2005 we are developing a MD simulations code for PC computers [1]. The computer code is written in C++ object oriented programming language. The aim of our work is twofold: a) to develop a fast computer code for the study of random walk of guest atoms in Be crystal, b) 3 dimensional (3D) visualization of the particles motion. In this case we mimic the motion of the guest atoms in the crystal (diffusion-type motion), and the motion of atoms in the crystal-lattice (crystal deformation).

Nowadays, it is common to use Graphics Devices in intensive computational problems. There are several ways to use this extreme processing performance, but never before was so easy to programming these devices as now. The CUDA (Compute Unified Device) Architecture introduced by nVidia Corporation in 2007 is a very useful for every processor-hungry application. A Unified-architecture GPU include 96-128, or more stream processors, so the raw calculation performance is 576(!) GFLOPS. It is ten times faster, than the fastest dual Core CPU [Fig.1].

Our improved MD simulation software uses this new technology, which speed up our software and the code run 10 times faster in the critical calculation code segment. Although the GPU is a very powerful tool, it has a strongly paralleled structure. It means, that we have to create an algorithm, which works on several processors without deadlock. Our code currently uses 256 threads, shared and constant on-chip memory, instead of global memory, which is 100 times slower than others. It is possible to implement the total algorithm on GPU, therefore we do not need to download and upload the data in every iteration. On behalf of maximal throughput, every thread run with the same instructions.
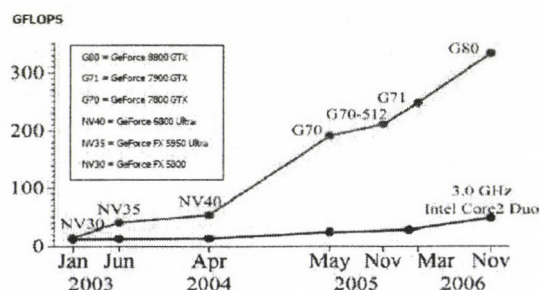
Figure 1. Calculation performance differences between GPUs and CPUs.

[1] I. Lévay and K. Tőkési, ATOMKI Annual Report 2005 (2006) 83.

9.1 Hebdomadal Seminars

January 25
A simple model for prosperity and decline of civilizations
T. Bíró *(Research Institute for Particle and Nuclear Physics /RMKI/, Budapest)*

February 1
Left-right asymmetry in the photo-ionisation of outer atomic shells
S. Ricz

February 21
A computer-assisted existence proof for photonic band gaps
M. Plum *(University of Karlsruhe)*

March 1
Radionuclide metrology in the fields of food and environment
Zs. Szántó

March 27
State of affairs
M. Pálinkás, R. Lovas

April 25
Commemoration for Dr. Edward Teller
E. Voisin *(USA)*

April 26
Development of experimental methods for the high-energy physics
Search for charged Higgs-bosons at the L3 experiment and
development of a precision alignment system for the CMS detector at CERN
Z. Szillási *(University of Debrecen)*

May 24
E. Wigner's years at school
Gy. Radnai *(Eötvös Loránd University, Budapest)*

May 31
Nanometer resolution depth profile analysis
K. Vad

June 2
Experimental study of the astrophysical p-process in capture and elastic scattering reactions
Gy. Gyürky

June 21
Noble gases dissolved in water in the twenty first century
i.e., what was my engagement in Heidelberg
L. Palcsu

June 28
Single ionization by short laser pulses
D. Arbo *(Institute for Astronomy and Space Physics, Buenos Aires)*

September 6
  Status and opportunities of FLAIR
  E. Widmann *(Stefan Meyer Institute for Subatomic Physics, Vienna)*

September 13
  Hyperdeformed band in ^{36}Ar populated in the ^{24}Mg+^{12}C elastic scattering
  A. Lépine-Szily *(University of Sao Paolo)*

September 20
  Search for gravitational waves: LIGO, VIRGO and LISA
  Zs. Frei *(Eötvös Loránd University, Budapest)*

September 27
  Characterization of materials and radiation damage induced changes using heavy ion beams
  M. Jakšić *(Ruder Bošković Institute, Zagreb)*

October 4
  LHC 2007: Collection and processing of data at ATLAS
  A. Krasznahorkay, Jr.

October 8
  Perspective of neutrino beam science
  E. Ejiri *(RCNP-Osaka, NIRS & CTU)*

October 11
  Migration of helium in SiO$_2$
  E. Szilágyi *(Research Institute for Particle and Nuclear Physics /RMKI/, Budapest)*

November 15
  Introduction of new colleagues in Atomki
  G. Christian, E. Corniani, J. Farkas, J. Imrek, R. Janovics, L. Papp, Z. Szoboszlai, C. Yalcin

November 22
  Three-body cluster states in ^{6,9}Be
  P. Papka *(iThemba LABS, South Africa)*

December 11
  Resonant X-ray emisson spectroscopy
  M. Kavčič *(Institut Jožef Stefan, Ljubljana)*

9.2 List of Publications

The list of the Institute's publications can be found on-line at:

http://www.atomki.hu/p2/years/yea02007.htm

Author index